THE COQUIHALLA VOLCANIC COMPLEX, SOUTHWESTERN BRITISH COLUMBIA

by

ROBERT G. BERMAN

B.A., Amherst College, 1975

A THESIS SUBMITTED IN PARTIAL FULFILLMENT OF
THE REQUIREMENTS FOR THE DEGREE OF
MASTER OF SCIENCE

in

THE FACULTY OF GRADUATE STUDIES
Department of Geological Sciences

We accept this thesis as conforming
to the required standard

THE UNIVERSITY OF BRITISH COLUMBIA

June, 1979

In presenting this thesis in partial fulfilment of the requirements for an advanced degree at the University of British Columbia, I agree that the Library shall make it freely available for reference and study. I further agree that permission for extensive copying of this thesis for scholarly purposes may be granted by the Head of my Department or by his representatives. It is understood that copying or publication of this thesis for financial gain shall not be allowed without my written permission.

Department of Geological Sciences

The University of British Columbia
2075 Wesbrook Place
Vancouver, Canada
V6T 1W5

Date July 6, 1979

Coquihalla Mountain viewed from Hidden Creek. A diorite stock forms the core of the mountain, and cuts an older andesite intrusive which forms the ledge in the foreground. An andesite dome occurs on the left side of the photograph.

ABSTRACT

The Coquihalla Volcanic Complex consists of calc-alkaline acid to intermediate extrusive and intrusive rocks which have an areal extent of roughly 30 km², near Hope, British Columbia. The oldest and most voluminous members of the complex are rhyolitic pyroclastic rocks (variably welded lithic-crystal lapilli tuff, vitric tuff, and crystal-lithic lapilli tuff), that have an overall thickness of approximately 1600 m. Later igneous activity produced numerous andesite to dacite domes, dykes, and sills. A late stage diorite to quartz-diorite stock forms the core of Coquihalla Mountain.

Most pyroclastic rocks rest unconformably on the Jurassic to Cretaceous Eagle pluton. Monolithologic avalanche breccias formed in the southern portion of the map area, where pyroclastic rocks were deposited against a fault scarp with uplifted Lower Cretaceous Pasayten Group rocks. In the southeastern part of the area, monolithologic avalanche breccias formed in response to tilting and uplift of the underlying Eagle pluton as the basin subsided.

All tuffaceous rocks are characterized by vitroclastic textures, and contain phenocrysts of plagioclase(An 40-20), biotite, quartz, and minor potassium feldspar and titanomagnetite. Andesites are porphyritic with phenocrysts of plagioclase(An 76-30), calcic augite, magnesio- to tschermakitic hornblende, and titanomagnetite. Glomeroporphyritic clots consist of plagioclase, aluminous augite, and titanomagnetite. Porphyritic dacites contain phenocrysts of plagioclase(An 60-35), hornblende, titanomagnetite, and minor apatite. The diorite

stock consists of orthopyroxene, clinopyroxene, plagioclase, titanomagnetite, and ilmenite, with interstitial quartz and potassium feldspar.

Three K-Ar dates average 21.4±0.7 Ma, and are concordant with a Rb-Sr isochron (22.3±4 Ma with initial $^{87}Sr/^{86}Sr$ = 0.70370±0.00008) based on seven whole rock samples which span the entire compositional range of the suite. These results indicate that the Coquihalla Volcanic Complex is coeval with calc-alkaline centres in the Pemberton Volcanic Belt.

The whole rock compositions of members of the Coquihalla Volcanic Complex show a range in silica contents from 54 to 76 weight per cent (volatile-free). In relation to increasing silica content, chemical variations within the suite are characterized by enrichment of K_2O, Na_2O, Rb, and Nb, and depletion in Al_2O_3, TiO_2, MgO, MnO, CaO, P_2O_5, Cr, Ni, V, and Sr. The elements Ba, Ce, Nd, and Zr show enrichment throughout most of the suite, but depletion in the most felsic members.

Interpretation of chemical variations of whole rocks and constituent phenocrysts suggests that the chemical diversity of the suite is governed by fractional crystallization. The results of quantitative major and trace element modelling indicate that 1) hornblende dacites can be derived from basaltic-andesites by 50% crystallization of a mixture of plagioclase, hornblende, clinopyroxene, titanomagnetite, and apatite, and 2) rhyolites can be derived from dacites by roughly 45% crystallization of a mixture of plagioclase, hornblende, biotite, titanomagnetite, and apatite.

Basaltic andesite compositions are consistent with

derivation from basaltic liquids (modified by olivine fractionation) that are produced by partial melting of hydrous mantle peridotite above the subducted Juan de Fuca plate.

TABLE OF CONTENTS

ABSTRACT i

TABLE OF CONTENTS iv

LIST OF TABLES vii

TABLE OF FIGURES AND PLATES viii

ACKNOWLEDGEMENTS xi

Introduction 1

Location And Access 1

Previous Work 1

Objectives 3

Regional Geology 3

Tectonic Setting 4

Geology of the Coquihalla Volcanic Complex 7

Stratigraphy 7

Extrusive Rocks 7

Intrusive Rocks 12

Breccia Fans and Sheets 17

Source of Ash Flow Eruptions 20

Structural Relations 21

Alteration 22

Age 23

Geological History 24

General Chemistry and Regional Correlation 26

Tectonic Implications 29

Petrology and Geochemistry 32

Petrography 32

Intrusive Rocks 32

Extrusive Rocks 38

Alteration Assemblages 42
Mineral Chemistry 44
Pyroxene 44
Hornblende 48
Plagioclase 48
Biotite 52
Iron-Titanium Oxides 52
Discussion 56
Geochemistry 57
Classification 57
Comparison with Cascade Calc-alkaline Suites 58
Discussion 60
Petrogenesis 67
Major Element Model 71
Trace Element Model 77
Discussion 85
Andesite Genesis 87
Conclusions 89
References 91
Appendix I: Whole-Rock Analytical Data 103
Appendix II: Representative Mineral Analyses 110
A: Pyroxene Analyses 111
B: Hornblende Analyses 113
C: Plagioclase Analyses 114
D: Biotite Analyses 115
E: Magnetite Analyses 116
F: Ilmenite Analyses 117
G: Analyses of Secondary Minerals 118

Appendix III: Compilation of Mineral/Liquid Distribution Ccefficients 119

Appendix IV: Contributions to Laboratory Analytical Techniques 128

A: Operating Conditions For Trace Element Analysis By X-ray Fluorescence Spectrcmetry 129

B: Trace Element Reduction Program 141

C: Determination of Total Water and Carbon Dioxide 150

D: Determination of Ferrous Iron 156

Appendix V: Computer Programs 159

A: Mass Absorption Computation 160

B: Whole-rock Tabulaticn Program 162

C: Whole-rock Plot Program 164

D: Mineral Tabulation Program 167

E: Mineral Plot Program 170

LIST OF TABLES

Table 1: Potassium-Argon Analytical Data 23

Table 2: Strontium Isotopic Data 25

Table 3: Representative Modal Analyses 33

Table 4: Major Element Model--Basaltic-andesite to Dacite . 75

Table 5: Major Element Model--Dacite to Rhyolite 76

Table 6: Trace Element Modelling Results 81

Table 7: Operating Conditions for XRF Analysis of Cr-V 135

Table 8: Operating Conditions for XRF Analysis of Ba 136

Table 9: Operating Conditions for XRF Analysis of Ni 137

Table 10: Operating Conditions for XRF Analysis of Nb-Zr-Y-Sr-Rb 138

Table 11: Operating Conditions for XRF Analysis cf Ce-Nd ..139

Table 12: Concentrations and Mass Absorption Coefficients for Standard Rocks 140

TABLE OF FIGURES AND PLATES

Figures

Frontispiece: Coquihalla Mountain

Figure 1: Location map 2

Figure 2: Tectonic setting of southwestern British Cclumbia 5

Figure 3: Differential weathering of flattened pumice 9

Figure 4: Bedding planes in lapilli tuffs 9

Figure 5: Trough cross-bedding in lapilli tuffs 11

Figure 6: Pyroclasitic breccia 11

Figure 7: Andesite dome 14

Figure 8: Radiating columnar joints in andesite dome 14

Figure 9: Hornblende dacite dome 16

Figure 10: Avalanche breccia composed of Pasayten Group clasts 18

Figure 11: Avalanche breccia north of Coquihalla Mountain . 18

Figure 12: Q'-Ol'-Ne' projection for Coquihalla Volcanic Complex and Pemberton Volcanic Belt rocks 27

Figure 13: AFM diagram for Coquihalla Volcanic Complex and Pemberton Volcanic Belt rocks 28

Figure 14: Sieve-textured plagioclase phenocryst 34

Figure 15: Fiamme structure in densely-welded tuff 34

Figure 16: Lithophysae In pneumatolytically altered tuffs . 40

Figure 17: Devitrification in pumice fragment cf vitric tuffs 40

Figure 18: Saussuritized plagioclase phenocryst 43

Figure 19: Formation of sericite in plagioclase phenocryst 43

Figure 20: Vug minerals in hornblende dacite 45

Figure 21: Partial sphenitization of titancmagnetite phenocryst 46

Figure 22: Formation of sphene and rutile from titano-magnetite phenocryst 46

Figure 23: Triangular An-Ab-Or diagram showing Coquihalla Volcanic Complex feldspar compositions 49

Figure 24a: Triangular diagram showing normative (An+Ab)-Or-Q compositions of Coquihalla Volcanic Complex whole-rocks 51

Figure 24b: Triangular diagram shcwing normative Ab-Or-Q ccmpositions of Coquihalla Volcanic Complex whole-rocks 51

Figure 25: Triangular diagram showing compositions of Coquihalla Volcanic Complex titanomagnetites and ilmenites 53

Figure 26: Normative plagioclase versus colour index classification diagram 59

Figure 27: Harker diagrams for Al_2O_3, FeO, and CaO 61

Figure 28: Harker diagrams for MgO, Na_2O, and K_2O 62

Figure 29: Harker diagrams for TiO_2, P_2O_5, and MnO 63

Figure 30: Harker diagrams for Cr, Ni, Nb, and Y 64

Figure 31: Harker diagrams for V, Zr, Rb, and Sr 65

Figure 32: Harker diagrams for Nd, Ce, and Ba 66

Figure 33: Calculated trace element correlaticn fcr partial melting and fractioanal crystallization processes 70

Figure 34: Correlation between Rb and Nb 72

Figure 35: Correlation of Ce, Nd, Zr, and Ba with Rb Concentration 86

Figure 36: Apparatus for determination of H_2O and CO_2 151

Plates

Plate I: Geology of the
Coquihalla Volcanic Complex ..... ~~(back pocket)~~

Plate II: Sample Locality Map ..... ~~(back pocket)~~

Plate III: Cross-sections of the
Coquihalla Volcanic Complex ..... ~~(back pocket)~~

} in Special Collections

ACKNOWLEDGEMENTS

I wish to thank R.L. Armstrong for supervision of all stages of this project, providing invaluable help in my field work, and for discussions and suggestions for the improvement of the final manuscript and maps. I am also grateful to D.J. Whitford for helpful discussions and critical reading of this thesis. In addition, I wish to express my appreciation to Jane leroux for her patient assistance with my field work, L.C. Pigage for many beneficial discussions and for his assistance in operation of computer programs for reduction of microprobe analyses and petrogenetic modelling, G.T. Nixon for stimulating discussions and assuming the burden of improving major element analytical procedures, K. Scott for helping with strontium isotopic measurements, J. Harakal for performing argon analyses, and finally J. Knight for assisting with operation of the electron microprobe. I am also grateful to E.H. Perkins for making available several sophisticated plotting programs.

National Research Council of Canada Grant A-8841 to R.L. Armstrong provided funding for this project.

Introduction

Location and Access

The Coquihalla Volcanic Complex lies approximately 32 km northeast of Hope and 32 km west of Princeton, British Columbia (Figure 1); the centre of the area is at longitude 121°03' and latitude 49°32'.

Access to most of the area is via a shepherd's trail (Plate I) that branches from the Jim Kelly Creek logging road, which starts at the mile 14 mark of the Tulameen River Road, southwest of the town of Tulameen. The northwestern portion of the area can be approached from the Coquihalla River road, approximately 35 km northeast of Hope.

Previous Work

Cairnes (1924) named and described the rocks comprising the Coquihalla Volcanic Complex. His map (1:63,360) shows an undifferentiated volcanic series which rests unconformably on all surrounding country rocks. He estimated a maximum thickness of 4500 feet (1370 m) for the volcanic rocks, and described them as consisting of widespread pyroclastic rocks and rhyolite flows, lesser amounts of basaltic flows, numerous dykes, and a large diorite intrusion forming the core of Coquihalla Mountain. His interpretation that basaltic rocks are the oldest members and pyroclastic rocks the youngest members of the complex is not supported by the present study. On the basis of structural evidence, he estimated that the volcanic complex was of Miocene age.

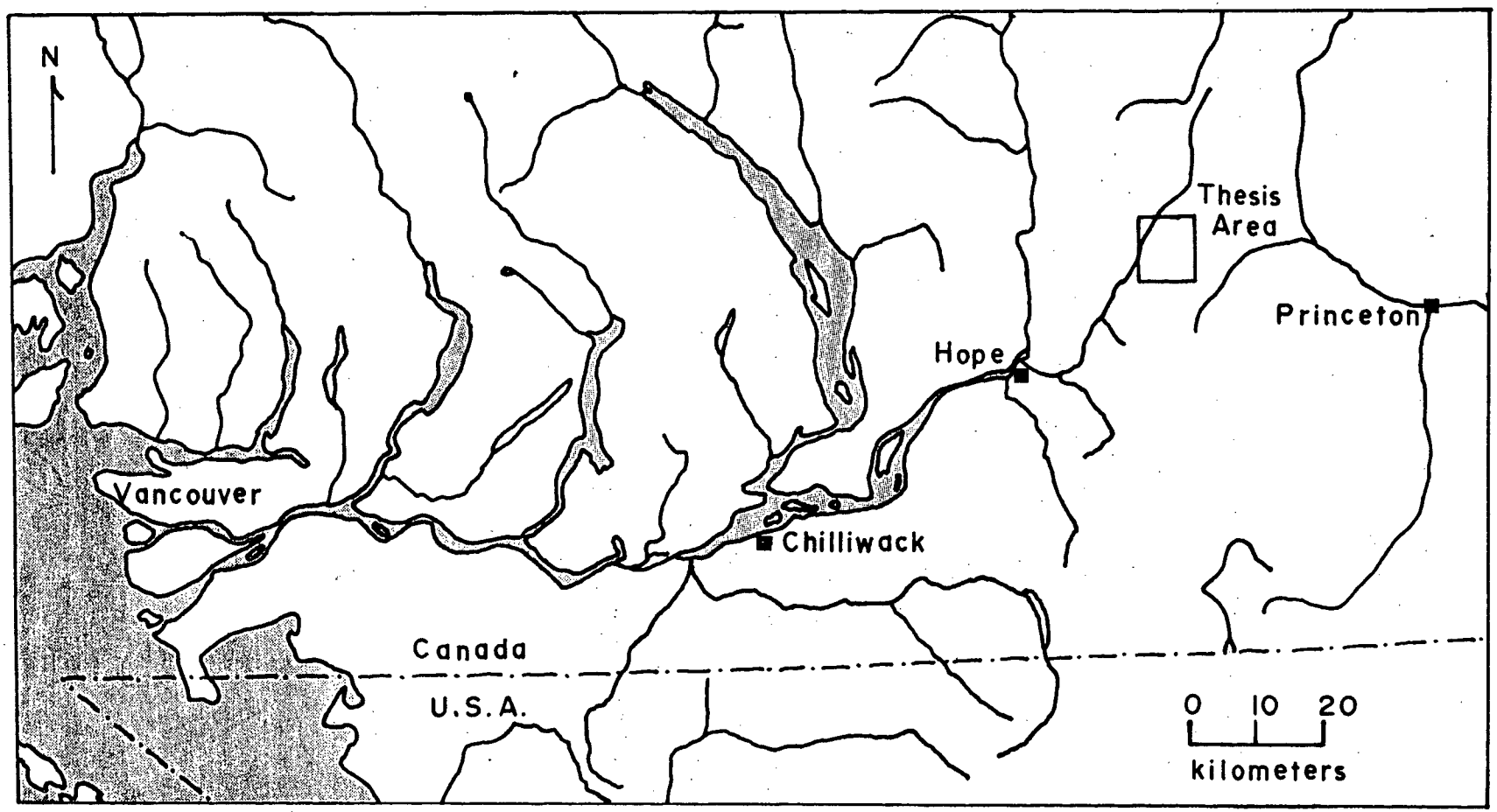

FIGURE 1: Map of southwestern British Columbia showing location of the thesis area.

Objectives

The present investigation was designed as a field and laboratory study of the Coquihalla Volcanic Complex. The objectives of the study were: 1) to map the rocks comprising the Coquihalla Volcanic Complex, 2) to determine their age using isotopic techniques, 3) to determine their mineralogical and chemical characteristics, 4) to correlate the Coquihalla Volcanic Complex with other volcanic centres, and relate this volcanism to the Cenozoic tectonic setting of southwestern British Columbia, and finally 5) to determine the genetic relationships between members of the Complex and to evaluate relevant petrogenetic models.

Regional Geology

The Coquihalla Volcanic Complex occurs in the northern part of the Cascade Mountains, near the physiographic boundaries with the Coast Mountains on the west and the Interior Plateau on the east. This boundary roughly corresponds to the tectonic division between the Coast Plutonic Complex and the Intermontane Belt.

The volcanic complex is in contact with the Jurassic-Cretaceous Eagle granodiorite on all sides except on the south where it is in contact with the Lower Cretaceous Pasayten Group. The Eagle is a large pluton of coarse grained, equigranular granodiorite to diorite with a variably developed northwesterly trending foliation (Monger, 1969). The Pasayten Group unconformably overlies the Eagle pluton (Monger, 1969), and consists of 8000 feet (2440 m) of non-marine conglomerate, sandstone, and pelite (Cairnes, 1924).

East of the mapped area the Eagle pluton intrudes Upper Triassic greenstones of the Nicola Group, composed of altered submarine flows and flow breccias, with intercalated shales and limestones. Mafic to intermediate rocks are more abundant than rhyolite and chemical data for Nicola volcanics indicate that both alkaline and sub-alkaline members are present (Souther, 1977).

The western boundary of the Eagle pluton is formed by the Pasayten Fault, along which considerable vertical and right lateral movement is inferred (Coates, 1974). The fault appears to have been inactive since mid-Cretaceous time (Staatz et al., 1971). Clastic rocks of the Lower Cretaceous Jackass Mountain Group are in contact with the Eagle pluton along this fault, but elsewhere lie unconformably on the Eagle pluton (Coates, 1974).

On the west side of the Coquihalla River, granitic and granodioritic rocks of the Oligocene Needle Peak Pluton intrude the Eagle and Jackass Mountain Group rocks.

Tectonic Setting

The present tectonic setting of southwestern British Columbia and the geographic and temporal distribution of late Cenozoic volcanic centres is depicted in Figure 2. North of latitude 50°N, the right lateral Queen Charlotte Fault separates the North American plate from the Pacific plate; south of 50°N, a subduction zone forms the boundary between the North American plate and the Juan de Fuca plate. This subduction zone appears to be presently active on the basis of evidence reviewed by Riddihough and Hyndman (1976). The Juan de Fuca-Pacific plate

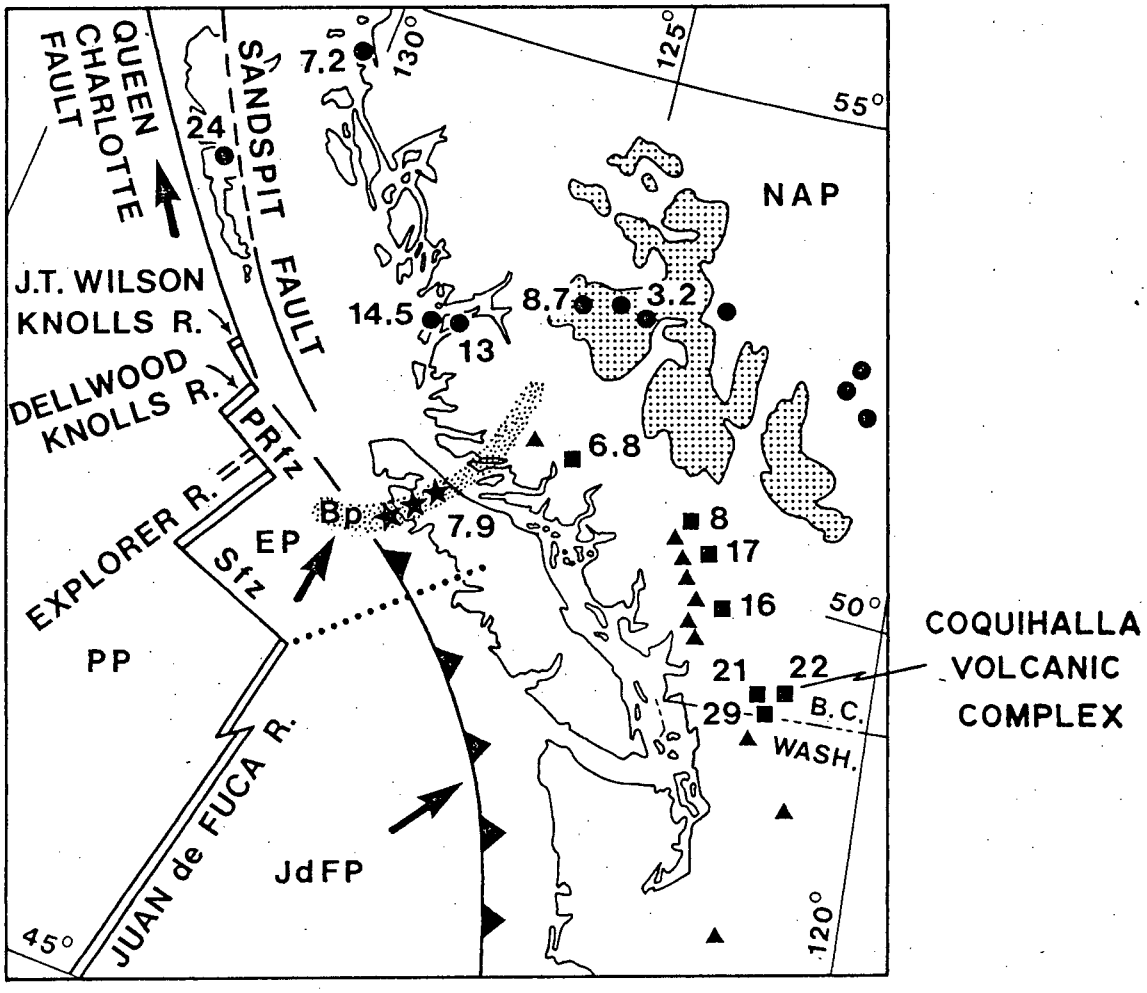

FIGURE 2: Present plate tectonic setting of southwestern British Columbia, showing extent of Pemberton Volcanic Belt (squares), Garibaldi Volcanic Belt (triangles), Anahim Volcanic Belt (circles), Alert Bay Volcanic Belt (stars), and oldest K-Ar ages in Ma. Stipled area shows the extent of Miocene plateau lavas (Souther, 1977). PP-Pacific plate, EP-Explorer plate, JdFP-Juan de Fuca plate, NAP-North American plate, BP-brooks Peninsula, PRfz-Paul Revere fracture zone, Sfz-Sovanco fracture zone. Dotted line is possible EP-JdFP boundary. Diagram modified from Bevier, et al., 1979.

boundary is a spreading ridge system (Barr and Chase, 1974).

Subduction of the Juan de Fuca plate beneath North America has produced arc and back-arc volcanism (Souther, 1977). Calc-alkaline volcanism is observable as the Pleistocene to Recent Garibaldi Volcanic Belt and the Miocene Pemberton Volcanic Belt. Alkaline Miocene and younger plateau and valley lavas occur in a typical back-arc setting.

Geology of the Coquihalla Volcanic Complex

Stratigraphy

The Coquihalla Volcanic Complex covers approximately 30 square km, and is exposed at elevations between 840 and 2160 m (2750-7100 feet). Outcrop is excellent above 1500-1700 m; below this level, dense vegetation makes detailed mapping impossible. Mapping was done on 1:15000 aerial photographs, and the final map was compiled on a 1:15000 enlargement of National Topographic Series Map No. 92H/11. The geology of the Coquihalla Volcanic Complex is presented in Plate I.

The Coquihalla Volcanic Complex consists of acid to intermediate extrusive and intrusive rocks which lie unconformably on, and in fault contact with, Eagle granodiorite and Pasayten Group rocks. Field work was confined to mapping the volcanic rocks up to the contacts with surrounding rocks; all contacts on Plate I that separate pre-Miocene rocks are taken from Cairnes (1924) and Monger (1969).

Igneous rocks have been divided into eight map units based on mineralogical and textural properties. Avalanche breccias and minor amounts of epiclastic conglomerate and sandstone are also present.

Extrusive Rocks

Tuffaceous pyroclastic rocks represent the oldest members of the complex. All display vitroclastic textures, are of rhyolitic composition, and contain phenocrysts of plagioclase, biotite, quartz, and minor potassium feldspar and magnetite.

Textural variations allow their subdivision into three map units, which, with local exceptions, are conformable with stratigraphic horizons. Contacts between these subdivisions are generally gradational.

The terminology used in the following field descriptions is consistent with that of Smith (1960a; 1960b), Fisher (1966), and Gary, et al. (1972).

Moderately- to densely-welded, lithic-crystal lapilli tuffs (Mtl) comprise the oldest pyroclastic unit, and have a total thickness of roughly 550 m (1800 feet). These rocks generally form massive, little-fractured outcrops more resistant to weathering than other pyroclastic units, and range in colour from light grey to light brownish grey; darker colours are correlated with greater degrees of welding. They are composed of 20-50% granitic xenoliths, less than 5% mudstone clasts, 10-15% pumice fragments, and 15-30% phenocrysts set in vitroclastic matrices that show pronounced development of coarse-granular (0.05-0.13 mm) devitrification products. Xenoliths average 1-2 cm in size but occasionally are up to 15 cm; pumice fragments up to 4 cm in length are not uncommon. Foliation is well displayed by the alignment of flattened pumice fragments which in many places are differentially weathered out of the rock matrix (Figure 3). Vapour phase crystallization of alkali feldspar and quartz is common within this unit and a distinctive pneumatolytic alteration zone is shown on Plate I.

Moderately-welded to densely-welded vitric tuffs (Mtv) crop out on the two ridges above the Coquihalla River Valley, and have a total thickness of roughly 120 m (400 feet). Densely-

FIGURE 3: Differential weathering of flattened pumice fragments in moderately-welded tuff.

FIGURE 4: Moderately-welded lapilli tuff. Fractures are parallel to bedding.

welded varieties are grey to dark grey in cclour, while moderately-welded varieties are grey to pinkish grey. These rocks are characterized by less than 5% granitic xenoliths and 5-15% phenocrysts in vitric matrices composed of devitrified ash and pumice fragments up to 4 cm in length. Minor interbedded rheoignimbrites display prominent flow banding and contain pumice fragments up to 3 cm in size.

Non-welded to moderately-welded crystal-lithic lapilli tuffs (Mt), approximately 915 m (3000 feet) thick, represent the youngest pyroclastic unit. They display mottled appearances with xenoliths, feldspar, quartz, and biotite phenocrysts set in light greenish grey ash matrices. These rocks commonly weather along bedding planes into irregular planar sheets (Figure 4). This unit is composed of 10-30% plutonic quartz and feldspar xenocrysts and xenoliths of predominantly granitic composition ranging in size up to 20 cm; phenocrysts ccmprise 15-40% of these rocks. Matrices consist of variably devitrified glass shards and pumice fragments which show only slight deformation and flattening. Well-sorted, fine grained ash fall tuff forms thin, discontinuous lenses near the top of this unit.

Several outcrops display trough cross bedding (Figure 5) in structures approximately 3 m wide. These structures appear to be related to scouring and deposition by successive surges of ash-laden gas. Interpretation of lamination directions suggests a source for these deposits which was located just north of Coquihalla Mountain.

Throughout the entire ash flow succession, there is a conspicuous absence of features suggestive of cooling breaks

FIGURE 5: Trough cross-bedding in lapilli tuff. Outcrop is 4 metres wide.

FIGURE 6: Pyroclastic breccia with small, angular clasts and large, rounded clasts.

between individual ash flows; possible exceptions are the occurrence of several topographic steps within the oldest pyroclastic unit, which probably reflect varying degrees of welding. The lack of any regular bedding within a 300 m section of this unit exposed above the Coquihalla River Valley is consistent with descriptions of intracaldera ash flows (Elston et al., 1976).

A discontinuous explosion breccia (Mvbr) crops out at an elevation of approximately 1830 m (6000 feet), and is best exposed on the divide-forming ridge (Figure 6). This unit ranges from 15-45 m (50-100 feet) in thickness, and is composed of 75-80% granitic clasts set in a coarse grit matrix of angular quartz and feldspar crystals and a small amount of vitroclastic material. Clast sizes average 5-10 cm but clasts up to 30 cm are common; most are highly angular although larger sizes tend to be rounded. Bedding within this unit is defined by sharp changes in proportions of clasts and matrix in adjacent layers. In several places this breccia lies above a thin (up to 20 cm) sandstone (Ms), which suggests that it represents the product of a vent clearing eruption after a short interval of volcanic quiescence.

Intrusive Rocks

Flow-banded rhyolite (Mr) at the base of Coquihalla Mountain consists of phenocrysts and xenocrysts of quartz and feldspar in a cryptocrystalline matrix. Steep inward-dipping flow banding on the north side of Coquihalla Mountain, and almost horizontal flow banding on the east side, suggests that this unit represents the remnant of a rhyolite dome that was

later intruded by the Coquihalla Mountain diorite stock.

One other intrusive rhyolite (Mr) occurs near the northernmost boundary of the area. It is characterized by a fresh glassy matrix with up to 15% granitic xenoliths, and phenocrysts of feldspar, biotite, and quartz.

Igneous rocks of intermediate-mafic composition crop out at elevations above 1650 m (5400 feet). Although columnar jointing in one dacite unit is suggestive of the colonnade and entablature characteristic of extrusive lavas, no features indicative of flow tops or bottoms have been found. For this reason, all intermediate-mafic rocks are considered to be intrusive.

Pyroxene (Map) and hornblende (Mah) andesites form dykes, sills, and domes which are greatly more resistant to erosion than surrounding pyroclastic rocks. These rocks are dark greenish grey to greyish black, and are all characterized by porphyritic textures, while matrices range from holocrystalline to aphanitic. Phenocrysts are plagioclase, pyroxene, hornblende, and magnetite.

Dykes are commonly 5-10 m thick, pinch and swell along strike, and have steep contacts with 60-85° dips. Columnar joints perpendicular to contacts are commonly well developed, and flow banding defined by the alignment of feldspar and mafic phenocrysts is parallel to contacts.

Andesite domes up to 0.5 km in diameter are invariably surrounded by large talus aprons (Figure 7), and show well developed columnar jointing that forms radiating patterns near contacts with surrounding rocks (Figure 8). Heterogeneity within

FIGURE 7: Hornblende andesite dome exposed on ridge northeast of Coquihalla Mountain. Diameter of dome is approximately 0.35 km.

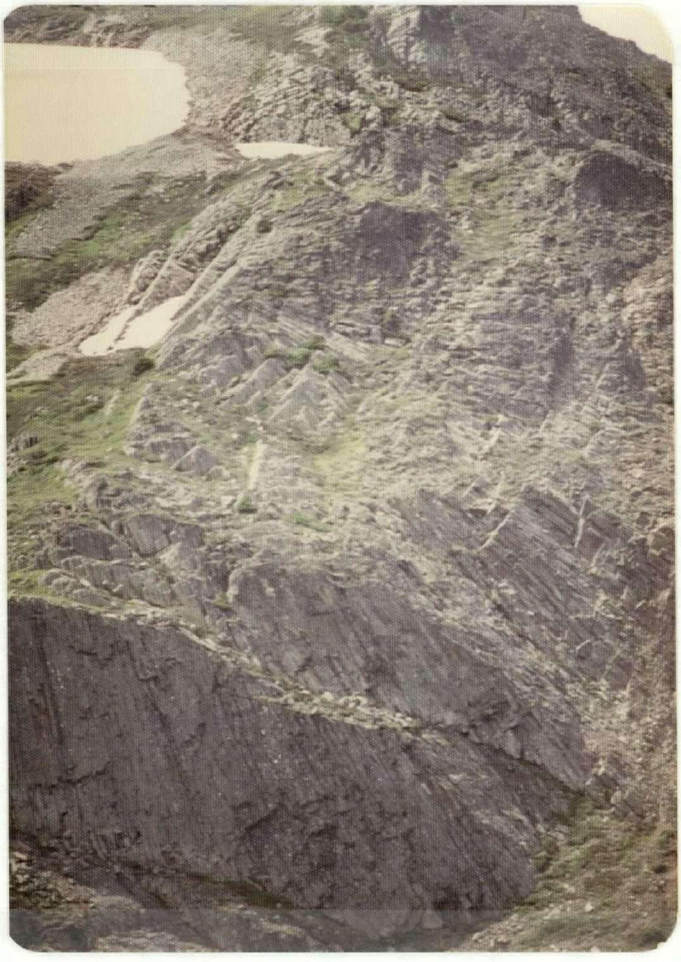

FIGURE 8: Radiating columnar joints in hornblende andesite dome shown in Fig. 7.

individual domes is reflected by contrasts in phenocryst proportions and chemical composition. Although these variations are usually slight and unrelated to regular zonation, the large dome east of Coquihalla Mountain is unique in that its core is composed of holocrystalline pyroxene andesite whereas the rest of the dome consists of more felsic, fine grained hornblende andesite.

Hornblende dacite (Md) is much less abundant than andesite, and occurs as dykes and domes (Figure 9). These rocks are light grey to greenish-grey in hand specimen, are porphyritic, and contain phenocrysts of plagioclase, hornblende, magnetite, and occasionally apatite.

A diorite to quartz diorite stock (Mcq) forms the core of Coquihalla Mountain (frontispiece) and crosscuts an earlier rhyolite dome and andesite dyke. The stock is coarse grained and composed of plagioclase, two pyroxenes, iron-titanium oxides, and lesser amounts of interstitial quartz and potassium feldspar. Zonation within the intrusion is pronounced, especially in the southern portion of the body, where the intrusive rock grades from quartz diorite at the contact to diorite near the peak of Coquihalla Mountain. The most mafic portion of the intrusion lies on the north side of Coquihalla Mountain. Flow banding near the contacts of the stock dip steeply inward and generally parallel the orientation of major fractures within the diorite.

Relative ages of the intrusive rocks of the Coquihalla Volcanic Complex are difficult to ascertain because of the general lack of crosscutting relations. Coquihalla Mountain

FIGURE 9: Hornblende dacite dome. Diameter of dome is approximately 0.75 km.

stock probably represents a late stage intrusion as it cuts an andesite dyke similar to other large andesite intrusives in the area, although several thin andesite dykes crosscut the northern portion of the stock. In comparison to andesite domes, the coarser grain size of the stock suggests that it crystallized at a later time, under a thicker accumulation of pyroclastic rocks. The irregular, ductily deformed contacts of the pyroxene andesite dyke which cuts the northern part of the stock indicate that this dyke was intruded before the stock had completely solidified.

Breccia Fans and Sheets

Contacts of the volcanic rocks with surrounding rocks along the southern and southeastern boundaries are characterized by the presence of faults marked by the occurrence of distinctive monolithologic avalanche breccias (Mbr). To the southwest, volcanic rocks contact Pasayten Group sediments along a fault (Jim Kelly Creek fault) that dips northeast at approximately 85°; preferential erosion of pyroclastic rocks along this fault has produced a steep scarp above Unknown Creek. Vertical displacement is unknown and the relationship of this fault with the Pasayten Fault in the Coquihalla River Valley has not been investigated.

A distinctive, ledge-forming breccia appears to have formed through large scale avalanching from the uplifted block southwest of the fault. The breccia is characterized by poorly sorted, angular clasts of Pasayten sediments up to 2 m in size, set in a matrix of clay and fine grained shale clasts (Figure

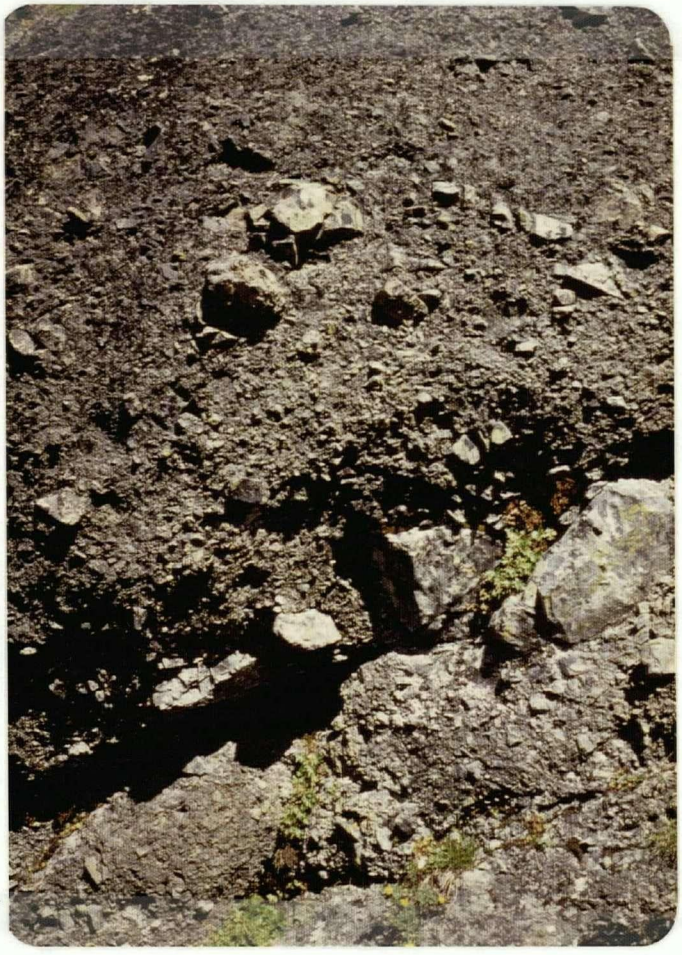

FIGURE 10: Avalanche breccia composed of Pasayten Group clasts up to 1 metre across. Width of photograph is approximately 5 metres.

FIGURE 11: Pasayten avalanche breccia forming prominent ledge on the north side of Coquihalla Mountain. Ledge is roughly 30 metres thick.

10). Granitic rocks are less than 5% of the clasts in this unit. This breccia sheet is approximately 30 m thick, crops out on the north (Figure 11) and southwest sides of Coquihalla Mountain, and is cut by later andesitic dykes and Coquihalla Mountain stock. It appears to thin and pinch out north of Coquihalla Mountain. The absence of this unit on the northwest side of Coquihalla Mountain suggests that a topographic high, near the present site of the mountain, may have existed at the time of deposition. This topographic high may be related to the vent area of the ash flow tuffs. The occurrence of a 10 m thick sandstone and conglomerate lens at the same elevation but farther to the northwest, implies that deposition of this breccia took place during an hiatus in volcanic eruptions.

A small breccia fan is exposed in cross section at an elevation of 1800 m (5900 feet) just north of the Jim Kelly Creek fault trace on the ridge southwest of Coquihalla Mountain. This outcrop is lithologically similar to that described above, but generally displays a more heterogenous mixture of fine and coarse grained sedimentary rock clasts. Thin clastic dykes consisting of sand cut the breccia, and probably formed as a result of the entrapment of fluid-rich sediments beneath the rapidly deposited breccia. At the top of the ridge the fault is buried by ash flows, which appear to have filled and overflowed the fault-bounded basin, and now rest unconformably on Pasayten Group rocks.

A similar Pasayten clast breccia occurs east of the divide on the north side of Jim Kelly Creek. Alignment of occasional rectilinear andesite clasts within this unit suggests

northwesterly dips of 20-25 degrees. This breccia grades laterally to the north and stratigraphically upwards into a breccia characterized by the dominance of Eagle granodiorite clasts over Pasayten clasts. The formation of this breccia is related to localized tilting of the underlying Eagle grancdiorite so that the unconformity is rotated frcm typical 25-30°, up to 70° westward dips. This unit is similar to monolithologic breccias described by Lambert (1974) at Bennett Lake, B.C., and consists of angular clasts up to 30 cm in size set in a coarse-grit matrix of fragmented quartz and feldspar grains with minor clay material. Bedding is typically absent, but in several areas, rough alignment of clasts and large scale lithologic layering indicate dips up to 70° west. Occasional blocks of Eagle up to 20 m across occur with little intervening matrix. Pyroclastic rocks that dip approximately 45° west unconformably overlie the western boundary of this breccia.

The implication of these overlapping relationships of breccias, pyroclastic rocks, and faults is that basin subsidence was rapid, and contemporaneous with faulting, tilting of the basal unconformity, and basin-filling volcanism.

Source of Ash Flow Eruptions

Field relations in the Coquihalla Volcanic Complex are similar to those described in "trap-door" type cauldrons, but there is no evidence for ash flow eruption along the basin-bounding fault. Similarity of Coquihalla ash flcw sequences with intracaldera ash flows (Elston et al., 1976) is interpreted as indicating close proximity to the source area and confinement of

ash flows within a basin formed in part by subsidence along faults in the southern part of the map area. The lack of sorting and large clast size in the pyroclastic breccia north and east of Coquihalla Mountain support the interpretation that associated ash flows are near the source of eruptions.

The relatively small volume of ash flow material preserved in the Coquihalla Volcanic Complex (50 km^3) suggests that the source for these eruptions was a central vent (Smith, 1960a). Although a source vent was not identified in the field, several lines of reasoning indicate that it may have been located near the present-day site of Coquihalla Mountain. The absence of the Pasayten-clast avalanche breccia unit on the northwest side of Coquihalla Mountain suggests that a topographic high, possibly a source vent, was present at the time of breccia deposition. The pinching out of a distinctive ledge-forming ash flow sheet to the northwest, and the location of vitric tuff units only on ridges west of Coquihalla Mountain, are both consistent with a source area located near Coquihalla Mountain, and cross-bedding in ash flow deposits also indicates a similar source location. The late-stage intrusion of the Coquihalla Mountain stock might have been guided by preexisting fracture and conduit systems related to the vent area formed during earlier pyroclastic eruptions.

Structural Relations

Except in the southern part of the map area, pyroclastic rocks rest nonconformably on the Eagle grancdiorite. Contacts along the eastern side of the area dip gently to the west at

angles less than 30°; along the north and west sides of the area, contacts dip inward at steeper angles up to 45°.

Deformation of rocks within the Coquihalla Volcanic Complex is slight in comparison to that in surrounding rocks of the map area. Bedding strikes conform to the regional north-northwest trend and dips range up to 45°, but rarely exceed 30°. Bedding attitudes within pyroclastic rocks are locally quite variable, reflecting the influence of original topography on ash flow deposition. On a larger scale, bedding attitudes define two folds with northerly-trending axes (Plate I).

Alteration

Alteration of members of the Coquihalla Volcanic Complex is quite variable and is predominantly fracture controlled. High concentrations of secondary iron, visible as brownish stains, occur around dykes on the north side of Coquihalla Mountain, and along the Jim Kelly Creek fault trace separating volcanic from Pasayten Group rocks. Alteration of andesites and dacites most commonly involves the variable saussuritization of plagioclase phenocrysts, chloritization of mafic phenocrysts, and the development of calcite and sericite in matrices. The degree of alteration can range from negligible to pronounced over a distance of several metres. Alteration is most evident in areas characterized by multiple crosscutting intrusive relations.

Alteration of pyroclastic rocks consists predominantly in iron oxide coatings on matrix material, occasional albitization of feldspar phenocrysts, and iron leaching leading to the formation of green biotite.

TABLE 1: Potassium-Argon Analytical Data

No.[1]	Rock type	Analysis	%K[2]	$^{40}Ar^*$[3]	$\frac{^{40}Ar^*}{^{40}Ar\,(total)}$	Age (Ma)[4]
318	diorite	whole rock	1.89±.01	1.676	0.560	22.7±0.8
164	hb dacite	hornblende	0.348±.002	0.272	0.197	20.0±0.9
173	vitric tuff	biotite	5.70±.015	4.780	0.463	21.4±0.7

[1] Sample localities: 318 (49°32'N,121°03'W), 164 (49°33'N,121°03'W), 173 (49°34'N,121°04'W)

[2] Potassium analyses by K. Scott by atomic absorption; errors are deviation from mean value of duplicate analyses

[3] Argon analyses by J. Harakal using MS10 mass spectrometer; Ar* refers to radiogenic argon; all values x 10^{-6} cm^3 g^{-1} STP

[4] Constants used in calculation (Steiger and Jager, 1977): $\lambda_\varepsilon = 5.81 \times 10^{-10}/yr$ $\lambda_\beta = 4.962 \times 10^{-10}/yr$ $^{40}K/K = 1.167 \times 10^{-2}$ atom% errors are one standard deviation

Age

The sample locations of rocks used for isotopic determinations are shown in Plate II.

Results of three potassium-argon determinations are presented in Table 1. The three samples give the same age within the estimated error of the technique. The average age of the three samples is 21.4±0.7 Ma.

Strontium isotopic compositions were determined for seven whole rock samples that span the compositional range diorite-andesite-dacite-rhyolite. Results are presented in Table II. An isochron can be fit within the analytical error of all points,

and this gives an age of 22.4±0.6 Ma, with an initial $^{87}Sr/^{86}Sr$ ratio of 0.7037.

Ages determined from both isotopic systems are in good agreement and indicate that the Coquihalla Volcanic Complex is of early Miocene age.

Geological History

Three cross sections are presented in plate III, which offer a visual summary of structural relations and intrusive body shapes.

Eruption of voluminous ash flows on a pre-Miocene erosional surface may have been initiated by tensional forces causing movement along the southern boundary fault, or activation of this fault may have taken place in response to emptying of a shallow magma chamber by early ash flow eruptions. Accumulation of pyroclastic rocks was greatest along this fault in the southwestern part of the area, and the weight of pyroclastic rocks may have accelerated tilting of the Eagle granodiorite unconformity that forms the southeastern boundary of the area. Concomitant with faulting, tilting, and subsidence, avalanche breccias periodically formed on oversteepened exposures of Pasayten and Eagle rocks. After the accumulation of nearly a thousand metres of pyroclastic material, a period of volcanic quiescence ensued, during which localized conglomerate and sandstone, and the large sheet of Pasayten breccia were deposited. Ash flow eruptions then resumed until another short break in volcanic activity, marked by the occurrence of thin sandstone lenses. Then vent clearing eruptions produced the

TABLE 2: Strontium Isotopic Data

No.[1]	SiO_2[2]	Rb[2]	Sr[2]	Rb/Sr[3]	$^{87}Sr/^{86}Sr$[4]
251	54.2	20.5	578	0.035±1.0%	0.7036±0.00014
318	57.1	55.3	489	0.113±0.5%	0.7039±0.00012
192	67.0	62.2	490	0.127±0.1%	0.7039±0.00014
240	67.0	81.4	369	0.221±0.9%	0.7039±0.00015
319	71.8	87.8	184	0.478±0.9%	0.7041±0.00017
173	73.8	83.8	120	0.700±0.6%	0.7044±0.00015
712	77.1	91.8	95.3	0.964±0.7%	0.7046±0.00009

Calculated Isochron Date[5]

22.3 ± 4Ma with initial $^{87}Sr/^{86}Sr$ = 0.70370 ± 0.00008

[1] Sample localities: 251(49°32'N, 121°03'W), 318(49°32'N, 121°03'W), 192(49°33'N, 121°02'W), 240(49°33'N, 121°03'W), 319(49°32'N, 121°03'W) 173(49°34'N, 121°04'W), 712(49°34'N, 121°04'W)

[2] SiO_2, Rb, and Sr determined by X-ray fluorescence; SiO_2 in wt. %, volatile-free; Rb, Sr in parts per million

[3] Errors represent deviations from mean of replicate analyses of Rb and Sr

[4] Sr ratios normalized to a value of 0.71022 for NBS Standard Sr 987
Errors in measured $^{87}Sr/^{86}Sr$ are one sigma

[5] Isochron calculated using computer program described by McIntyre et al. (1966), using $\lambda = 1.42 \times 10^{-11}$/yr

pyroclastic breccia on the ridge north and east of Coquihalla

Mountain. Movement along the Jim Kelly Creek fault ceased, and subsequent ash flows filled and overflowed that edge of the basin.

Finally numerous andesite and dacite hypabyssal intrusives were emplaced. Coquihalla Mountain stock is probably related to a final diapiric rise of fresh magma which crystallized under the blanket of previously-formed volcanic rocks. A few steeply dipping dykes postdate the stock. Circulation of fluids along fractures concentrated around intrusive contacts produced localized low-grade alteration.

Post-Miocene uplift tilted and warped the volcanic rocks. Erosion removed what may have been extensive volcanic cover from the surrounding area, and uncovered the diorite stock of Coquihalla Mountain.

General Chemistry and Regional Correlation

Twenty-six whole-rock analyses were performed by X-ray fluorescence spectrometry. Analytical techniques and results are presented in Appendix I. Figure 12 is a normative Q'-Ol'-Ne' diagram which shows that all rocks are distinctly subalkaline according to the classification scheme of Irvine and Baragar (1971). The trend of whole-rock analyses on an AFM diagram (Figure 13) is clearly calc-alkaline, and the rocks plot in the field of orogenic volcanics on an MgO-Al_2O_3-FeO diagram (Pearce et al., 1977).

Also plotted in Figures 13 and 14 are available analyses of rocks which form the Pemberton Volcanic Belt (Figure 2). Analyses of the Chilliwack Batholith, Mt. Barr batholith, and

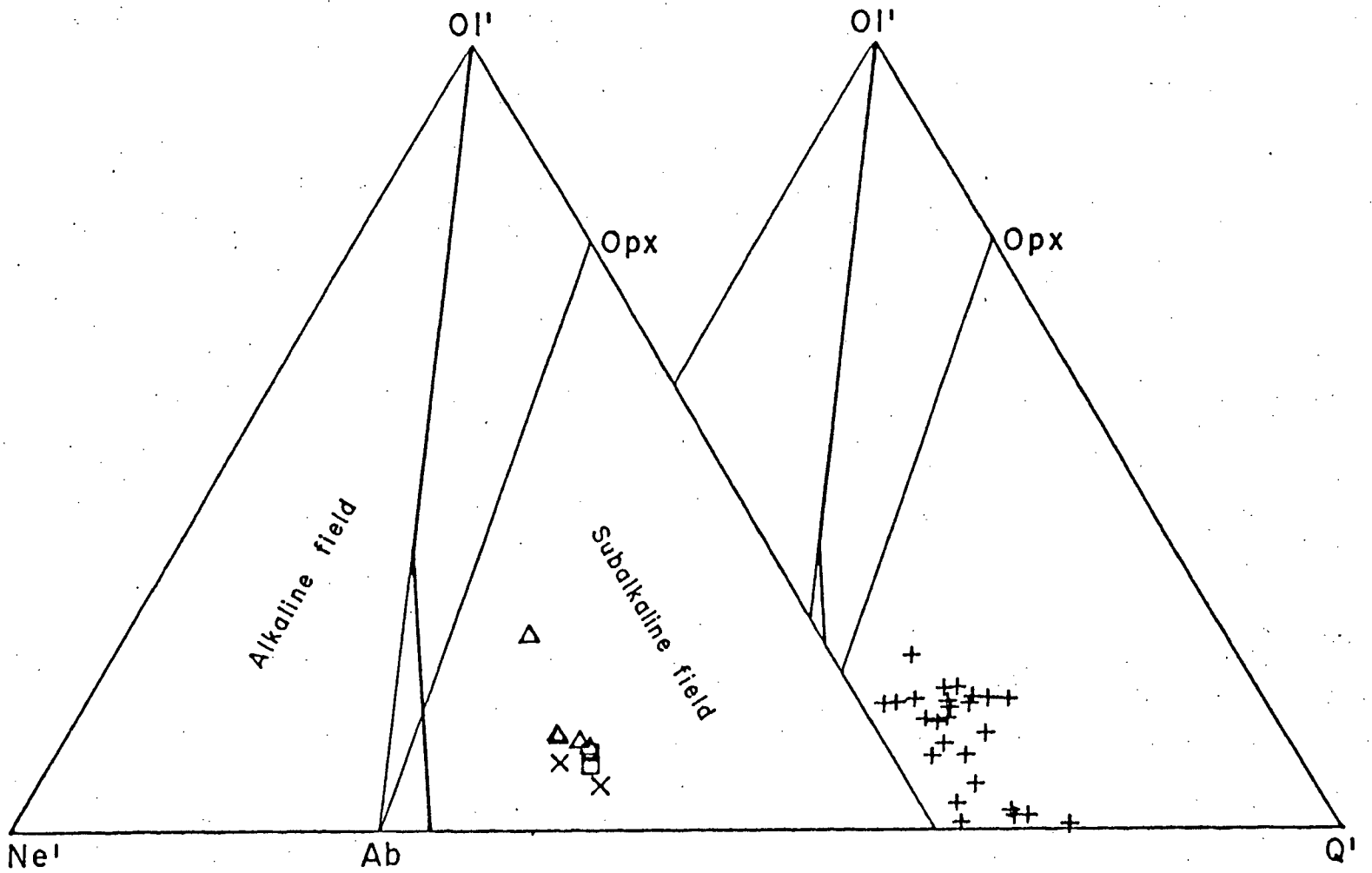

FIGURE 12: Ol'-Ne'-Q' basal triangle of the Cpx-Ol-Ne-Q tetrahedron, projected from Cpx. The heavy lines separate the fields of alkaline and subalkaline rocks (Irvine and Baragar, 1971). Symbols: + - Coquihalla Volcanic Complex, other symbols for the Pemberton Volcanic Belt: □ - Mt. Barr Batholith, △ - Chilliwack Batholith, X - Williams Peak Stock.

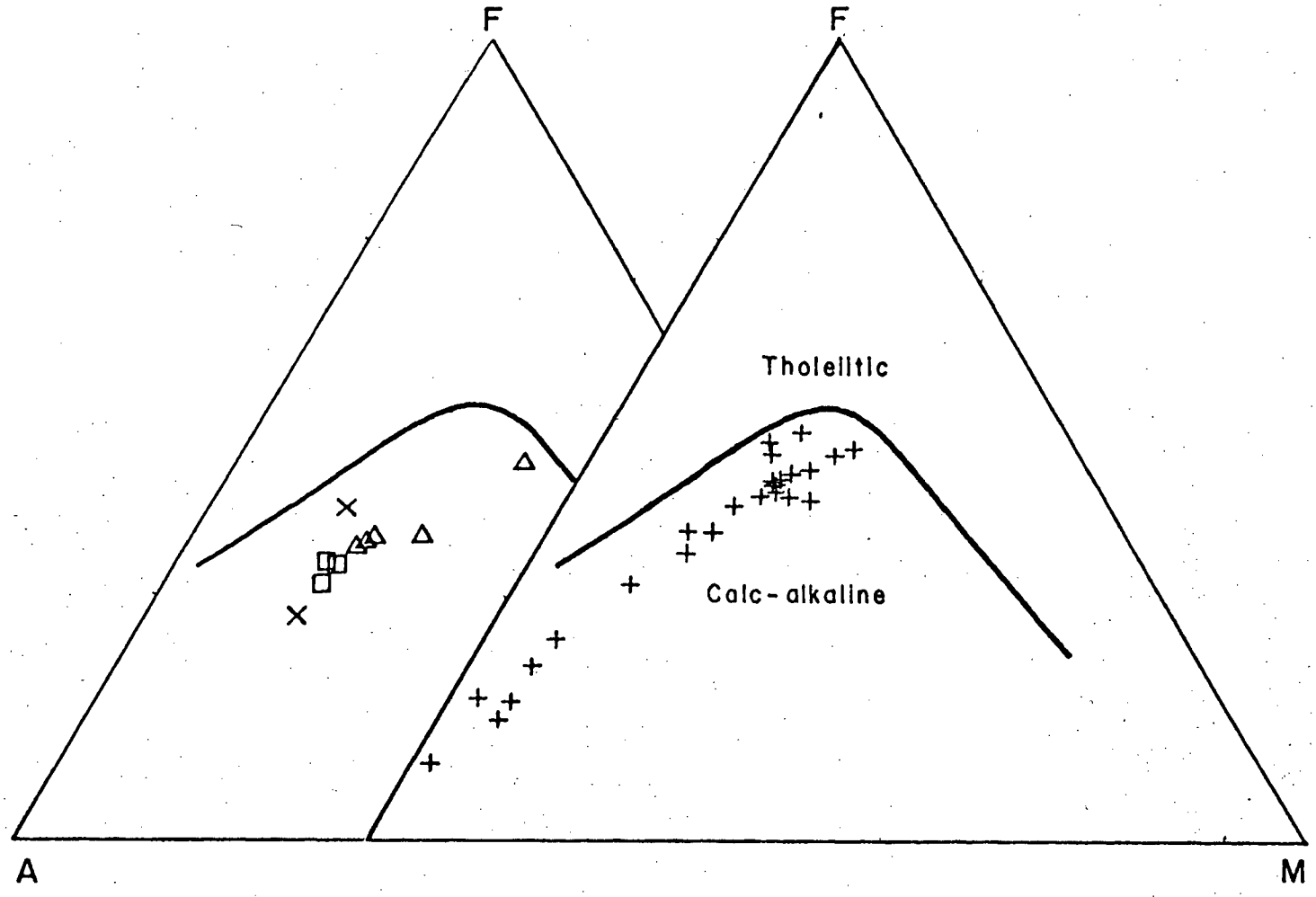

FIGURE 13: AFM diagram with curve separating the fields of tholeiitic and calc-alkaline rocks(Irvine and Baragar, 1971). A=Na_2O+K_2O, F=$FeO+0.8998Fe_2O_3$, M=MgO, all in weight percent. Symbols as in Fig. 12.

Williams Peak Stock (from Richards, 1971) clearly plot in the same field as rocks of the Coquihalla Volcanic Complex. This similarity in chemistry and age warrants consideration of the Coquihalla Volcanic Complex as a member of the Pemberton Volcanic Belt, and suggests that the Coquihalla Volcanic Complex represents the hypabyssal and volcanic equivalent of the plutons that comprise the southern portion of the Pemberton Volcanic Belt. The apparent differences appear to be related to depth of erosion.

Tectonic Implications

In recent years, the association of calc-alkaline suites with areas of subduction along continental margins and island arcs has been clearly demonstrated (cf. Wyllie, 1973). In British Columbia, subduction of the Juan de Fuca plate and Explorer subplate has given rise to the 2 Ma to present Garibaldi Volcanic Belt (Green, 1977; Bevier et al., 1979), and Souther (1977) has suggested that the origin of the Pemberton Volcanic Belt is similarly related to Juan de Fuca plate subduction in the Miocene.

The trend of both volcanic belts is roughly parallel, with the Pemberton Belt lying approximately 75 km east of the Garibaldi Belt. This displacement of the Garibaldi Belt to the west could be accounted for by:

1) greater subduction rates during the Miocene with associated depression of isotherms along the subducted slab, resulting in magma genesis at greater depths further from the active trench,

2) decrease in the width of the Juan de Fuca plate from Miocene to the present, so that Miocene subduction involved a cooler oceanic plate and consequent greater isctherm depression as above, or

3) accretion of sediments and/or oceanic crust onto the trench wall, so that the position of the active trench shifted west with time (Dickinson, 1973).

The observed greater K_2O contents of members of the Coquihalla Volcanic Complex as compared with rocks of the Garibaldi Volcanic Belt lend support to either of the first two models (Hatherton and Dickinson, 1969). Calculations of Juan de Fuca plate spreading rates based on magnetic anomalies west of the Juan de Fuca ridge (Pitman III et al., 1974), indicate an average spreading rate (half-rate) of 3.2 cm per year for the period from 32-9.5 Ma. Comparison with calculations of Riddihough (1977) indicates that this rate is slightly less than spreading rates from 9.5-4.5 Ma, and equal to or slightly greater than spreading rates from 4.5 Ma to the present.

It appears, then, that spreading rates of the Juan de Fuca ridge were not significantly different in the Miocene, but models 1 and 2 are also critically dependent on Pacific-North American plate interactions over the time period in question. Riddihough (1977) assumed constant relative motion for the last 10 million years in his modelling of plate interactions in southwestern B.C., and calculations based on global tectonic models appear to indicate that present directions of motion are applicable for the last 20 million years (Minster et al., 1974; Clague and Jarrard, 1973). From studies on the Gulf of

California, however, Larson (1972) inferred that North American-Pacific plate interaction involved a 20° more westerly component prior to 10 Ma. Until such discrepancies are resolved, calculations of North America-Pacific plate, and hence Juan de Fuca-North America plate interactions remain highly speculative for the time period from Miocene to the present.

Petrology and Geochemistry

Petrography

The following descriptions summarize the petrographic features of rocks of the Coquihalla Volcanic Complex, and are based on a study of more than 150 thin sections. Representative modal analyses are presented in Table 3.

Intrusive Rocks

Pyroxene andesites are characterized by porphyritic textures with phenocrysts of plagioclase, clinopyroxene, and magnetite representing 35-60% of the rocks. Matrices are composed of fine grained aggregates of plagioclase laths, anhedral clinopyroxene and magnetite, and glass. One andesite which forms the core of a large dome has a holocrystalline matrix of the same mineralogy, with additional minor amounts of interstitial quartz and potassium feldspar.

Plagioclase comprises between 45-65% of the phenocryst mode, and ranges in size up to 3 mm. Most grains are subhedral to euhedral, contain inclusions of magnetite and minor apatite, and show pronounced compositional zonation. Normal zoning ranging from An 76 to An 35 is most prevalent; oscillatory zoning, when present, is confined to the outer sections of crystals and probably reflects fluctuations in water pressure during the latter stages of phenocryst growth. Many phenocrysts display sieve textures similar to those reported by Wise (1969) and Green (1977), in which ovoid cores riddled with glass

TABLE 3: Representative Modal Analyses of Coquihalla Volcanic Complex Igneous Rocks

		Phenocrysts									
No.	Rock Type	Pl	Cpx	Opx	Hb	Bi	Mt	Q	Ksp	Ap	Gndms
632	diorite	62.9	7.6	18.0	-	-	5.8	3.0	3.0	-	-
251	prx andesite	61.8	29.3	-	-	-	8.8	-	-	-	43.1
61	prx andesite	55.5	36.1	-	-	-	8.4	-	-	-	60.9
252	hb andesite	61.9	22.6	-	5.5	-	10.0	-	-	-	60.0
4	hb andesite	64.2	22.3	-	4.3	-	13.1	-	-	0.9	56.9
283	hb dacite	52.9	8.0	-	35.8	-	11.3	-	-	0.4	60.7
192	hb dacite	65.3	-	-	23.5	-	10.1	-	-	1.2	67.2
173	vitric tuff	83.6	-	-	-	15.1	1.4	-	-	-	93.0
712	vitric tuff	76.1	-	-	2.2	4.3	4.4	13.0	-	-	94.2

Modal analyses based on over 600 points counted

Phenocryst modes recalculated to 100%

inclusions are enclosed by clear, generally euhedral rims (Figure 14). Resorption zones are interpreted as forming through decreases in liquidus temperatures related to pressure drops (Vance, 1965); short intervals of crystallization then followed prior to eruption. Plagioclase microphenocrysts show little zonation, and their compositions range from An 75 to An 35.

Clinopyroxene represents 25-40% of the phenocryst mode of pyroxene andesites. Crystals have an average size of 0.25 mm, but range up to 3 mm in length. Phenocrysts generally display a

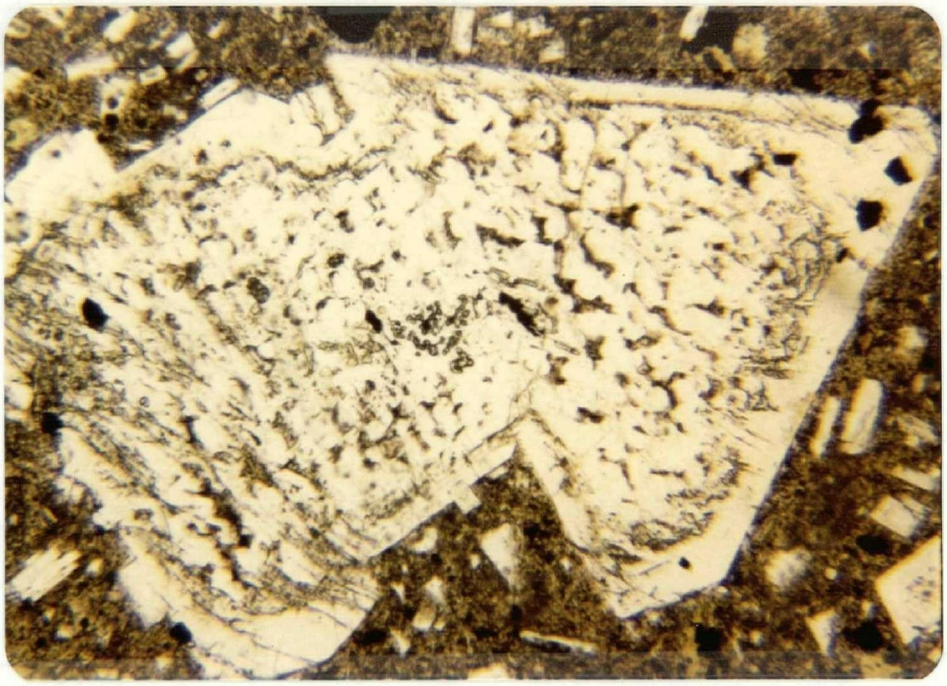

FIGURE 14: Sieve-textured plagioclase phenocryst in pyroxene andesite. Inclusions are glass, clinopyroxene, and titanomagnetite. Note inclusion-free rim. Width of photomicrograph is 2.9 mm.

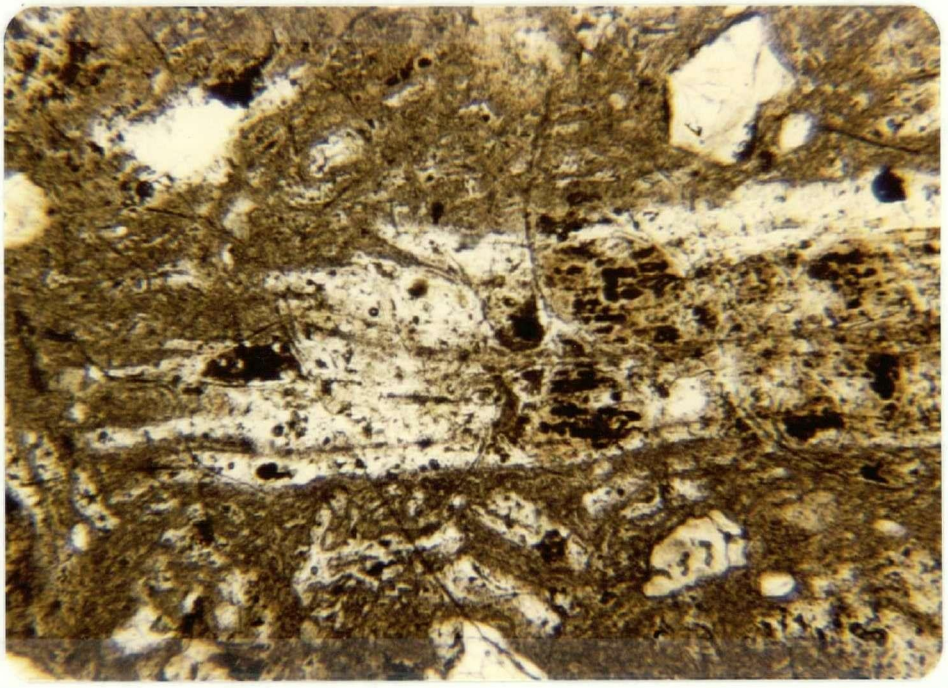

FIGURE 15: Flattened pumice fragment in densely-welded vitric tuff, showing well-developed fiamme structure. Width of photomicrograph is 2.9 mm.

combination of subhedral to euhedral faces and larger phenocrysts show moderate compositional zonation from Mg-rich cores to Fe-rich rims. Tiny rounded inclusions of magnetite and rarely ilmenite, and small laths of plagioclase are common.

Anhedral magnetite, commonly with pronounced embayments, occurs up to 0.5 mm in size, and comprises 5-10% of the phenocryst mode. Magnetite inclusions in plagioclase and pyroxene are indicative of its early crystallization.

Apatite and zircon are scarce accessory minerals which form tiny prismatic inclusions in plagioclase.

Glomeroporphyritic clots up to 5 mm across are present in most pyroxene andesites and consist of aggregates of clinopyroxene, plagioclase, and magnetite, with an average grain size of 0.1-0.25 mm. Grain boundaries within clots are anhedral to subhedral, but euhedral crystal faces commonly protrude into the matrices. Plagioclase compositions are generally less anorthite-rich than phenocryst cores; pyroxene compositions show a marked increase in Al and Ti substitution over phenocrysts.

Hornblende andesites are characterized by similar textures and mineralogy as pyroxene andesites, with the addition of 1-10% hornblende to the phenocryst mode. Hornblende ranges in length up to 2.5 mm, and generally displays subhedral crystals invariably rimmed by oxides thought to have formed by oxidation during or subsequent to eruption. Hornblende phenocrysts contain inclusions of plagioclase, magnetite, and apatite; plagioclase phenocrysts rarely contain tiny, subhedral hornblende inclusions.

Glomeroporphyritic clots in hornblende andesites are

mineralogically and texturally identical with those in pyroxene andesites.

Hornblende dacites are porphyritic with 30-40% phenocrysts in fine grained matrices composed of feldspar, Fe-Ti oxides, minor mafic minerals, and glass. Modally dominant plagioclase phenocrysts up to 4 mm in size show less pronounced zonation than andesitic plagioclase; compositions range from An 60 to An 35. Microphenocrysts have compositions similar to phenocryst rims.

Hornblende phenocrysts and chlorite pseudomorphs after hornblende up to 5 mm in length, represent 15-35% of the phenocryst mode, and display euhedral to slightly rounded crystal faces. Oxide reaction rims are less common than in hornblende andesites and several dacites contain hornblende phenocrysts which show no signs of oxide development. Anhedral to subhedral inclusions of plagioclase are commcn.

Clinopyroxene microphenocrysts have an average size of 0.2 mm, and represent less than 10% of the phenocryst mode. Crystals are euhedral and show no zonation.

Magnetite, representing approximately 10% of the phenocryst mode, occurs as anhedral to subhedral phenocrysts and microphenocrysts up to 1 mm in size. Smaller subhedral grains occur as inclusions in hornblende, and less commonly in plagioclase.

Subhedral to euhedral apatite is more common than in andesites, ranges in length up to 0.3 mm, and generally occurs as inclusions in plagioclase. Minor zircon needles also occur within plagioclase phenocrysts.

Glomeroporphyritic clots are rare in dacites and textures are indicative of disequilibrium between the clot minerals and matrix. Mineral grains in contact with the matrix are rounded and embayed, and vermicular blebs of glass commonly occur at grain boundaries within the clots. Up to 35% hornblende is present in these clots, and their compositions are identical to those of phenocrysts in dacites and andesites.

Coquihalla Mountain stock is composed of medium grained two-pyroxene diorite to orthopyroxene-biotite quartz diorite; felsic rocks occur on the southwestern side of Coquihalla peak.

Rocks within the stock vary considerably in grain size but exhibit similar textures. Most diorites display euhedral to slightly rounded plagioclase up to 3mm in size, set in an equigranular matrix of pyroxene and plagioclase ranging in size from 0.3-0.5 mm. Less commonly, the matrix grain size is 0.1-0.2 mm. A chill zone along the southern contact of the stock has an average grain size of 0.05-0.15 mm, with plagioclase grains rarely exceeding 0.5 mm.

Pyroxenes are anhedral to subhedral with irregular, slightly embayed boundaries. Abundant minute inclusions of magnetite and ilmenite, form wormlike blebs in many places. In felsic rocks pyroxenes are generally rimmed by biotite.

Poikilitic plagioclase grains enclose pyroxenes and show pronounced zonation (An 75-30), both normal and oscillatory. In many phenocrysts, rounded cores containing abundant glass, oxide, and pyroxene inclusions have inclusion-free subhedral to euhedral rims. Smaller plagioclase laths in the matrix are unzoned.

Quartz and potassium feldspar form interstitially to plagioclase and pyroxene. In more felsic rocks, the development of graphic texture is common.

Extrusive Rocks

The petrography of the three pyroclastic units are discussed separately, although similarities, especially in phenocryst populations and in welding textures, do exist between the units. Characteristic textures and compositions are presented for each group as a whole; localized exceptions were observed but not mapped in the field. In general there is a decrease in the degree of welding and amount of vapour phase crystallization progressing stratigraphically upwards; these variations are interpreted as resulting from gradual decreases in the temperature of pyroclastic extrusives over the period of rhyolitic volcanism.

Terminology used to describe welding and crystallization textures conforms to that presented by Smith (1960b) and reviewed by Lambert (1974, pp. 20-35).

Lithic-crystal lapilli tuffs are moderately- to densely-welded and consist of 30-50% vitroclastic matrix composed of devitrified, comminuted glass and pumice fragments up to 4 cm in length. Length to width ratios of pumice fragments range from 2.5:1 up to 15:1, and average 6:1. Many large pumice fragments are collapsed to the point of displaying little or no vesicular structure, show signs of deformation especially where moulded around crystal or lithic fragments, have variably developed fiamme structure (Figure 15), and are aligned in subparallel

fashion so as to impart a well-defined eutaxitic foliation.

Devitrification is coarse-granular to granophyric, and commonly spherulitic. Vapour phase crystallization, resulting in aggregates of feldspar and quartz or tridymite, is evident in many rocks, but is most pronounced in a thin pneumatolytically altered zone shown on Plate I. In some places eutaxitic foliations are occasionally deflected around lithophysae (Figure 16), indicating that vapour phase crystallization may have preceded welding or that the cavities expanded after welding.

Phenocrysts up to 1.5 mm across comprise 15-30% of these rocks and consist predominantly of subhedral to euhedral plagioclase, with lesser amounts of anhedral quartz, euhedral biotite, and orthoclase. Skeletal plagioclase grains are common, and show variable degrees of albitization.

Lithic fragments are predominantly granitic in composition, and comprise 20-50% of these rocks. Clast size ranges up to 10 cm, and averages about 5-6 mm; clast outlines range from slightly rounded to sharply irregular.

Vitric tuffs are moderately- to densely-welded and composed of more than 80% vitroclastic matrix consisting of devitrified glass shards and flattened pumice fragments that are up to 4 cm in length. Devitrification is generally fine-granular in texture, but larger glass shards commonly display distinctive spherulites with coarse-granular quartz rims surrounding remnant glass cores or fine grained intergrowths of quartz and feldspar. In some rocks, larger collapsed pumice fragments exhibit concentric ring structures suggestive of incipient devitrification (Figure 17), and prominent perlitic fractures.

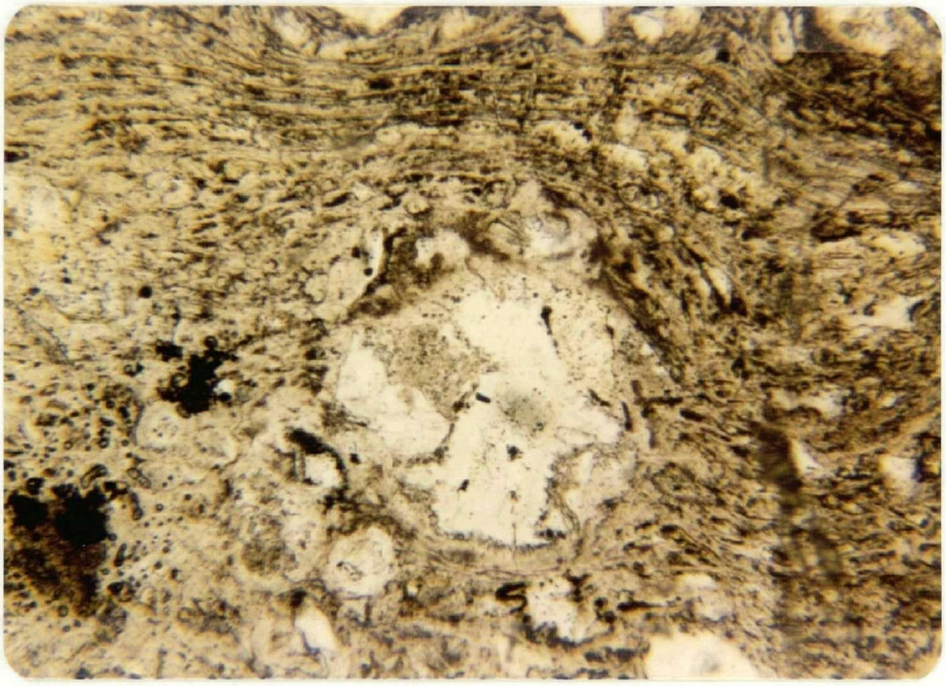

FIGURE 16: Vapour phase crystallization of alkali feldspar and quartz in pneumatolytically altered zone of lapilli tuffs. Note deflection of eutaxitic foliation around cavity. Width of photomicrograph is 2.9 mm.

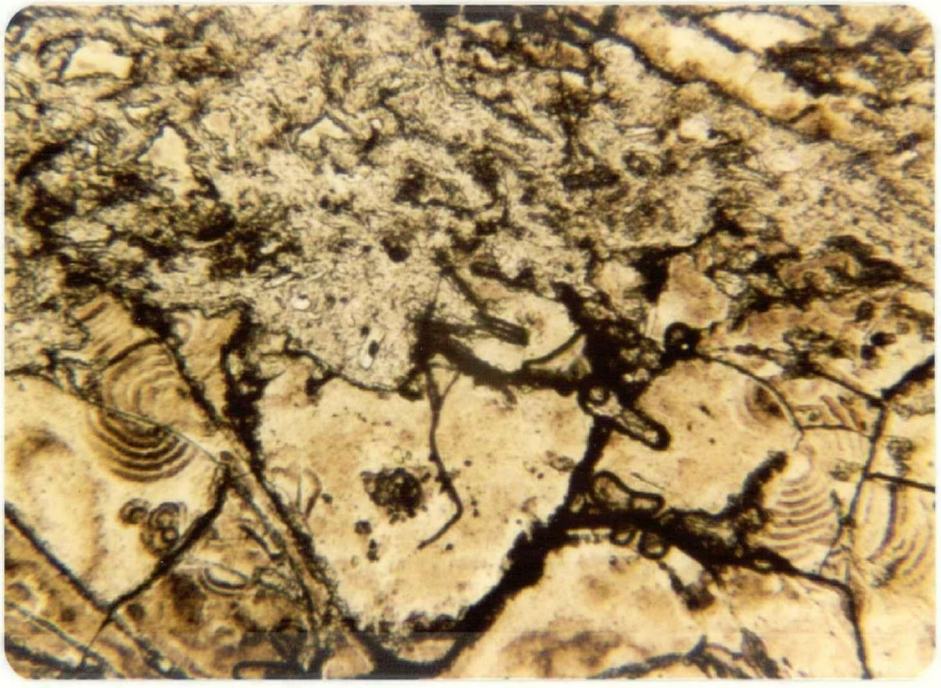

FIGURE 17: Concentric ring structures indicative of incipient devitrification in densely-welded vitric tuff. Width of photomicrograph is 1.9 mm.

In densely-welded rocks, the outlines of pumice fragments can be recognized only in crossed polarized light, because of their tendency to produce coarser grained devitrification products. Length to width ratios of pumice fragments are similar to those described above. Vapour phase crystallization has not been recognized in rocks of this unit.

Phenocrysts represent 5-15% of vitric tuffs, and lithic fragments comprise less than 5% of these rocks. Phenocrysts are predominantly subhedral, fragmented plagioclase (An 20-30), with small amounts of quartz, euhedral biotite, and minor orthoclase and magnetite. Small inclusions of apatite in plagioclase, and zircon, apatite, and rutile in biotite phenocrysts are common.

Lithic fragments are granitic, with composite grains of quartz and feldspar, and quartz xenocrysts being most common. Fragments are commonly less than 1 mm across, but do occur up to 2.5 cm; most display irregular, fractured outlines with little or no rounding.

Non-welded to moderately-welded crystal-lithic lapilli tuffs consist of 35-60% ash matrix, which, in plane polarized light, varies in colour from dark yellowish orange to dark reddish brown; dark colours are probably due to the dissemination of fine grained iron oxide throughout the matrix. Devitrification in these rocks is finer grained than in the lower ash flow units.

Non-matrix components in these rocks consist of up to 40% pumice fragments, 10-30% lithic fragments, and 15-40% phenocrysts. Pumice fragments up to 0.5 mm in length generally display original vesicular textures, with no flattening of

vesicles in non-welded varieties, and slight flattening of vesicles in moderately-welded rocks. Length to width ratios range from 1.5:1 to 6:1, and average 2.5:1. Devitrification of pumice fragments is fine- to medium-granular.

Phenocrysts display the same form and mineralogy as vitric tuffs, with the exception of greater percentages of biotite in crystal-lithic tuffs.

Lithic fragments average 0.3 to 0.6 mm across, but commonly range up to 10 cm. Smaller fragments are angular in shape, whereas larger clasts are commonly rounded. Granitic clasts and xenocrysts of quartz and feldspar predominate over mudstone and fine grained volcanic clasts.

Alteration Assemblages

As discussed above, alteration appears to be largely fracture controlled with dramatic variations in the extent of alteration being evident in rocks only metres apart. Metamorphic assemblages are low-grade, and the formation of chlorite from pyroxene and hornblende is most common.

Saussuritization is frequently displayed in andesites and dacites, but is rare in rhyolitic rocks. Plagioclase phenocrysts are more susceptible to this alteration process than groundmass plagioclase, and display mats of stubby epidote crystals within patchy intergrowths of calcite, chlorite, and sericite (Figure 18).

Plagioclase phenocrysts in andesites and diorites also display an unusual alteration involving the formation of sericite in a particular plagioclase zone which, in most places,

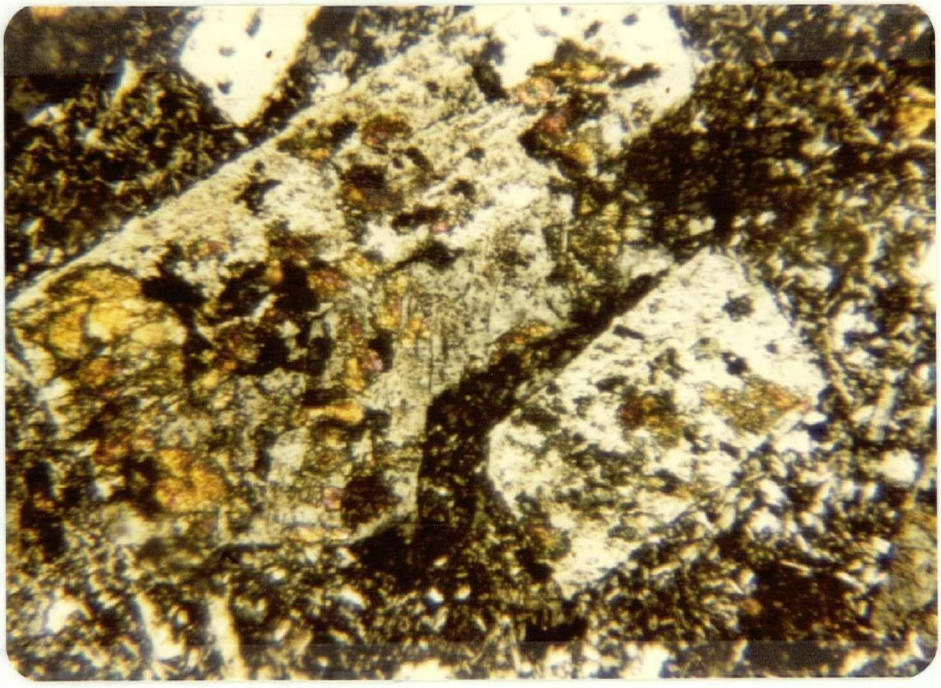

FIGURE 18: Saussuritization of plagioclase phenocryst in andesite. High birefringent minerals are predominantly epidote, with minor calcite. Width of photomicrograph is 1.9 mm.

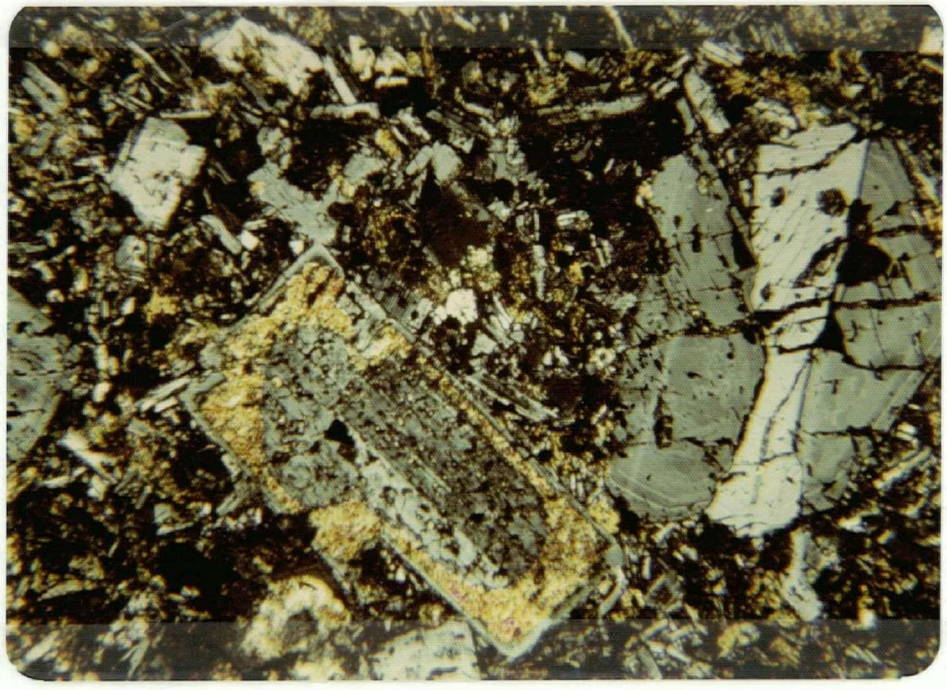

FIGURE 19: Sericite confined to a particular plagioclase zone in pyroxene andesite. Note unaltered core and rim. Width of photomicrograph is 2.9 mm.

is contained within an outer unaltered rim (Figure 19).

Vugs in andesites and dacites are fringed with fibrous chlorite and filled with quartz, epidote, or prehnite (Figure 20). Partial sphenitization of titanomagnetite phenocrysts is evident in one dacite (Figure 21). Where this reaction has gone to completion, rutile crystals surround secondary sphene and outline the original magnetite crystal shape (Figure 22).

Compositions of secondary minerals are listed in Appendix IIg; the high iron content of prehnite probably accounts for its unusually low 2V, between 20-30°.

Mineral Chemistry

All mineral analyses were performed on the electron microprobe; analytical procedures are described in Appendix II.

Pyroxene

Representative analyses are presented in Appendix IIa. End members and ferric iron contents were calculated by the procedure of Cawthorne and Collerson (1974).

Andesites and dacites contain calcic augites, while diorites of Coquihalla stock contain hypersthene in addition to calcic augite. Normal zonation in both pyroxenes is slight, and primarily involves substitution of Fe for Mg.

The most striking chemical variations appear between phenocrysts and pyroxenes in andesite crystal clots. The latter contain up to 4.63 % Al_2O_3, 1.09% TiO_2, and 6.51% calcium-tschermak's molecule. On a plot of Al^{VI} versus Al^{IV}, clot pyroxenes define a distinct high-Al^{IV} group considered to be

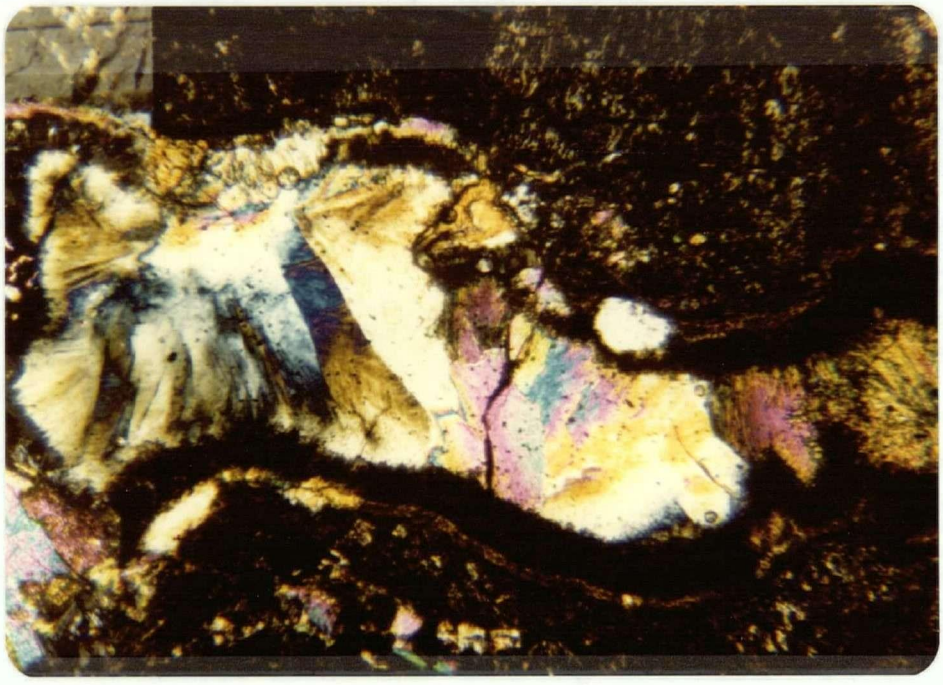

FIGURE 20: Vug in hornblende dacite fringed with chlorite(black), and filled with prehnite(high and anomalous birefringence) and epidote(left side of photomicrograph). Width of photomicrograph is 2.9 mm.

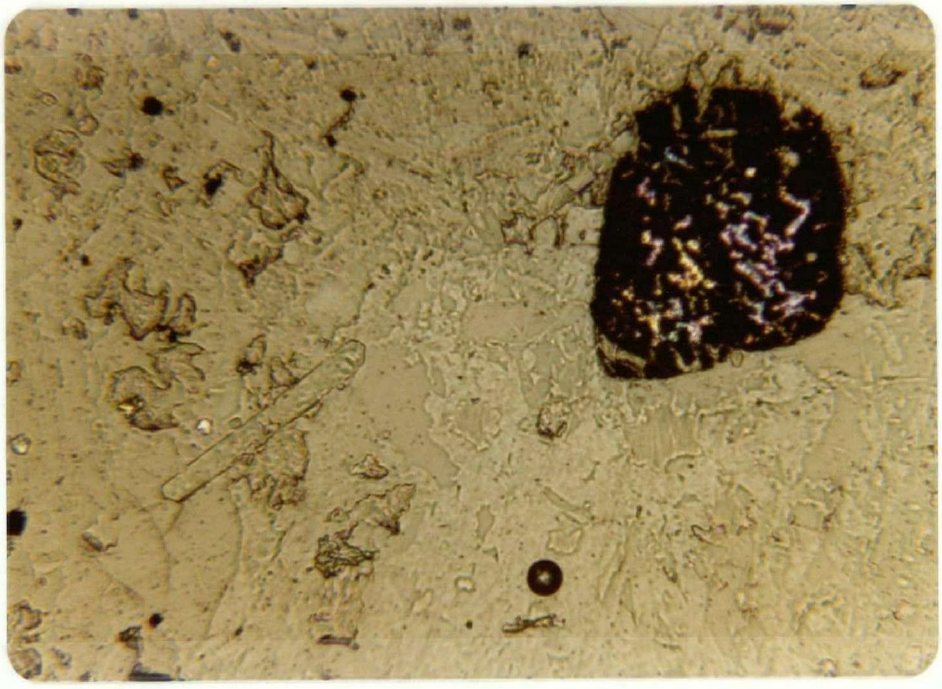

FIGURE 21: Partial sphenitization of titanomagnetite phenocryst in hornblende dacite. Note rodlike apatite microphenocrysts. Width of microphotograph is 0.75 mm.

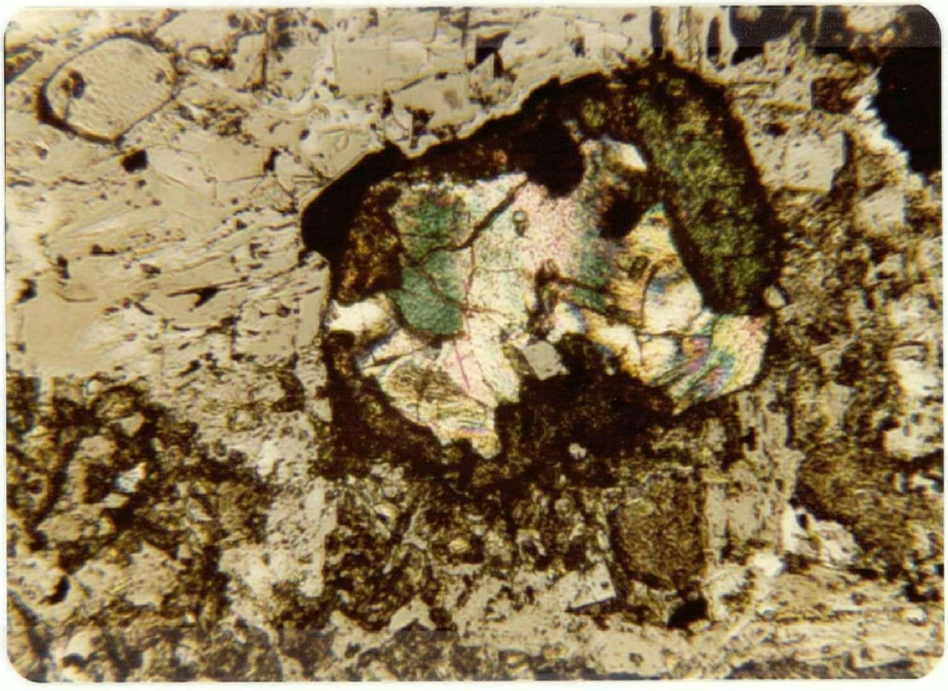

FIGURE 22: Rutile crystals surround secondary sphene, and outline the original shape of a titanomagnetite phenocryst in hornblende dacite. Width of microphotograph is 0.75 mm.

representative of high pressures of crystallization (Aoki and Kushiro, 1968). Alternately, high Al content of clot pyroxenes may indicate crystallization prior to plagioclase; phenocrysts crystallizing after plagioclase will display lower Al contents due to incorporation of Al into the plagioclase crystal structure (Barberi et al., 1971). Subtitutuion of Ti for Al in the pyroxene structure (Verhoogen, 1962) causes these elements to vary sympathetically.

The absence of orthopyroxene from andesites and dacites may be related to crystallization at lower pressures than the diorite stock, as experimental studies (cf. Bultitude and Green, 1968; 1971) indicate that orthopyroxene stability is favoured by high pressures under hydrous conditions. Experimental results of Eggler (1972) on a Paricutin andesite suggest, however, that water content may be the more important factor in controlling orthopyroxene stability; orthopyroxene was fcund to be the liquidus phase at all values of X_{H_2O}, but increasing X_{H_2O} moved the appearance of clinopyroxene closer to the liquidus. These results are poorly understood at the present time, for experimental runs by Green (1972) on similar natural compositions produced no orthopyroxene at or near the liquidus.

Crystallization temperatures calculated by the method of Wood and Banno (1973) from coexisting pyroxenes in Coquihalla stock indicate a range frcm 1050° to 1170° Celsius.

Hornblende

Representative analyses are presented in Appendix IIb. Ferric iron contents were calculated by charge balance considerations summarized in Appendix Vd.

Amphiboles are similar in composition to those reported from other calc-alkaline suites (Green, 1977) and from experimental studies of natural andesites (Green, 1972). Lower Al contents than hornblende produced in experimental runs at 9-10 kb (Green and Ringwood, 1968) suggest that Coquihalla hornblendes crystallized below these values.

Coquihalla Volcanic Complex hornblendes straddle the boundary between the fields of magnesio-hornblende and tschermakitic hornblende (Leake, 1978). Compositional zonation is slight in large phenocrysts (rims enriched in Fe relative to Mg) and non-existent in microphenocrysts. Hornblende compositions from all dacites and andesites are surprisingly uniform, and they plot as a single cluster with respect to Ca, Mg, Fe contents. The only systematic variation appears to be a decrease in Al and Na+K with increasing silica content of the host rocks.

Plagioclase

Representative analyses of phenocryst, microphenocryst, and groundmass feldspars are presented in Appendix IIc, and plotted in Figure 23. Although phenocryst zonation produces considerable overlap, there is a systematic decrease in anorthite content through the series diorite-andesite (An 76-30), dacite (An 60-35), and rhyolite (An 40-20). These compositional variations

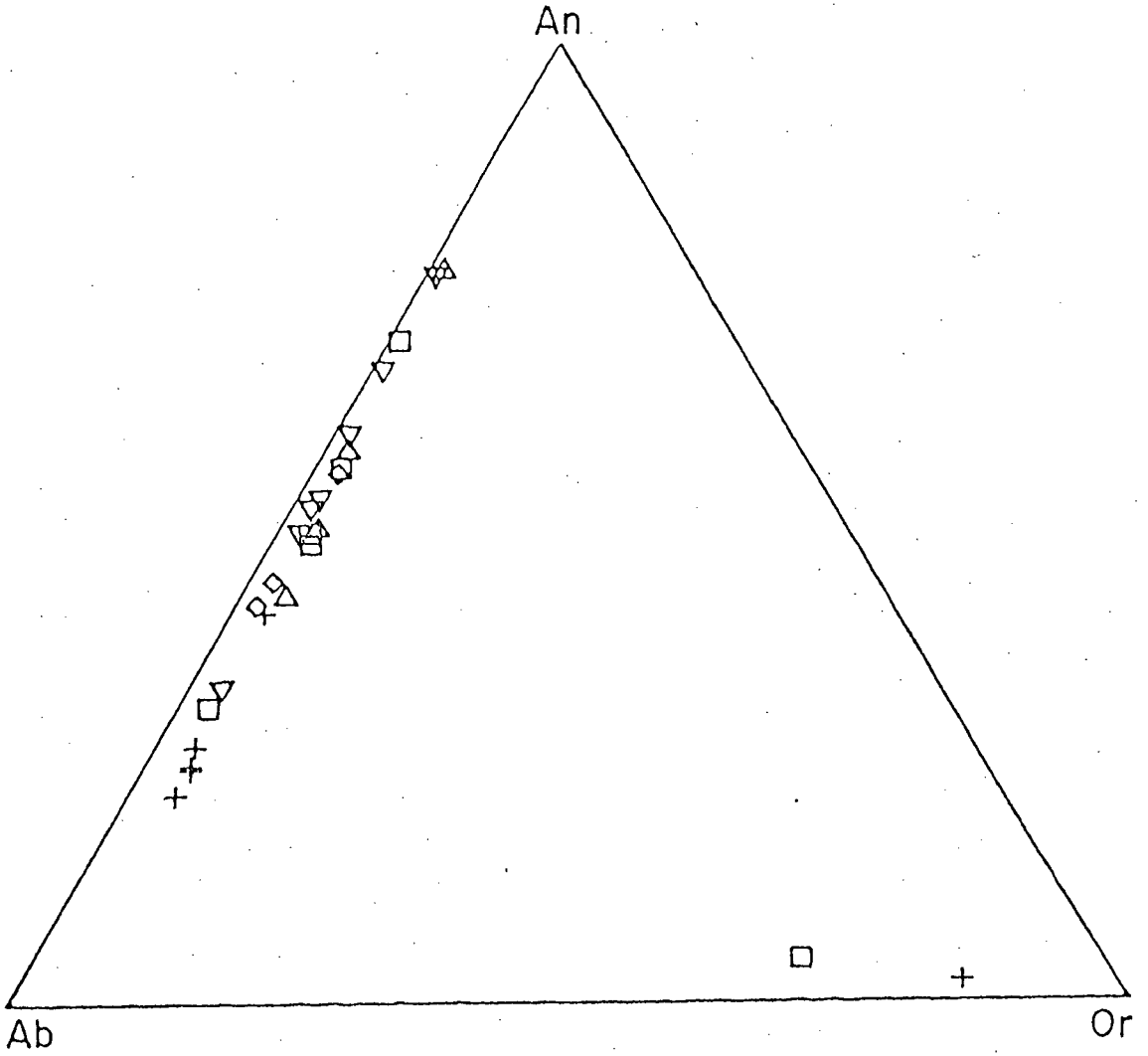

FIGURE 23: Feldspar phenocryst and microphenocryst compositions in terms of mol.% end-members. Symbols: □ diorite, △ pyroxene andesite, ▽ hornblende andesite, ◊ dacite, + rhyolite.

seem to reflect decreasing temperatures of crystallization throughout the series.

Attempts to calculate equilibration temperatures utilizing the plagioclase thermometer of Kudo and Weill (1970), as modified by Mathez (1973), proved unsuccessful due to problems in obtaining consistent microprobe analyses of groundmass compcsitions.

Potassium rich feldspars occur as sparse euhedral phenocrysts in some rhyolites, and as interstitial grains in Coquihalla Mountain diorites. The greater amount of solid solution towards albite of the latter feldspars are indicative of higher temperatures of crystallization than rhyolite phenocrysts. Rhyolite phenocrysts, however, display less sclid solution (Or 84) than expected for potassium feldspar in equilibrium with plagioclase of An 20-40 composition (Carmichael et al., 1974; Tuttle and Bowen, 1958), and they may have undergone subsolidus reequilibration.

The normative whole rcck components (An+Ab)-Or-Q and Ab-Or-Q of Coquihalla Volcanic Complex rocks are recalculated to 100% and plotted in Figures 24a and 24b. The important role of plagioclase crystallization in the evolution of these rocks is displayed in the whole-rock trends directly away from the plagioclase apex (Figure 24a).

The most felsic of the rhyolites plotted in Figure 24b plots very near to the experimentally determined ternary minimum for the system Ab-Or-Q at water pressures of 1000 bars (Tuttle and Bowen, 1958). The occurrence of sparse quartz phenocrysts in this rock indicates that the quartz-feldspar field boundary was

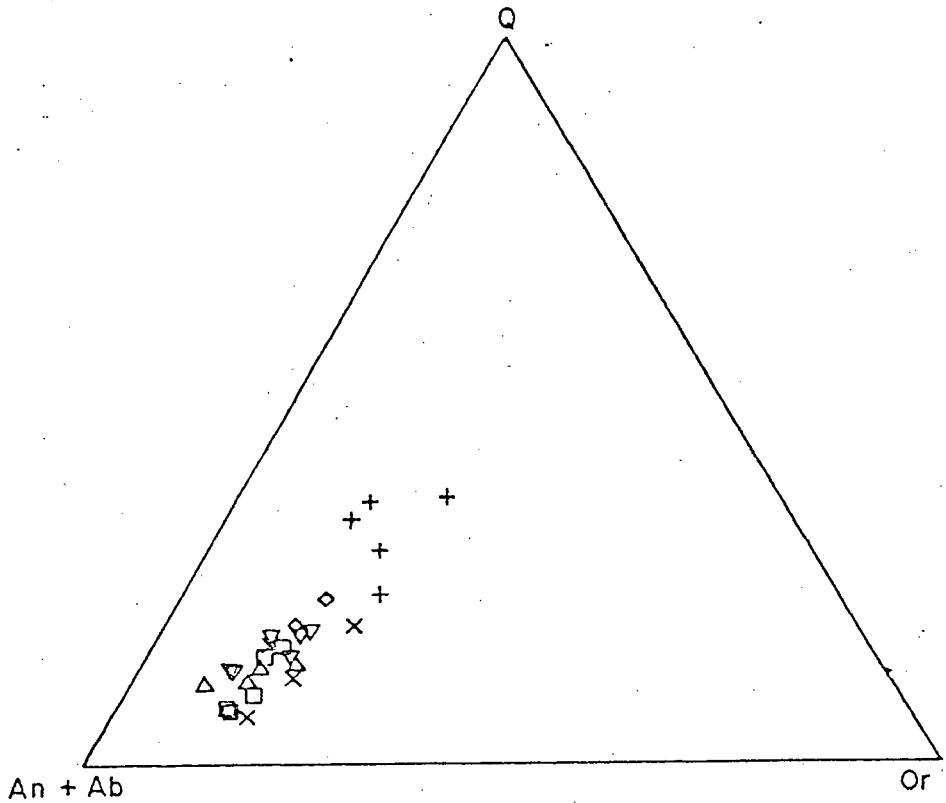

FIGURE 24a: Normative whole-rock compositions plotted in terms of (An+Ab)-Or-Q triangular diagram. Symbols as in Fig. 23.

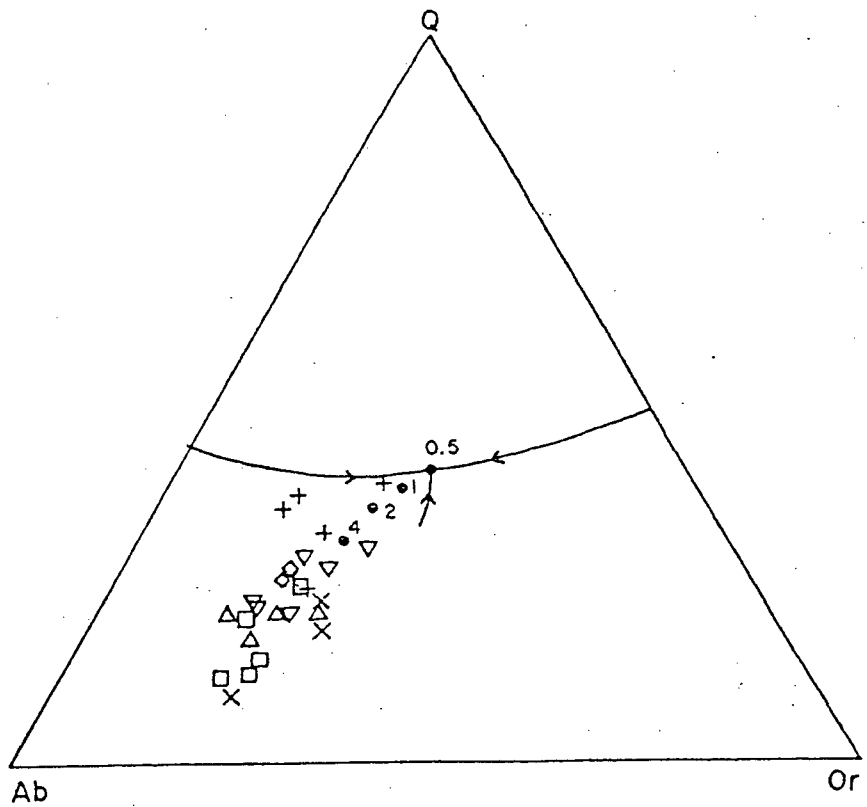

FIGURE 24b: Normative whole-rock compositions plotted in terms of Ab-Or-Q triangular diagram. Solid circles with numbers show the positions of ternary minima for different values of pH_2O(kb), taken from Tuttle and Bowen (1958). Symbols as in Fig. 23.

reached. Comparison of water pressure with water content for this system (Tuttle and Bowen, 1958) allows the magmatic water content for this rhyolite to be estimated at 3-4 weight per cent. Low normative orthoclase contents of two of the plotted rhyolites are probably related to significant amounts of biotite fractionation as discussed in a later section.

Biotite

Representative analyses are presented in Appendix IId. Coquihalla Volcanic Complex biotites display higher Fe/(Fe+Mg) ratios than phenocrysts in Garibaldi andesites, and they contain up to 1.25% BaO. Phenocrysts are unzoned, but show increasing Fe/(Fe+Mg) ratios with increasing silica content of host rocks. Biotites in Coquihalla stock have less Al and more Si than those in rhyolites. The composition of biotites in granitic xenoliths differ markedly from the volcanic biotites, having higher Fe/(Fe+Mg) ratios and lower Ti contents.

Iron-Titanium Oxides

Representative analyses of titanomagnetites and ilmenites are presented in Appendix IIe and IIf, and plotted in Figure 25. Titanomagnetite is a ubiquitous phenocryst, microphenocryst, and groundmass phase in all Coquihalla Volcanic Complex rocks. The occurrence of ilmenite is limited to phenocrysts and microphenocrysts in the most mafic diorite of Coquihalla stock, sparse inclusions in andesitic pyroxenes, occasional microphenocrysts in dacites, and rare inclusions in rhyolitic plagioclase. The modal prevalence of titanomagnetite over

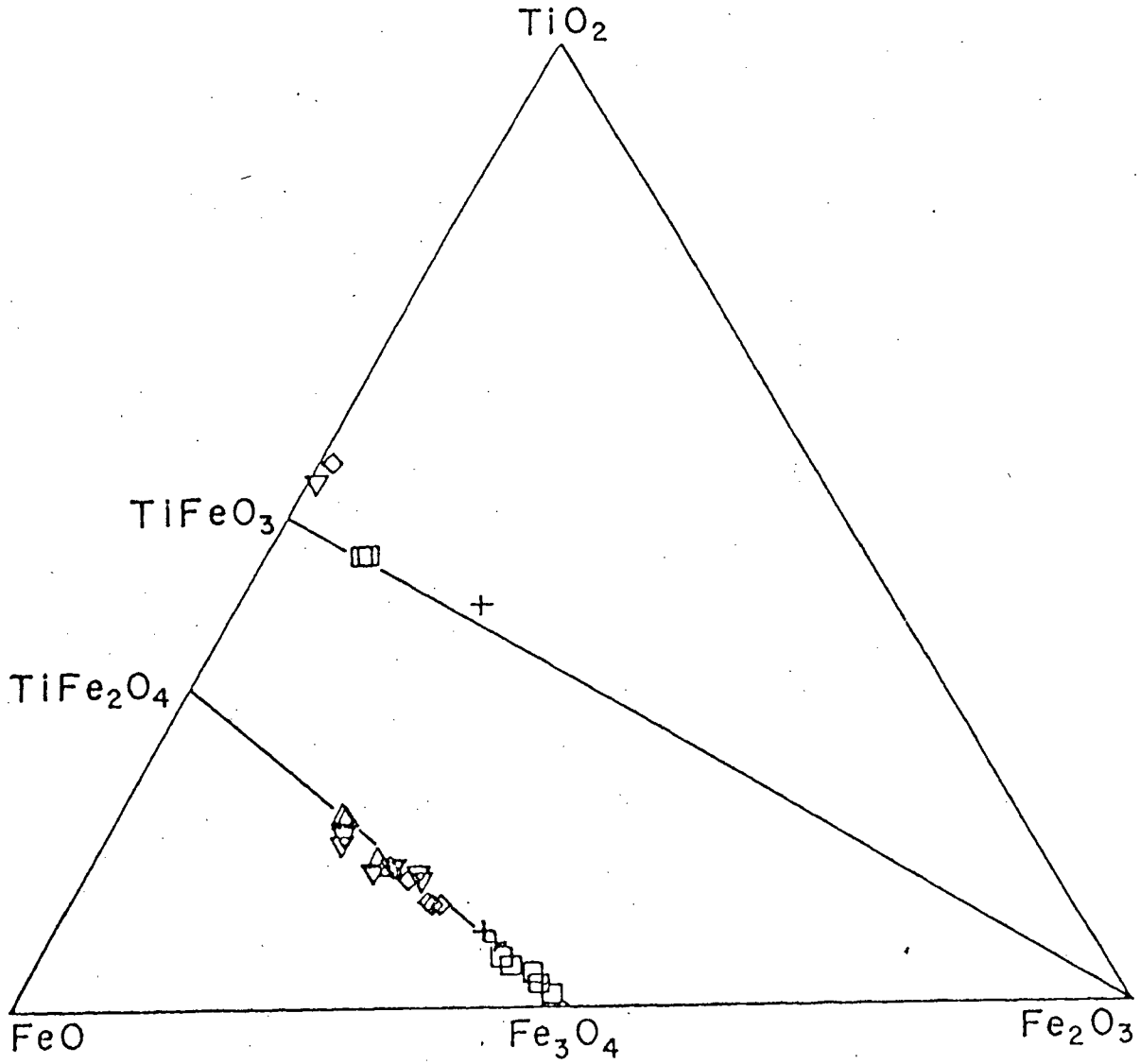

FIGURE 25: Compositions of titanomagnetite and ilmenite phenocrysts and microphenocrysts, plotted in terms of TiO_2, FeO, and Fe_2O_3. Symbols as in Fig. 23.

ilmenite probably reflects complex interactions of factors such as titanium availability, silica activity, and oxygen fugacity (Haggerty, 1976).

Most titanomagnetite grains are optically and compositionally homogenous; hematization of rims is common. Ilmenite inclusions in pyroxene or plagioclase show no signs of alteration or exsolution; in a few rocks, groundmass grains exhibit irregular patches of hematite probably related to post-crystallization oxidation.

Titanomagnetites contain up to 3.96% Al_2O_3, 1.37% V_2O_3, and 2.89% MnO. Al and V decrease, and Mn increases with increasing silica content of host rocks. Ilmenites contain up to 10.56% MnO as their main minor element impurity. Coquihalla Volcanic Complex ilmenites are higher in MnO than those reported from other calc-alkaline suites (Carmichael, 1967; Green, 1977) and resemble ilmenites from peralkaline suites in this respect (Haggerty, 1976).

The general lack of coexisting titanomagnetite and ilmenite in Coquihalla Volcanic Complex rocks prevents determination of unique temperature, oxygen fugacity conditions using the experimental results of Buddington and Lindsley (1964). One andesite with coexisting spinel and rhombohedral phases gives a result of less than 600°C with fO_2 less than 10^{-23} atmospheres. Although the recasting of microprobe analyses into end member components follows the procedures of Buddington and Lindsley as modified for minor elements by Anderson (1968), and takes into account attempts by Mazullo et al., (1975) to calibrate this thermometer for MnO-rich oxides, this calculated temperature and

oxygen fugacity appear much too low when compared to other calc-alkaline suites (Gill, 1978). This inconsistency probably derives from the incompatibility of applying the pure 3 component experimental results to natural systems containing up to 10 weight per cent MnO in ilmenite; post-crystallization oxidation would also contribute to low temperature results.

Coexisting groundmass oxides in one diorite of Coquihalla stock yield a solidus temperature of 640°C and fO_2 equal to 10^{-16} atmospheres. This temperature is lower than experimentally determined water-saturated solidi of similar compositions (Robertson and Wyllie, 1971), and perhaps reflects re-equilibration under slow cooling conditions.

Oxygen fugacities determined from coexisting oxides show that most orogenic andesites crystallized under fO_2 conditions parallel to but approximately one log unit above the Ni-NiO buffer (Gill ,1978). Carmichael (1967) has shown that estimated fO_2 for calc-alkaline suites show systematic variations depending on the phenocryst assemblages in equilibrium with oxide minerals. Olivine-bearing rocks plot along the QFM buffer, orthopyroxene-bearing rocks fall along the Ni-NiO buffer, and biotite- and hornblende-bearing rocks fall above the Ni-NiO buffer. Oxygen fugacities tend to remain constant (Green, 1977) or increase slightly (Carmichael, 1967) with increasing acidity of host rocks.

Ulvospinel contents of titanomagnetites show continuous decreases with increasing silica content of host rocks, although titanomagnetites of Coquihalla stock are displaced to lower ulvospinel contents. This systematic decrease can be accounted

for by steadily decreasing temperatures of crystallization throughout the suite. Assuming oxygen fugacities along the Ni-NiO buffer for pyroxene andesites, and slightly above it for amphibole- and biotite-bearing dacites and rhyclites, temperature estimates vary from 925°C for andesites to 675°C for rhyolites. Lower ulvospinel contents of diorites suggest crystallization at lower temperatures under conditions of higher pH_2O, although, as mentioned above, subsolidus reequilibration may have taken place.

Discussion

Comparison of crystallization sequences in Coquihalla Volcanic Complex rocks with those produced in experimental studies of natural andesites allows some estimation of various intensive parameters involved in the formation of this suite of rocks. Direct comparisons are subject to uncertainties insofar as oxide phases were found to have crystallized well below the experimental liquidi of Green (1972), Eggler (1972), and Eggler and Burnham (1973), while oxides are early forming phases in all Coquihalla Volcanic Complex rocks. Green's runs were all unbuffered, and the latter two experiments were run at the QFM and Ni-NiO buffers. Stabilization of oxide phases with respect to silicates by higher oxygen fugacities (Eggler and Burnham, 1973; Hamilton et al., 1964) suggests that the magmas crystallized at oxygen fugacities above the Ni-NiO buffer, and lends more credibility to the temperature estimates discussed above. It is important to note that early crystallization of Coquihalla Volcanic Complex oxides, and oxides in other calc-

alkaline suites (Carmichael, 1967) is inconsistent with the arguments of Eggler and Burnham (1973) that oxygen fugacities will not be sufficiently high to cause the appearance of oxides on the liquidi of calc-alkaline magmas.

Addition of water to andesite liquids causes pronounced depression of liquidus temperatures. Comparisen cf experimental results of Eggler (1972) and Green (1972) with pyroxene equilibration temperatures in diorites of Coquihalla stcck, suggests that the natural magmas contained 1-5% water at upper crustal pressures. Crystallization of orthopyroxene before plagioclase in these rocks also indicates water contents in diorite magmas greater than 2 weight per cent (Eggler, 1972). Reversal of this crystallization sequence in andesites suggests that these magmas contained less water, and supports the higher oxide mineral equilibration temperatures in andesites as compared to diorites.

Geochemistry

Whole-rock analyses of members of the Coquihalla Volcanic Complex are presented in Appendix I. Analytical prccedures for major elements are discussed in Appendix I, and procedures for trace element analyses are presented in Appendix IV.

Classification

The calc-alkaline rocks of the Coquihalla Vclcanic Complex have been subdivided according to the classification system proposed by Irvine and Baragar (1971), with mcdifications based on the terminology of Wise (1969). This system of classification

utilizes major element and normative compositions, calculated on a volatile-free basis, to subdivide the Coquihalla Volcanic Complex rocks into 4 groups: basaltic andesite, andesite, dacite, and rhyolite.

Figure 26 is a plot of normative plagioclase content versus normative colour index and shows the classification lines of Irvine and Baragar which delineate their fields of basalt, andesite, dacite, and rhyolite. The compositions of the two rocks (632 and 251) which fall well within the basalt field are termed 'basaltic andesite' in this study due to their lack of modal or normative olivine, and their petrographic similarity to other andesites within the suite. Rocks which fall on the dividing line are grouped with the andesites. The rock (283) which falls at the felsic end of the andesite field has been classified with the dacites due to its high silica (64 wt. %), differentiation index (68), and normative quartz (17.5), and its petrographic similarity to other dacites in the suite.

Comparison with Cascade Calc-alkaline Suites

Andesites of the Coquihalla Volcanic Complex are similar to calc-alkaline suites in western North America and worldwide, in that they are quartz-normative, have an average silica content of 59 wt. %, and show Mg/(Mg+Fe) ratios less than 0.55. Coquihalla Volcanic Complex andesites are similar to Cascade andesites in exhibiting initial $^{87}Sr/^{86}Sr$ ratios of 0.7037, as compared to an average value of 0.7037 for Cascade lavas (Church and Tilton, 1973).

Coquihalla Volcanic Complex andesites can be classified as

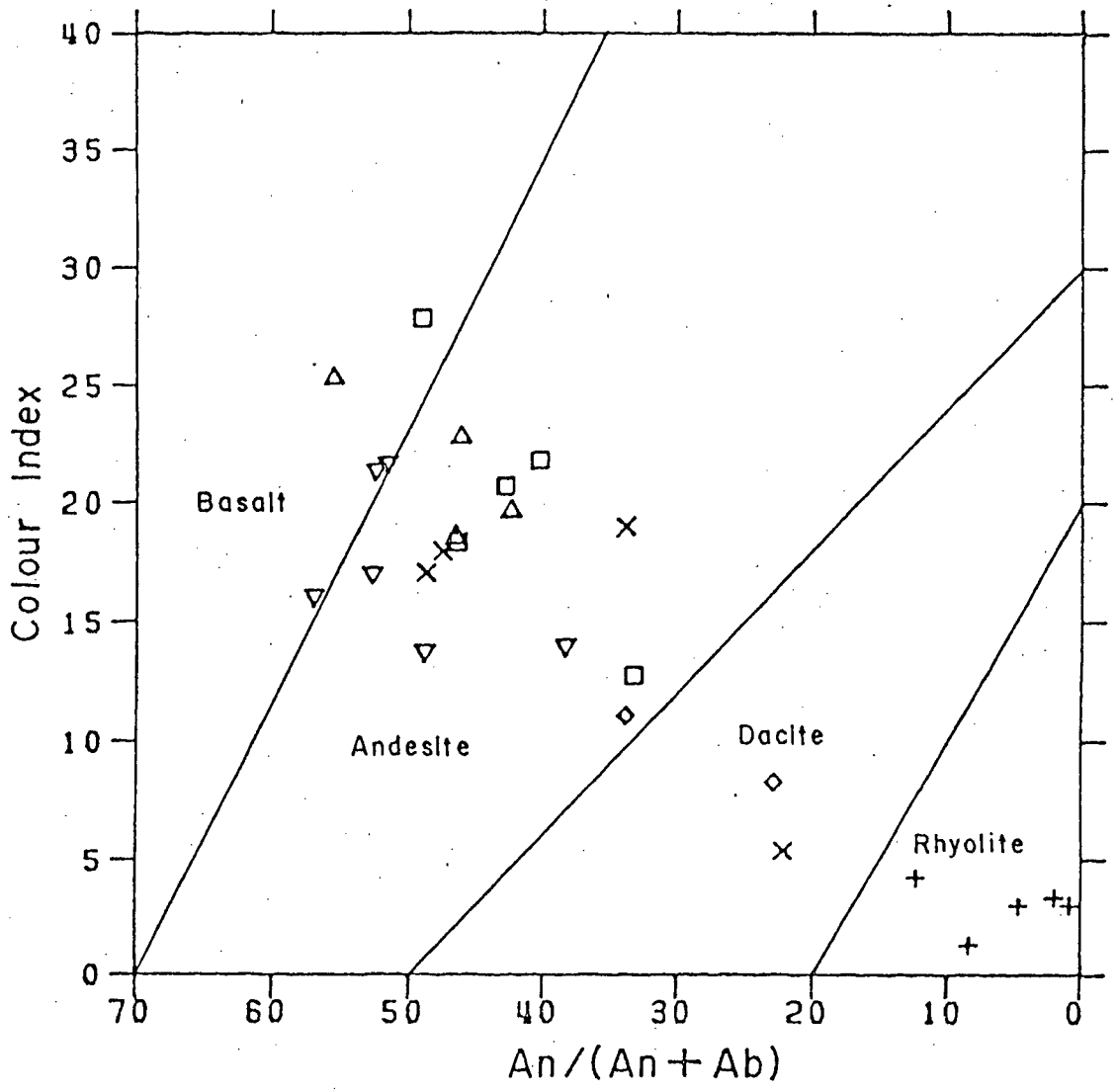

FIGURE 26: Normative plagioclase (100An/(An+Ab+5/3Ne)) versus normative colour index (ΣOl+Opx+Cpx+Hm+Ilm), with the classification lines of Irvine and Baragar (1971). Symbols as in Fig. 23; × altered rocks.

'average K_2O' andesites (Gunn, 1974) with K_2O contents distinctly higher than those for Cascade or Garibaldi andesites. In addition, Coquihalla Volcanic Complex rocks are enriched in Ba and Rb, and depleted in Ni and Cr relative to Cascade and Garibaldi lavas. Sr contents are similar to those of Cascade volcanics but less than those of Garibaldi lavas.

Discussion

Members of the Coquihalla Volcanic Complex display a range in silica contents (volatile-free) from 54 to 76 weight per cent. The compositional hiatuses around a silica content of 67% are thought to be related to a sampling bias towards andesitic and rhyolitic rocks.

Chemical variations within the suite (Figures 27-32) are characterized by enrichment of K_2O, Na_2O, Rb, and Nb in relation to increasing silica, and depletion of TiO_2, Al_2O_3, MgO, FeO, MnO, CaO, P_2O_5, Cr, Ni, V, and Sr. The elements Ba, Ce, Nd, and Zr all show enrichment throughout most of the suite, and depletion in the most felsic members of the suite.

In order to estimate the effect of alteration processes on whole rock compositions, four rocks, which showed pronounced development of secondary minerals, were analyzed and plotted with other 'unaltered' rocks in Figures 30 to 35. The main effect of alteration is an increase in H_2O and CO_2. The Harker diagrams (Figures 27-32) were constructed on a volatile-free basis, and they indicate that altered rocks plot slightly outside the main field of compositional variation for the elements Na, K, Ca, Mn, Ba, and Sr. The Na_2O-silica diagram is

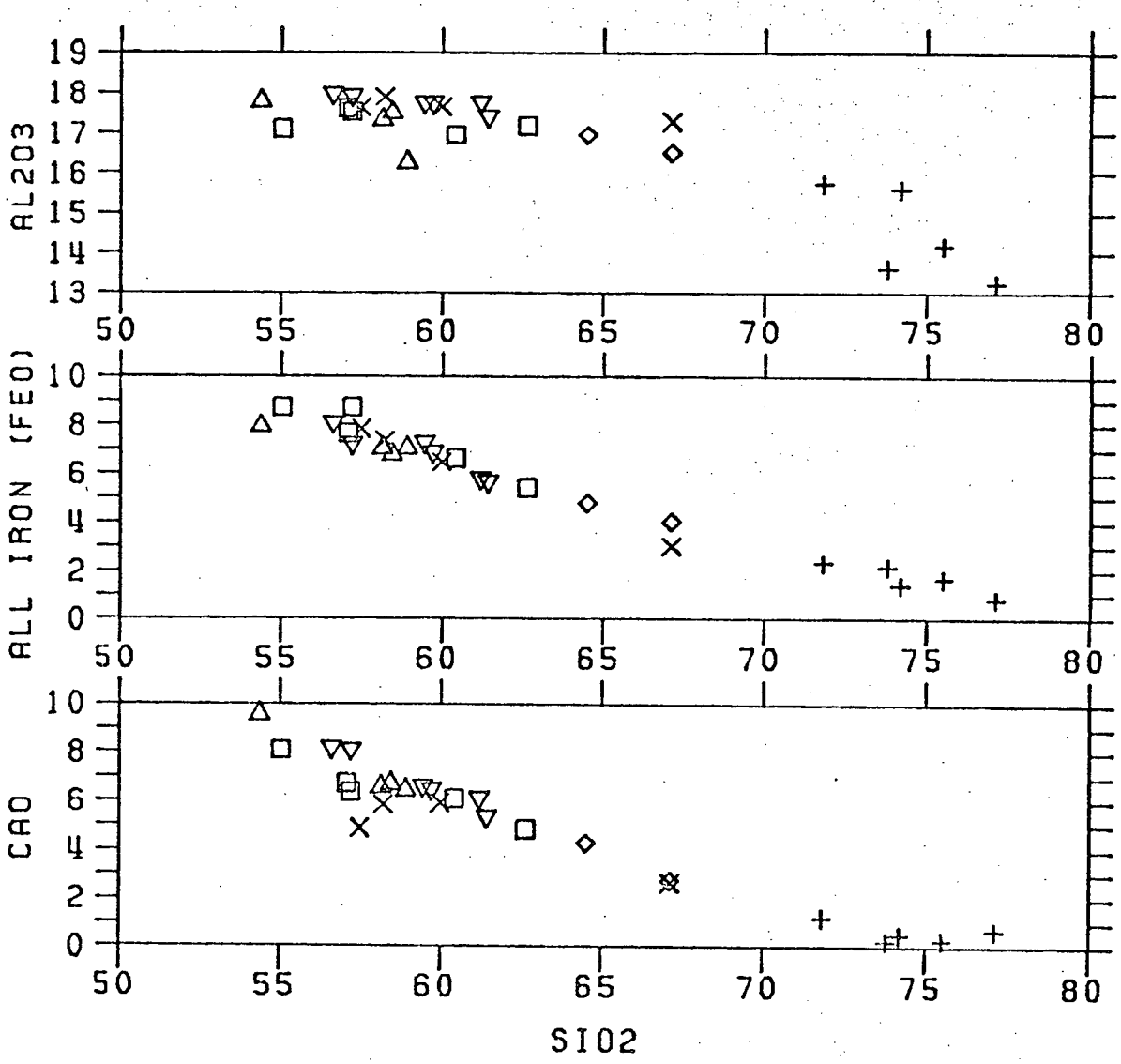

FIGURE 27: Harker variation diagrams. Values in weight percent, volatile-free. Symbols as in Fig. 26.

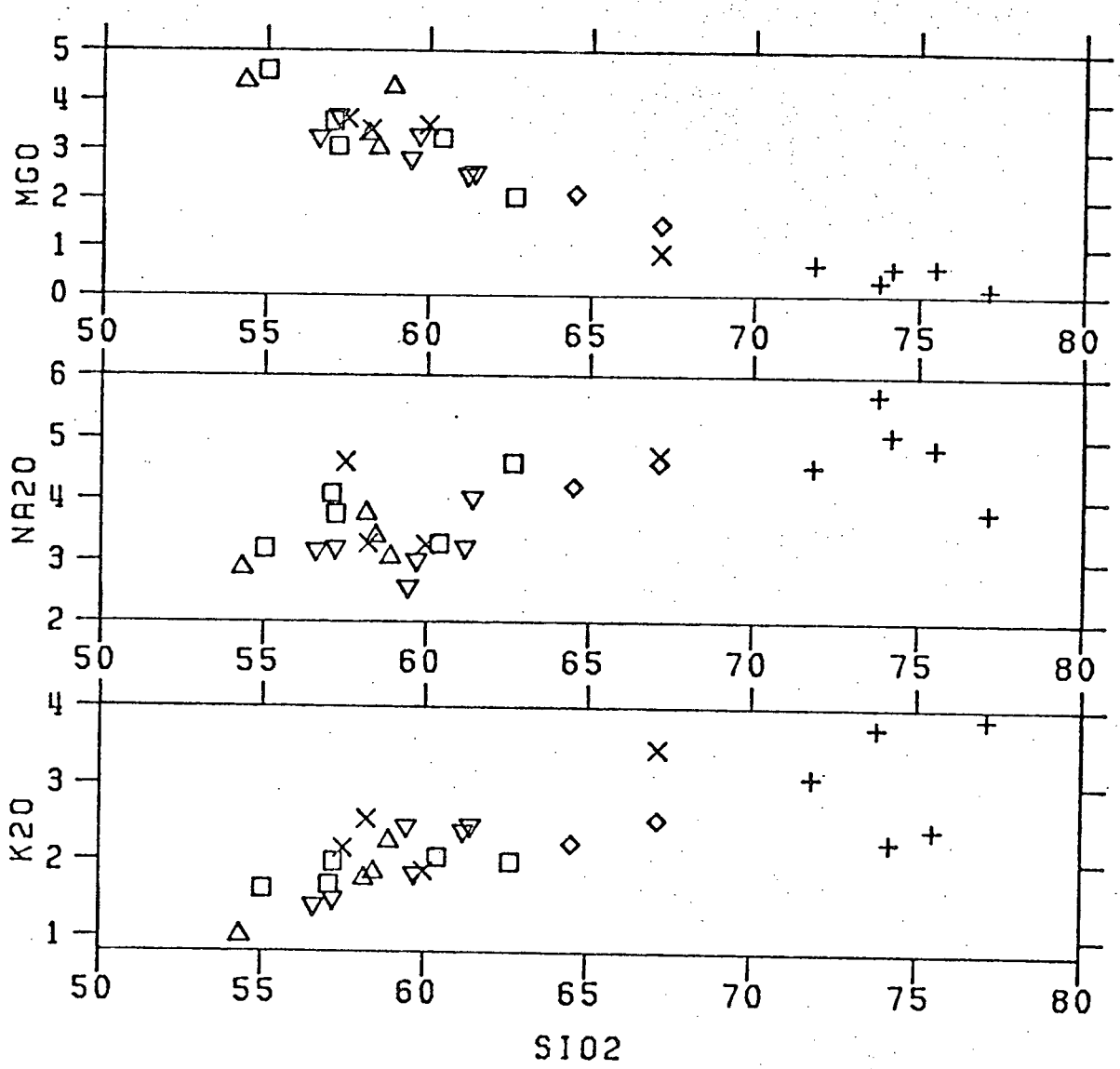

FIGURE 28: Harker variation diagrams. Values in weight percent, volatile-free. Symbols as in Fig. 26.

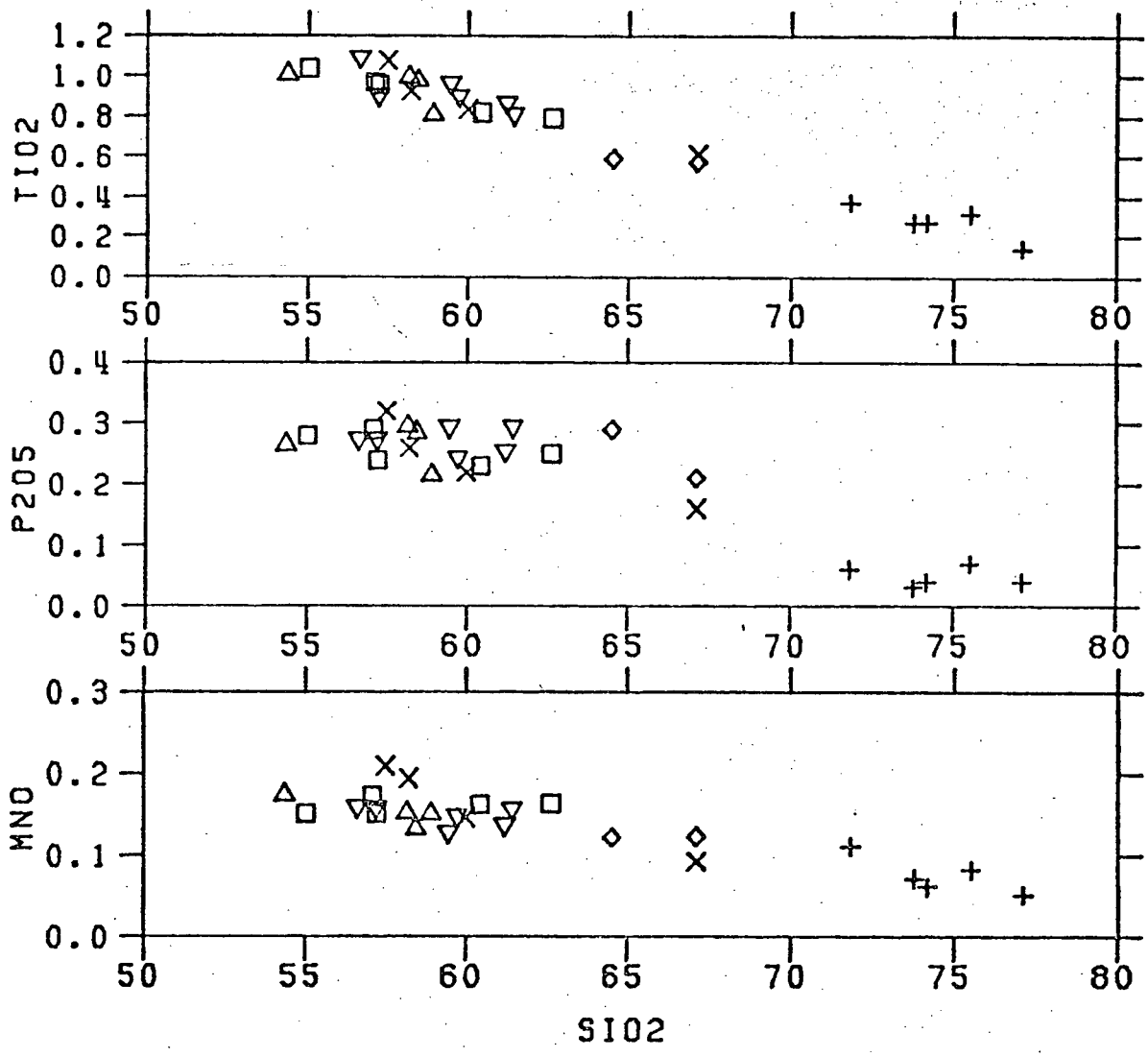

FIGURE 29: Harker variation diagrams. Values in weight percent, volatile-free. Symbols as in Fig. 26.

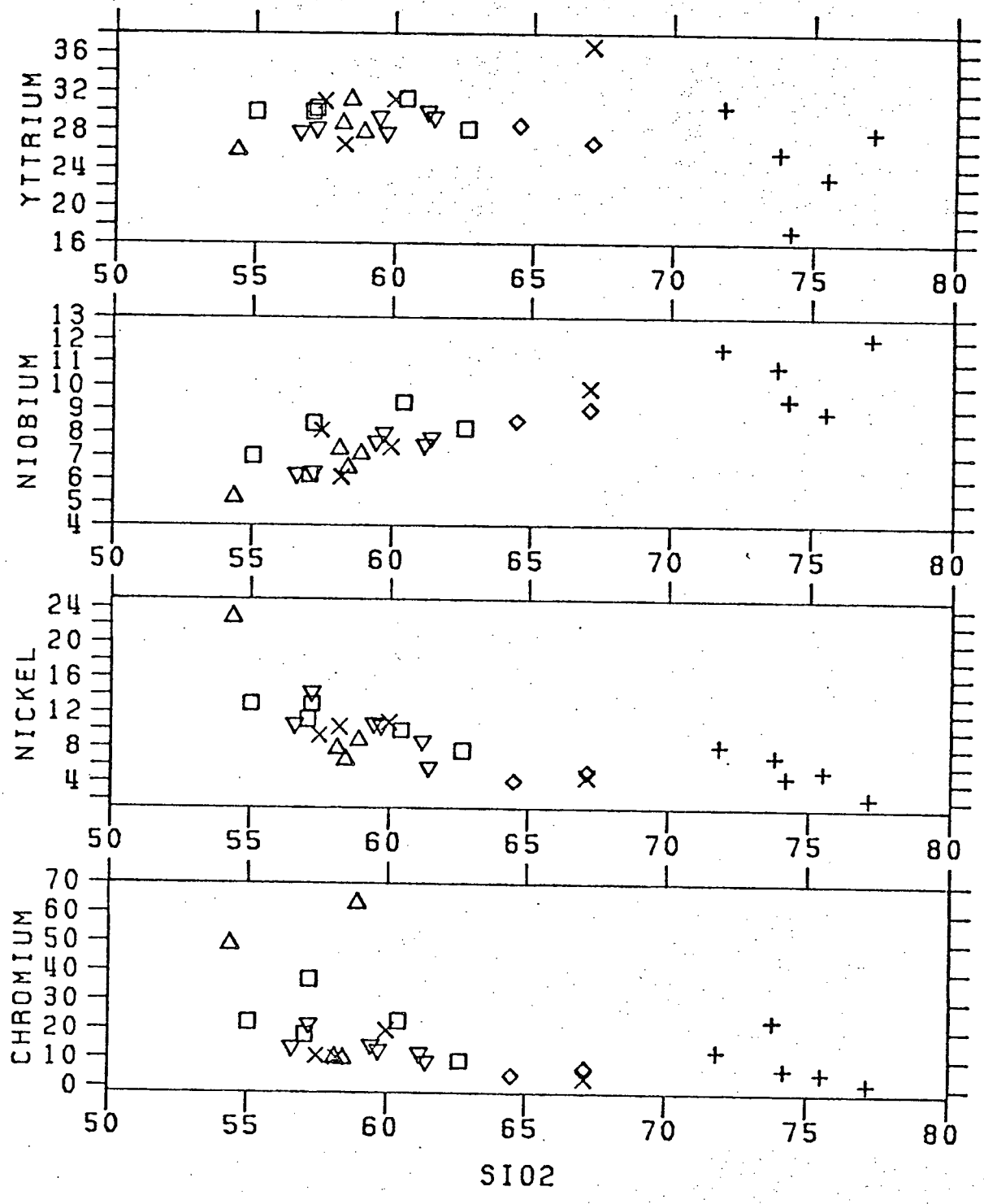

FIGURE 30: Harker variation diagrams. Oxide values in weight percent, volatile-free. Trace element values in parts per million. Symbols as in Fig. 26.

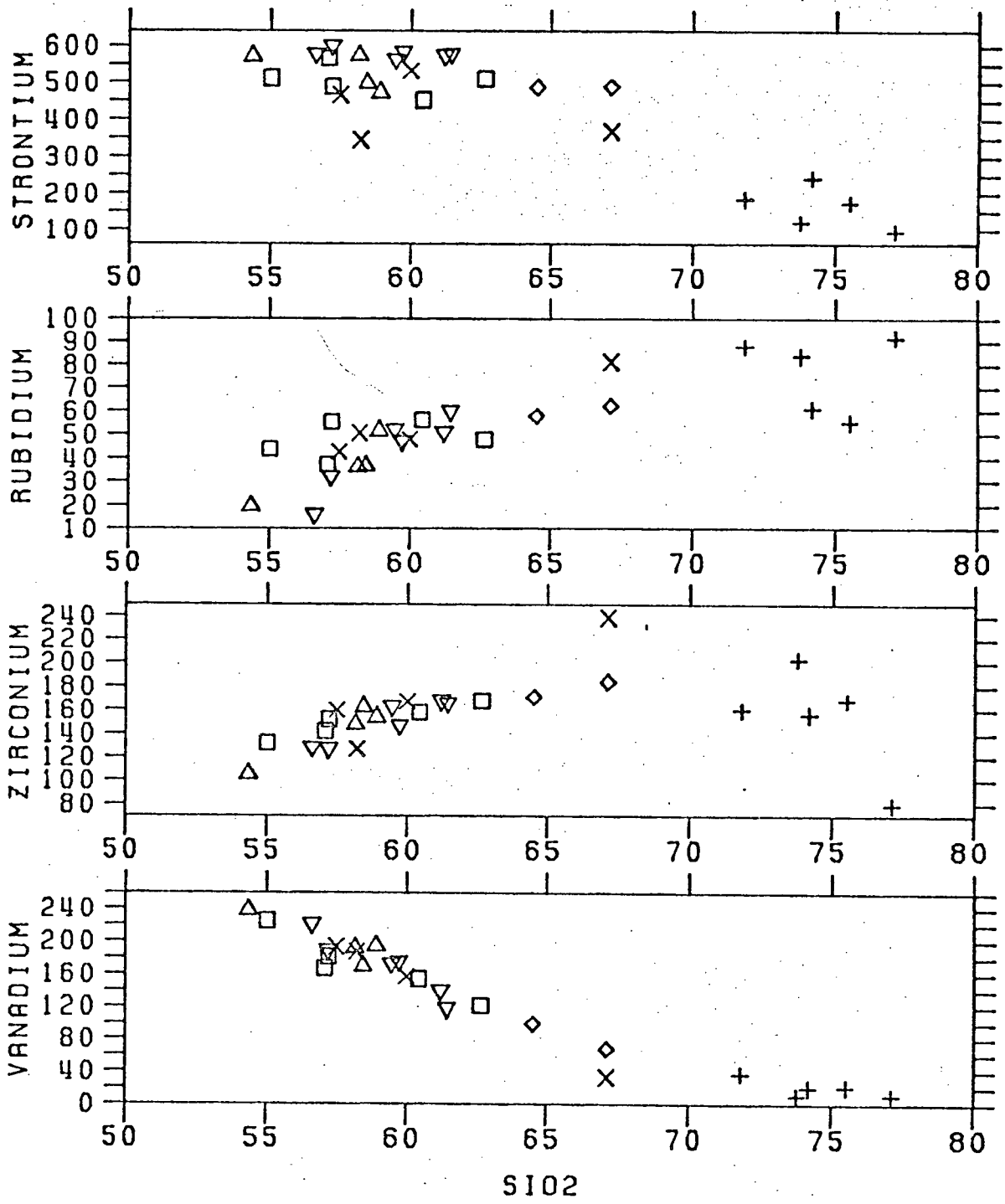

FIGURE 31: Harker variation diagrams. Oxide values in weight percent, volatile-free. Trace element values in parts per million. Symbols as in Fig. 26.

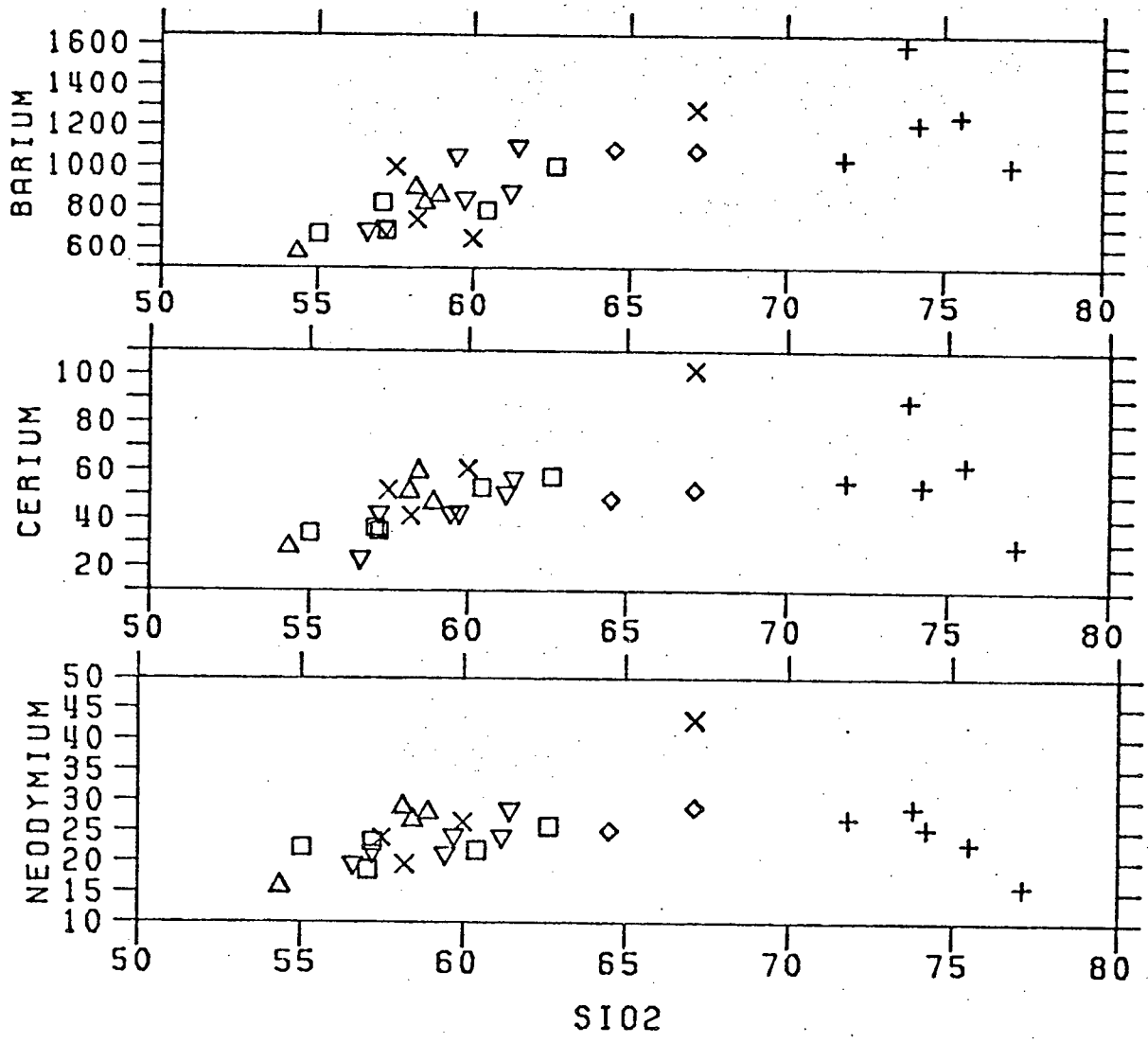

FIGURE 32: Harker variation diagrams. Oxide values in weight percent, volatile-free. Trace element values in parts per million. Symbols as in Fig. 26.

the only plot in which significant scatter appears among non-altered rocks. Depletion of Na_2O in some Coquihalla Volcanic Complex rhyolites could be due to alkali leaching of glasses (Lipman, 1965), but these variations are not accompanied by changes in Rb concentrations, which is generally regarded to be mobile during hydrothermal alteration (Chikhaoui et al., 1978). Moreover, the depletion of Na O is accompanied by decreases in Ce, Nd, Ba, and Zr, and the latter element is considered to be highly immobile during metamorphism (Smith and Smith, 1976; Winchester and Floyd, 1977).

In view of the small amount of scatter in chemical variation diagrams, and the small compositional effects on highly altered rocks, the chemical variations exhibited by members of the Coquihalla Volcanic Complex are regarded as reflecting the primary igneous history of these rocks. A model to account for the late-stage depletion of the above-mentioned elements is proposed below.

Petrogenesis

Models proposed for the genesis of silicic members of calc-alkaline suites (dacites and rhyolites) fall into three groups:

a) upper crustal anatexis (Ewart and Stipp, 1968; Ewart et al., 1971),

b) low pressure fractional crystallization of andesitic liquids (Nicholls, 1971; Ewart et al., 1973; Lambert et al., 1974), and

c) partial melting of quartz eclogitic upper mantle (Wilkinson, 1971).

A genetic relationship between members of the Coquihalla Volcanic Complex is suggested by relatively smooth chemical variations and strontium isotopic uniformity within the suite. Systematic variations of modal abundances, and the correlation of whole rock chemistry with constituent feldspar and titanomagnetite compositions, suggest that crystal fractionation played a dominant role in generating the petrological diversity within the Coquihalla Volcanic Complex. Although partial melting of an isotopically uniform source could also account for this diversity, arguments based on trace element constraints severely limit the applicability of this model.

The trace element distribution patterns within a suite of igneous rocks can be used to discriminate between the effects of partial melting and fractional crystallization as discussed by Ferrara and Treuil (1974). The trace element distribution produced by fractional crystallization is governed by the Rayleigh fractionation law (Arth, 1976):

Equ. 1.1 $$C_i^l/C_i^o = F^{(D_i+1)}$$

where C_i^l is the concentration of i in the remaining liquid

C_i^o is the concentration of i in the original liquid

F is the fraction of liquid remaining

D_i is the bulk solid/liquid distribution coefficient, defined as

Equ. 1.2 $$D_i = x_j k_{ij}$$

where x_j is the fraction of mineral j in the cumulate

k_{ij} is the solid/liquid distribution coefficient for mineral j and element i

For equilibrium partial melting, the trace element

distribution is governed by the following relation (Shaw, 1970):

Equ. 1.3 $$C_i^l / C_i^o = 1/(D_i + F(1 - D))$$

where C_i^o is the initial concentration of i in the solid

C_i^l is the concentration of i in the liquid formed

F is the fraction of melting

D_i is the bulk distribution coefficient defined in equ. 1.2

Elements for which the bulk distribution coefficient, D, is close to zero are concentrated in the liquid and have been called 'hygromagmatophile' (Ferrara and Treuil, 1974). Equations 1.1 and 1.3 are simplified for hygromagmatophile elements, and and both reduce to:

Equ. 1.4 $$C_i^l / C_i^o = 1/F$$

It can be seen from equ. 1.4 that the amount of liquid, F, can be estimated from the concentration ratio of two related rocks, and that plots of the variation of two hygromagmatophile elements will produce linear correlations for suites of rocks derived by either partial melting or fractional crystallization.

The two processes can be distinguished, however, on plots illustrating the variation of two trace elements which have slightly different degrees of proclivity for the liquid phase. Equations 1.1 and 1.3 were used to calculate the distribution of two trace elements with different, but constant values of D, as a function of F; it can be seen from Figure 33 that the partial melting process causes a much greater departure from linearity in trace element patterns than crystal fractionation processes if the two elements have slightly different bulk distribution coefficient values, even if neither element is

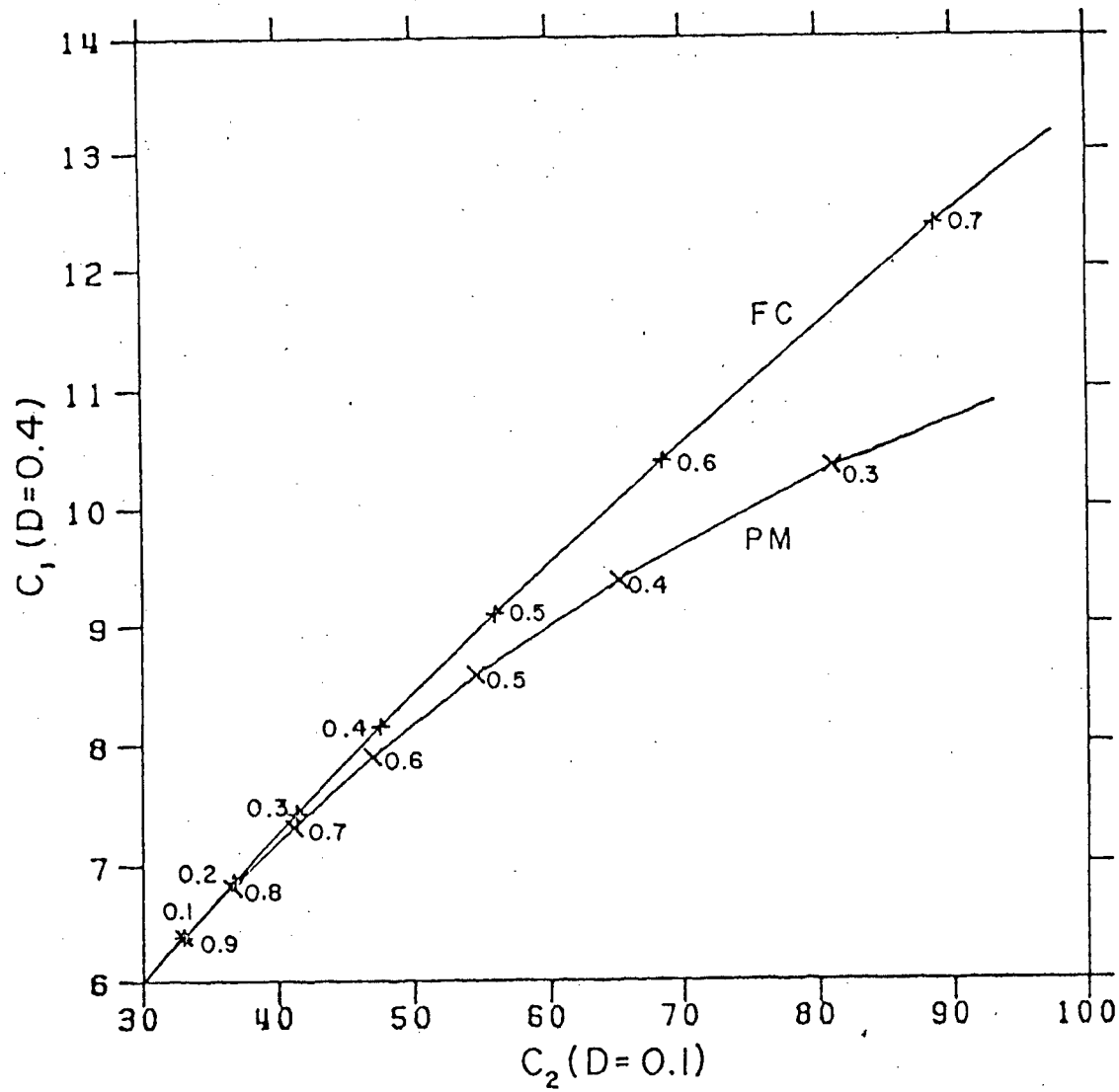

FIGURE 33: The calculated correlation curves of two trace elements C_1 and C_2 with different bulk distribution coefficients during partial melting (PM) and fractional crystallization (FC) processes. Numbers indicate the fraction of melt remaining or formed.

hygromagmatophile. It should be noted that calculated trace element distributions for other types of partial melting processes produce similar patterns to those shown in Figure 33 for the equilibrium case.

Of the trace elements analyzed in Coquihalla Volcanic Complex rocks, Zr, Nd, Ce, and Nb are commonly considered as hygromagmatophile (Ferrara and Treuil, 1974; Allegre et al., 1977). The only elements, however, which increase in concentration throughout the Coquihalla Volcanic Complex sequence andesite to rhyolite are Rb and Nb, and their enrichment rates indicate that bulk distribution coefficients are significantly greater than zero. The correlation of these two elements (Figure 34) closely matches the calculated fractional crystallization curve in Figure 33, and implies that the volcanic suite has been generated by crystal fractionation processes. In order for a partial melting process to produce this nearly-linear pattern, distribution coefficients for Rb and Nb would have to be almost equal; this is inconsistent with steadily increasing Rb/Nb ratios observed in Coquihalla Volcanic Complex rocks.

In addition to the above argument, it would be difficult to account for the depletion of Ce, Nd, Ba, and Zr in some rhyolites by partial melting of mantle of upper crustal material, in which bulk distribution coefficients for these elements are nearly zero.

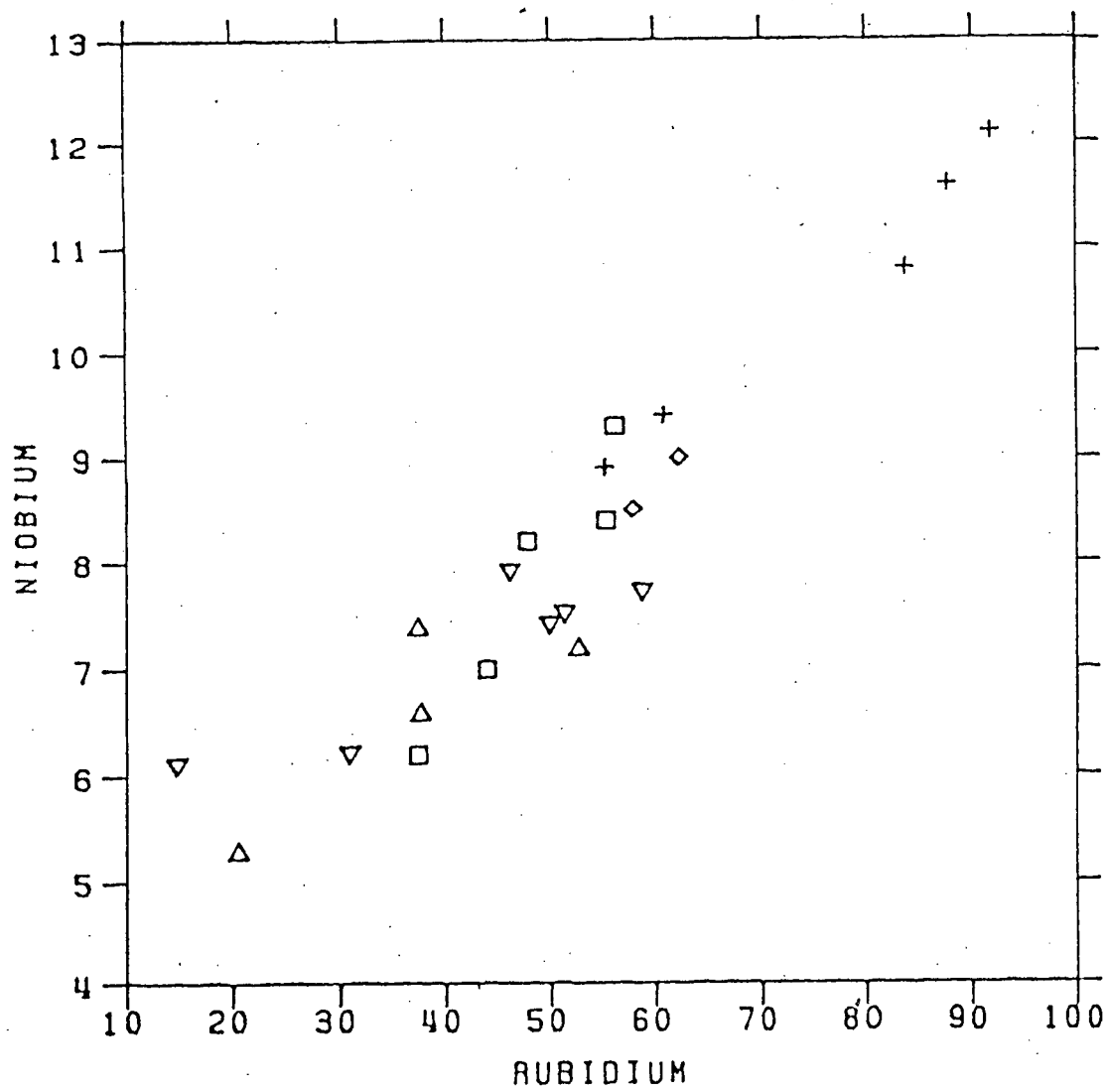

FIGURE 34: The observed correlation of rubidium and niobium in Coquihalla Volcanic Complex rocks. Symbols as in Fig. 26.

Major Element Model

In order to quantitatively test the fractional crystallization model, solutions were sought tc least squares mass balance equations which test whether the major element composition of a rock can be mathematically derived from that of another rock by subtraction of the compositions of phenocrysts observed in these rocks. Solutions by algorithms of Wright and Doherty (1970) or Bryan et al., (1969) seem inappropriate in that no allowance is made for analytical error in microprobe analyses of mineral phases. A program written by Albarede and Provost (1977) was used in this study and all mineral and whole-rock analyses were assigned standard deviations equal to 2% of the concentrations of each element present.

Modelling of the spectrum of Coquihalla Volcanic Complex compositions was divided into two steps: basaltic andesite-diorite to dacite, and dacite to rhyolite. This division is artificial in that the fractionation process is envisioned to be continuous. Different phenocryst populations between andesites and rhyolites, however, make it reasonable to formulate the modelling in this manner.

All members of the Coquihalla Volcanic Complex are porphyritic or holocrystalline, and it is not known whether phenocrysts represent cumulate phases or whether they crystallized from differentiated liquids. In order to minimize the effects of this uncertainty, averages of two whole rock compositions were used for the basaltic-andesite and dacite compositional stages. A crystal-poor vitric tuff was used for the rhyolite end member. Mineral compositions were taken from

microprobe analyses of phenocrysts in the modelled rocks and in rocks similar to them, except for the apatite analysis which was taken from Green (1977).

Results of each step of the model are presented in Tables 4 and 5. Both fitting steps produced adjusted mineral and whole rock compositions in which all residuals were less than the assumed 2% errors. Major element modelling indicates that:

A) hornblende dacites can be derived from basaltic-andesites by roughly 50% crystallization of a mixture of plagioclase (An75), hornblende, clinopyroxene, titanomagnetite, and apatite,

b) rhyolites can be derived from hornblende dacites by 30-40% crystallization of a mixture of plagioclase (An 42), hornblende, biotite, magnetite, and apatite, and

c) the quantity of rhyolitic magmas produced by fractional crystallization of basaltic-andesite liquids will be roughly equal to 25-30% of the original magma volume.

It should be noted that results of this modelling procedure are not overly sensitive to particular mineral or whole rock compositions; fitting of other whole rock pairs similar to the average compositions shown in Tables 4 and 5 generally produces results within two standard deviations of the calculated coefficients shown in these tables.

Modal abundances of phenocrysts in Coquihalla Volcanic Complex rocks (Table 3) are generally compatible with the mineralogical proportions of the calculated cumulates. Recent experimental work by Kushiro (1978) indicates that all fractionating phases are more dense than hydrous andesitic

4: MAJOR ELEMENT MODEL: STEP 1-- BASALTIC ANDESITE TO DACITE

	Ap	Hb	Pl	Mt	Cpx	Dacite
Mean	0.004	0.128	0.204	0.038	0.111	0.511
Sigma	0.001	0.028	0.015	0.003	0.025	0.020
Mineral %	0.82	26.35	42.20	7.80	22.84	

Fraction of liquid remaining 0.511

Initial Compositions

	Ap	Hb	Pl	Mt	Cpx	Dacite	Andesite
Si	0.0	45.20	49.17	0.07	50.38	65.63	54.54
Ti	0.0	2.63	0.07	8.19	1.09	0.58	1.03
Al	0.0	9.40	32.29	3.08	4.51	16.69	17.44
Fe	0.0	12.46	0.40	88.59	9.12	4.40	8.36
Mg	0.0	14.54	0.06	0.16	14.93	1.77	4.51
Ca	54.00	11.52	15.95	0.01	20.16	3.51	8.80
Na	0.0	2.19	2.55	0.02	0.32	4.39	2.99
K	0.0	0.49	0.16	0.0	0.0	2.38	1.33
P	40.00	0.0	0.0	0.0	0.0	0.23	0.28
Mn	0.0	0.36	0.04	0.80	0.24	0.12	0.17

Absolute Residuals[1]

	Ap	Hb	Pl	Mt	Cpx	Dacite	Andesite
Si	0.000	0.022	0.042	0.000	0.024	0.186	-0.253
Ti	0.000	0.015	0.002	0.028	0.004	0.011	-0.036
Al	-0.000	-0.015	-0.243	-0.001	-0.004	-0.171	0.365
Fe	-0.000	-0.018	-0.000	-0.237	-0.009	-0.012	0.069
Mg	-0.000	-0.063	-0.000	-0.000	-0.058	-0.008	0.062
Ca	0.016	0.027	0.081	0.000	0.068	0.014	-0.132
Na	0.000	0.005	0.009	0.000	0.001	0.054	-0.058
K	-0.000	-0.001	-0.001	-0.000	-0.000	-0.013	0.012
P	-0.012	-0.000	-0.000	-0.000	-0.000	-0.001	0.003
Mn	0.000	0.000	0.000	0.000	0.000	0.001	-0.002

Reduced Residuals[2]

	Ap	Hb	Pl	Mt	Cpx	Dacite	Andesite
Si	0.000	0.024	0.042	0.000	0.023	0.140	-0.228
Ti	0.002	0.204	0.097	0.153	0.102	0.356	-0.896
Al	-0.000	-0.071	-0.365	-0.008	-0.033	-0.485	0.989
Fe	-0.000	-0.067	-0.011	-0.132	-0.044	-0.108	0.366
Mg	-0.000	-0.203	-0.022	-0.004	-0.181	-0.145	0.565
Ca	0.015	0.110	0.238	0.003	0.161	0.158	-0.672
Na	0.001	0.074	0.132	0.007	0.027	0.501	-0.727
K	-0.000	-0.022	-0.027	-0.004	-0.013	-0.199	0.268
P	-0.015	-0.012	-0.019	-0.003	-0.010	-0.058	0.118
Mn	0.000	0.010	0.013	0.004	0.008	0.034	-0.070

[1] Difference between initial and final, adjusted compositions
[2] Absolute residuals divided by error (2%) of analyses

5: MAJOR ELEMENT MODEL: STEP 2-- DACITE TO RHYOLITE

	Ap	Hb	Pl	Mt	Bi	Rhyolite	
Mean	0.005	0.074	0.281	0.028	0.034	0.567	
Sigma	0.001	0.017	0.024	0.001	0.015	0.031	
Mineral %	1.18	17.46	66.67	6.71	7.98		
Fraction of liquid remaining			0.567				

Initial Compostions

	Ap	Hb	Pl	Mt	Bi	Dacite	Rhyolite
Si	0.0	43.62	58.23	0.31	38.62	77.02	65.63
Ti	0.0	2.93	0.10	5.35	4.07	0.14	0.58
Al	0.0	11.11	26.79	2.10	14.55	13.23	16.69
Fe	0.0	11.76	0.12	89.90	13.75	0.84	4.40
Mg	0.0	14.80	0.03	0.67	16.15	0.14	1.77
Ca	54.00	11.05	7.56	0.14	0.10	0.68	3.51
Na	0.0	2.50	7.23	0.08	0.75	3.79	4.39
K	0.0	0.35	0.21	0.08	7.01	3.80	2.38
P	40.00	0.0	0.0	0.0	0.0	0.04	0.23
Mn	0.0	0.31	0.0	0.90	0.55	0.05	0.12

Absolute Residuals[1]

	Ap	Hb	Pl	Mt	Bi	Dacite	Rhyolite
Si	-0.000	-0.023	-0.158	-0.000	-0.008	-0.553	0.711
Ti	0.000	0.011	0.003	0.012	0.009	0.007	-0.025
Al	-0.000	-0.007	-0.142	-0.000	-0.005	-0.075	0.204
Fe	-0.000	-0.005	-0.000	-0.099	-0.003	-0.001	0.012
Mg	-0.000	-0.054	-0.001	-0.000	-0.029	-0.002	0.023
Ca	0.049	0.035	0.067	0.000	0.000	0.005	-0.067
Na	0.000	0.000	0.002	0.000	0.000	0.001	-0.002
K	0.000	0.001	0.002	0.000	0.011	0.067	-0.058
P	-0.037	-0.000	-0.001	-0.000	-0.000	-0.003	0.007
Mn	-0.000	-0.002	-0.004	-0.001	-0.001	-0.009	0.018

Reduced Residuals[2]

	Ap	Hb	Pl	Mt	Bi	Dacite	Rhyolite
Si	-0.000	-0.026	-0.133	-0.000	-0.011	-0.354	0.534
Ti	0.003	0.146	0.156	0.091	0.086	0.326	-0.797
Al	-0.000	-0.029	-0.255	-0.003	-0.017	-0.263	0.578
Fe	-0.000	-0.020	-0.007	-0.055	-0.011	-0.022	0.115
Mg	-0.001	-0.171	-0.043	-0.007	-0.085	-0.095	0.407
Ca	0.045	0.145	0.394	0.005	0.006	0.156	-0.737
Na	0.000	0.001	0.010	0.000	0.000	0.012	-0.023
K	0.001	0.025	0.087	0.008	0.069	0.695	-0.863
P	-0.045	-0.016	-0.062	-0.006	-0.007	-0.130	0.271
Mn	-0.004	-0.070	-0.205	-0.039	-0.038	-0.434	0.816

[1] Difference between initial and final, adjusted compositicns
[2] Absolute residuals divided by error (2%) of analyses

liquids. The observation that plagioclase occurs in slightly greater amounts than predicted by these calculations may be related to the lower density, and hence slower settling rates of plagioclase, as compared to other fractionating phases. Experimental studies by Green (1972) and Eggler (1974) on natural and synthetic andesitic compositions demonstrate the feasibility of this proposed fractionation model.

It should be noted that the lack of precise stratigraphic control between rhyolites and intermediate volcanics in the field, and the use of average intermediate compositions do not necessarily imply derivation of all igneous rocks in stages from a single, stagnant, fractionating magma chamber. Coquihalla Volcanic Complex rhyolites and dacites appear to be derived by crystal fractionation of andesitic magmas, but the actual process may involve more than one magma chamber, or periodic replenishment of a single magma chamber by mafic melts.

Trace element model

Serious difficulties are presented in the use of trace elements to test the consistency of the results of major element modelling. The problem of whether analyzed rocks represent true liquids can be circumvented only with completely aphyric rocks. Errors related to analysis of a rock composed of cumulate phases and liquid are small for elements with distribution coefficients (D) near zero, but quite considerable for elements with large D values (Allegre et al., 1977).

The greatest problem in quantitative treatment of trace element distributions is the uncertainty in, and wide range of

values for mineral/liquid distribution coefficients (k). A large percentage of determinations of k values on analyses of phenocryst-matrix pairs in natural rocks. Distribution coefficients determined in this manner implicitly assume bulk equilibrium between mineral and liquid, and can give rise to spurious results when applied to Rayleigh fractionation models. Analytical results of Philpotts and Schnetzler (1970) clearly show phenocryst zonation with respect to trace elements, and k values calculated from zoned minerals in their study show differences up to an order of magnitude. As pointed out by Albarede and Bottinga (1972), apparent distribution coefficients calculated from zoned minerals will be higher than equilibrium values if $k > 1$, and lower than equilibrium values if $k < 1$.

In recognition of this problem, Zielinski (1975) has modelled trace element abundances using a bulk equilibrium fractionation equation. Although this presents an internally consistent approach, results are probably inappropriate for application to natural systems where Rayleigh-type processes appear to be active.

In addition to the problem of selecting appropriate k values, recent experimental studies (reviewed by Irving, 1978) demonstrate that k values vary considerably with intensive parameters such as composition of mineral and melt, temperature, and oxygen fugacity. Increases in k values with decreasing temperature and increasing silica content of melts appear to reflect the increasing polymerization and Si/O bond ratios in the melt structure (Irving, 1978). Discrepancies between apparent and experimental k values can in part be resolved by

more rigorous definition of distribution coefficients in terms of proposed equilibrium exchange reactions incorporating activity estimates of melt components (i.e. k values for Ni in olivine, Leeman and Lindstrom, 1978). At the present time, however very much more experimental work is necessary to extend this technique to other trace elements and the common minerals in volcanic rocks. In addition, the effect of water content of melts on distribution coefficient values is in need of experimental investigation.

In view of the above qualifications, it makes little sense to calculate trace element distributions using best estimates for k values. Graphical techniques can be used to calculate bulk distribution coefficients for suites of rocks (Allegre et al., 1977; Duchesne, 1978), and mineral percentages can be calculated if k values for individual minerals are chosen. The approach taken in this study is an inversion of this last procedure, in that k values are calculated from the mineral percentages given by major element modelling.

Rewriting equation 1.1 as:

Equ. 1.5 $$D = \ln(C_i^l/C_i^o)/\ln(F) + 1 \quad ,$$

it can be seen that the bulk distribution coefficient for any trace element can be calculated from the concentration ratio of whole rock pairs, combined with values of F derived from the major element model. Values for mineral distribution coefficients can then be computed utilizing the mineral fractions from the major element model (equation 1.2). Consistency of the trace element model can be judged by comparing these calculated k values with the ranges of values

quoted in the literature (Appendix III). A major benefit of this approach is that calculated distribution coefficients may provide valuable suggestions for further investigation by experimental techniques.

It should be noted that trace element modelling of this nature can be formulated such that solutions can be obtained by least squares fitting akin to the major element procedure. This approach has recently met with some success in quantitative modelling of batch partial melting processes (Minster and Allegre, 1978). Attempts to solve the problem in this manner, however, led to non-converging solutions due to the large errors associated with k values for many minerals.

The results of the trace element modelling are presented in Table 6. Modelling was again divided into two steps using the trace element concentrations of the same rocks used in the major element models. Bulk distribution coefficients were calculated in the manner described above. For each element, one mineral/liquid distribution coefficient was calculated (indicated by an asterisk in Table 6) from the bulk distribution coefficient after other minerals, with more constrained k values, were assigned values taken from the literature (Appendix III). This procedure is somewhat arbitrary and calculated k values can vary dramatically depending on the values chosen. Assumptions made in assigning k values, and results of these calculations are discussed below for each element.

TABLE 6: TRACE ELEMENT MODELLING RESULTS

STEP 1: BASALTIC ANDESITE TO DACITE

	D	Cpx	Hb	Plag	Mt	Ap
Cr	3.80	3.0	5.0	-	23*	-
V	2.53	2.8	4.0	-	10.7*	-
Ni	3.01	2.5	2.9	-	21.4*	-
Sr	1.16	0.12	0.46	2.4*	-	1.0
Ba	0.19	-	0.42	.19*	-	-
Rb	0.07	-	0.19*	.05	-	-
Nd	0.62	0.2	0.5	0.08	-	49.9*
Ce	0.30	0.1	0.3	0.09	-	19.6*

STEP 2: DACITE TO RHYOLITE

	D	Bio	Hb	Plag	Mt	Ap
Cr	3.05	7	5	-	24.2*	-
V	4.55	9.3*	4	-	46.5*	-
Ni	2.25	3.7	2.9	-	21.7*	-
Sr	3.86	0.4	0.46	5.6*	-	1
Ba	1.13	10.2*	0.42	0.35	-	-
Rb	0.26	2.4*	0.19	0.05	-	-
Nd	1.93	0.34	0.5	0.12	-	147*
Ce	1.98	0.32	0.3	0.2	-	153*

* Indicates calculated value
\- Indicates distribution coefficient value close to zero

Chromium

Step 1: Experimental work demonstrates that k(cpx) decreases with decreasing fO as Cr changes from +3 to +2 valence state (Schreiber and Haskin, 1976). The Table 6 value is adjusted to a higher value to account for the higher silica content and lower temperatures of crystallization in Coquihalla Volcanic Complex rocks as compared with the study cited. No experimental data are available on k(hb); the Table 6 value is calculated from the average hb/cpx concentration ratio for Cr in Coquihalla Volcanic Complex phenocryts, analyzed by microprobe. The calculated k(mt)

value (23) falls well within the range (1-58) found from studies of natural phenocryst-matrix pairs (Appendix III).

Step 2: K(hb) is taken from the results of step 1. No experimental work has been carried out on k(biotite), and the Table 6 value is taken from calculations by Leeman (1976). The calculated k(mt) value (24) is similar to that of step 1.

Vanadium

Step 1: K(cpx) decreases with increasing fO (Lindstrom, 1976) and the Table 6 value is taken from this study. K(hb) is taken from the average hb/cpx concentration ratio for V in Coquihalla Volcanic Complex phenocrysts. The calculated k(mt) value (11) agrees well with experimentally determined values at oxygen fugacities just above the QFM buffer (Lindstrom, 1976).

Step 2: Microprobe analyses of coexisting bictite and magnetite in Coquihalla Volcanic Complex rocks indicate that k(mt) is roughly five times k(biotite). The calculated k(mt) value (46) is within the range of values (24-63) calculated in natural systems; the higher value than calculated in step 1 may reflect a real variation of k(mt) with increasing silica content and lower temperature. The k(biotite) is much lower than that calculated by Andriambololona et al., (1975) for natural rocks.

Nickel

Step 1: K(cpx) and k(hb) are taken from the experimental results of Mysen (1978) which indicate that variations with temperature and pressure are slight. The calculated k(mt) value(21) is similar to values determined experimentally (Leeman, 1974; Lindstrom, 1976) and in natural systems.

Step 2: No experimental data are available of k(biotite) and

the Table 6 value is taken from calculations of Leeman (1976). The calculated k(mt) value(22) is similar to results of step 1.

Strontium

Step 1: K(cpx) is taken from the average value of experimental work by Sun et al., (1974) and Shimizu (1974). K(hb) is taken as an average value from studies on natural systems by Schnetzler and Philpotts (1970) and Ewart and Taylor (1969). K(apatite) is adopted from calculations by Sun and Hanson (1976). The calculated k(plag) value (2.6) agrees with estimates calculated for An-rich plagioclase (Korringa and Noble, 1971), and with experimental results of Drake and Weill (1975) for temperatures between 1100-1200°C.

Step 2: K(biotite) is taken from the average value for phenocrysts in dacites and rhyolites (Philpotts and Schnetzler, 1970). The calculated k(plag) value (5.4) is consistent with the results of Korringa and Noble (1971) for intermediate-composition plagioclase, and with Drake and Weill's (1975) experimental results when extrapolated to temperatures estimated for crystallization of Coquihalla Volcanic Complex rhyolites.

Barium

Step 1: K(cpx) is taken from the experimental work of Shimizu (1974). K(hb) is taken as the average value of Griffin and Murthy (1969) and Leeman (1976). The calculated k(plag) value (0.19) is similar to experimental results of Drake and Weill (1975), and is consistent with results for natural systems.

Step 2: K(plag) is taken from the lower temperature values of Drake and Weill (1975) and from the calculated values of

Korringa and Noble (1971) for intermediate composition plagioclase. The calculated k(biotite) value(10) is similar to natural phenocryst values determined by Schnetzler and Philpotts (1970).

Rubidium

Step 1: K(plag) is taken from the experimental work of McKay and Weill (1976; 1977), and k(cpx) from the results of Shimizu (1974) and Hart and Brooks (1974). The calculated k(hb) value (0.19) is within the range of values determined from natural phenocrysts.

Step 2: Using k(hb) of step 1, the calculated k(biotite) value (2.4) agrees well with natural phenocryst results of Higuchi and Nagasawa (1969).

Neodymium

Step 1: K(plag) is taken from the experimental results of Drake and Weill (1975) and Weill and McKay (1975). K(cpx) and k(hb) are taken from the experimental work of Frey (in Irving, 1978). The calculated k(apatite) value (50) is within the range of values detrmined by Nagasawa (1970) on natural phenocryst-matrix pairs.

Step 2: K(plag) is taken from the lower temperature experimental results of Drake and Weill (1975), and Weill and McKay (1975). No experimental data are available on k(biotite) and the Table 6 value is that of Schnetzler and Philpotts (1970). The calculated k(apatite) value (147) is higher than any estimates in the literature, and may, in part, reflect increasing silica content and lower temperatures of the melt. The presence of zircon inclusions in rhyolitic biotites would

lower the calculated value for k(apatite).

Cerium

Step 1: Sources of data are the same as used for neodymium calculations. The calculated k(apatite) value (20) is similar to results on natural systems, but is inconsistently low when compared to the ratio of apatite distribution coefficients for Ce and Nd (Nagasawa, 1970; Nagasawa and Schnetzler, 1971).

Step 2: The calculated k(apatite) value(153) is similar to that for Nd, but higher than values found for natural phenocrysts.

Discussion

The general agreement of calculated distribution coefficients (Table 6) with reported ranges of values found in the literature (Appendix III) offers excellent support for the proposed differentiation model.

Discrepancies in the trace element model for the rare earth elements may reflect sampling problems, where apatite phenocrysts in dacites could be considered as culmulate phases. The problem is compounded in rhyolites where rocks with higher modal percentages of apatite show much greater concentrations of Ce and Nd. If Rb content is used as an indicator for degree of differentiation (from equation 1.4), it is evident that Ce and Nd increase steadily in abundance until a sharp decrease is encountered in the most differentiated rhyolites (Figure 35). Similar trends are recorded for Zr and Ba, and lead to the conclusion that the depletion of these elements marks a point of increased fractionation of biotite, with concomitant removal of

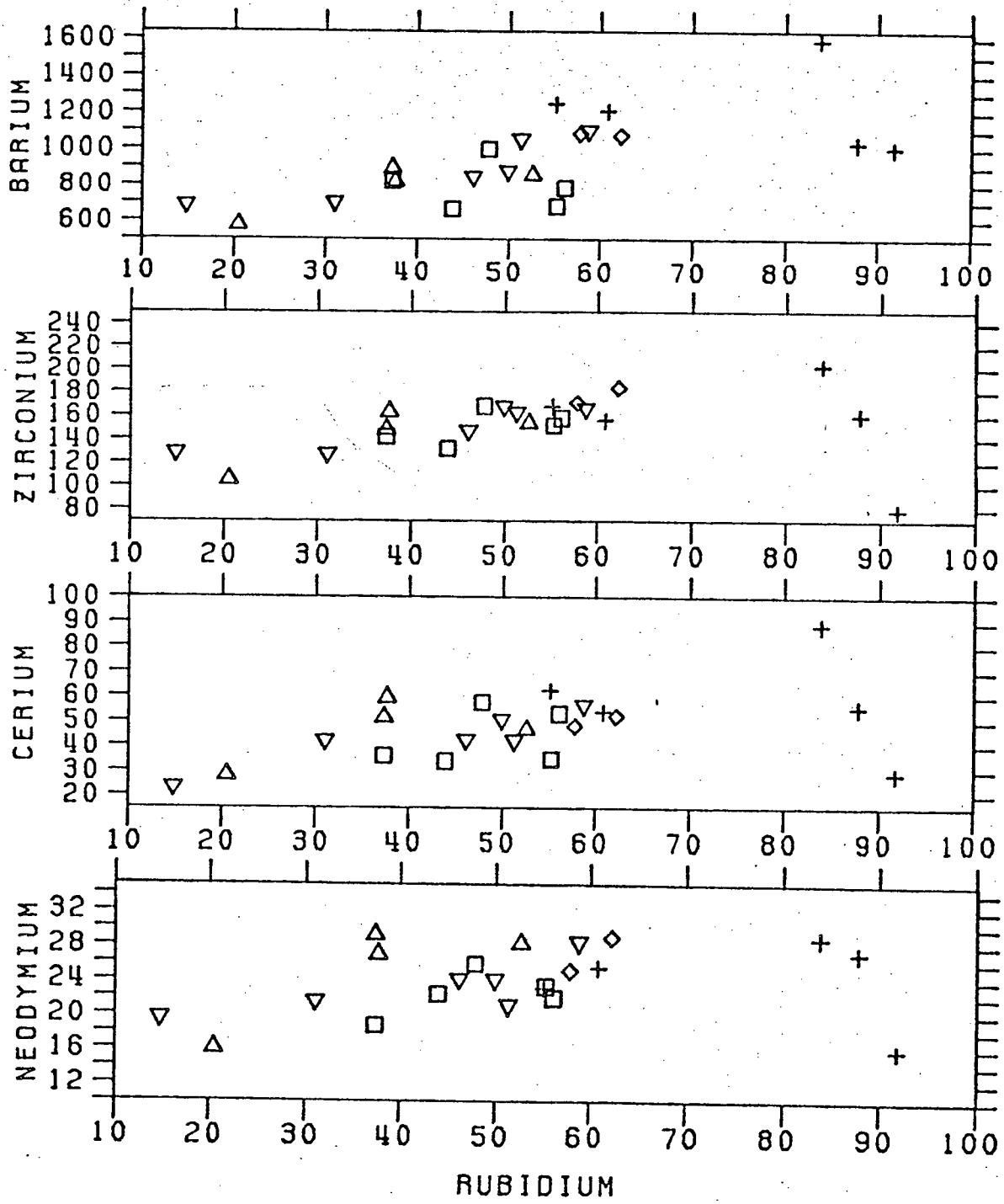

FIGURE 35: The correlations of rubidium with barium, zirconium, cerium, and neodymium in Coquihalla Volcanic Complex rocks. Symbols as in Fig. 26.

the abundant zircon, apatite, and rutile inclusions observed in rhyolitic biotites. Similar decreases in Zr content of rhyolites in New Zealand have been interpreted in an analogous fashion (Ewart et al., 1968).

It is interesting to note that the two rhyolite samples which show the greatest range of Ce, Nd, Zr, and Ba concentrations are only separated stratigraphically by approximately 75 m. The enriched sample (173) has roughly 15% biotite phenocrysts while the depleted sample (712) has less than 5%. The lower stratigraphic position of the depleted sample suggests that eruptions tapped a zoned magma chamber in which biotite had accumulated in lower levels, leaving residual liquids markedly depleted in characteristic trace elements.

Andesite Genesis

In recent years many different processes have been proposed to account for the petrogenesis of calc-alkaline andesite associated with subduction zones. These processes include partial melting of eclogitic oceanic crust (Green and Ringwood, 1968), partial melting of hydrous mantle peridotite (Kushiro, 1974; Mysen and Boettcher, 1975a; 1975b), fractional crystallization of basaltic magmas (Green and Ringwood, 1967; Osborn, 1969; Cawthorne and O'Hara, 1976), and mixing of basaltic and rhyolitic magmas (Eichelberger, 1978). The chemistry of Coquihalla Volcanic Complex rocks can be used to evaluate the roles of these various processes.

Mixing of basaltic magma with upper crustal material is unlikely in view of the uniform Sr isotopes within the volcanic

suite, and the lack of observed crustal xenoliths in Coquihalla Volcanic Complex andesites. Mixing of basaltic and rhyclitic magmas is not supported by the general lack of disequilibrium phenocryst assemblages and reversed zoned phenccrysts, and the nonlinearity of whcle-rock compositional variations.

The uniform yttrium contents of Coquihalla Vclcanic Ccmplex andesites argues against their derivation by partial melting of eclogitic cceanic crust, as the high distribution coefficient of garnet for Y would be reflected in variations in Y content of rocks formed by different degrees of partial melting. In addition, liquids produced by melting of high Na/K eclogitic oceanic crust would be expected to show higher Na/K ratios than those observed in Coquihalla Volcanic Complex rocks (Whitford, et al., 1979).

The low Mg/(Mg+Fe) ratios of Coquihalla Vclcanic Ccmplex andesites, and low Cr and Ni contents are incompatible with equilibrium of these rocks with mantle peridotite (Rceder and Emslie, 1970; Nicholls and Whitford, 1976). Experimental data of Nichclls and Ringwood (1973) show, however, that thcleiitic liquids produced by hydrous partial melting cf peridotitic assemblages at depths of 60-100 km, will undergo pronounced olivine fractionation as they ascend through the mantle and lower crust. Such high pressure accumulation of olivine, plus clinopyroxene or chrome-spinel can account satisfactcrily for the low Mg/(Mg+Fe) ratios, and low Ni and Cr ccntents of Coquihalla Volcanic Complex basaltic andesites. Subsequent residence in high level magma chambers would allcw fractionation of the low pressure phases involved in generating the chemical

spectrum through dacites and rhyolites.

Conclusions

The chemical characteristics of Coquihalla Volcanic Complex andesites are consistent with derivation through high pressure modification of parental basaltic magmas. The asscciation of the Coquihalla Volcanic Complex with subduction of the Juan de Fuca plate, and andesites in general with zones of lithospheric subduction, implies a genetic relationship such as outlined by Green (1977) or Mysen (1978b).

Generation of dacites and rhyolites by low pressure fractionation of andesitic liquids is supported by quantitative major and trace element modelling, as well as the results of experimental studies. This low pressure fractionation implies long term residence of magmas in the upper crust, and may be a consequence of the increased viscosity of andesitic liquids as they rise through the crust (Kushiro, 1978).

The observed stratigraphic sequence of the Coquihalla Volcanic Complex suggest a model in which tapping of the upper, differentiated portion of a high level magma chamber occurs, producing voluminous ash flow eruptions which tend to decrease in temperature with time. Periodic replenishment of the magma chamber with mantle-derived andesitic liquids maintains similar differentiation paths throughout the period of explosive volcanism. Production of late stage dacite, andesite, and diorite reflect decreasing residence time in the crust, possibly as a response to the increased development of conduit systems and fractures resulting from earlier eruptions.

Production of dacites and rhyolites by means of the proposed fractionation model requires the accumulation of large amounts of gabbroic material within the upper crust. No geophysical data are yet available with which to evaluate the extent of accumulation of gabbroic material underlying the Coquihalla Volcanic Complex.

REFERENCES

Abbey, S., 1977, Studies in "standard samples" for use in the general analysis of silicate rocks and minerals. Part 5: 1977 edition of "usable" values. Geol. Surv. Can. Paper 77-34, 31p.

Albee, A.L. And Ray, R.L., 1970, Correction factors for electron micoanalysis of silicates, oxides, carbonates, phosphates, and sulfates. Anal. Chem. 42 ,pp. 1408-1414.

Albarede, F. and Bottinga, Y., 1972, Kinetic disequilibrium in trace element partitioning betweeen phenocrysts and host lava. Geochim. Cosmochim. Acta 36 ,pp. 141-156.

Albarede, F. and Provost, A., 1977, Petrological and geochemical mass-balance equations: an algorithm for least-squares fitting and general error analysis. Computers and Geosciences 3 ,pp. 309-326.

Allegre, C.J., Treuil, M., Minster, J.-F., Minster, B. and Albarede, F., 1977, Systematic use of trace elements in igneous processes. Part I: fractional crystallization processes in volcanic suites. Contrib. Mineral. Petrol. 60,pp. 57-75.

Anderson, A.J., 1968, Oxidation of the LaBlacke Lake titaniferous magnetite deposit. Quebec J. Geol. 76 ,pp. 528-547.

Andriambololona, R., Lefevre, C. and Dupuy, C., 1975, Coefficient de partage des elements de transition dans les mineraux ferro-magnesians extraits des dacites. C. R. Acad. Sc. Paris, Serie D 281 .

Aoki, K. and Kushiro, I., 1968, Some clincpyroxenes from ultramafic inclusions in Dreiser Weiher, Eifel. Contrib. Mineral. Petrol. 18 ,pp. 326-337.

Arth, J.G., 1976, Behavior of trace elements during magmatic processes-- a summary of theoretical models and their applications. J. Res. U.S. Geol. Survey 4 ,pp. 41-47.

Barberi, F., Bizouard, H. and Varet, J., 1971, Nature of the clincpyroxene and iron-enrichment in alkalic and transitional basaltic magmas. Contrib. Mineral. Petrol. 33,pp. 93-107.

Barr, S.M. and Chase, R.L., 1974, Geology of the northern end of the Juan de Fuca plate ridge and sea-floor spreading. Can. J. Earth Sci. 11 ,pp.1384-1406.

Bence, A.E. and Albee, A.L., 1968, Empirical correction factors for the electron micro-analysis of silicates and oxides. J. Geol. 76 ,pp.382-403.

Bevier, M.L., Armstrong, R.L. and Souther, J.G., 1979, Miocene peralkaline volcanism in west-central British Columbia -- its temporal and plate tectonic setting. (in press).

Bryan, W.B., Finger, L.W. and Chayes, F., 1969, Estimating proportions in petrogenetic mixing equations by least squares approximation. Science 163 ,pp. 926-927.

Buddington, A.F. and Lindsley, D.H., 1964, Iron-titanium oxide minerals and synthetic equivalents. J. Petrol. 5 ,pp. 310-357.

Bultitude, R.J. and Green, D.H., 1968, Experimental study at high pressures on the origin of olivine nephelinite and olivine melilite nephelinite magmas. Earth Planet. Sci. Lett. 3 ,pp. 324-337.

Bultitude, R.J. and Green, D.H., 1971, Experimental study of crystal-liquid relationships at high pressures in olivine nephelinite and basanite compositions. J. Petrol. 12,pp. 121-147.

Cairnes, C.E., 1924, Coquihalla area, British Columbia. Geol. Soc. Can. Mem. 139 , 187 p.

Carmichael, I.S.E., 1967, The iron-titanium oxides of salic volcanic rocks and their associated ferromagnesian silicates. Contrib. Mineral. Petrol. 14 ,pp. 36-64.

Carmichael, I.S.E., Turner, F.J. and Verlhoogen,J., 1974, Igneous Petrology. McGraw-Hill Inc., New York, 739 p.

Cawthorne, R.G. and Collerson, K.D., 1974, The recalculation of pyroxene end-member parameters and the estimation of ferrous and ferric iron content from electron microprobe analyses. Amer. Mineralogist 59 ,pp. 1203-1208.

Cawthorne, R.G. and O'Hara, M.J., 1976, Amphibole fractionation in calc-alkaline magma genesis. Amer. J. Sci. 276 ,pp. 309-329.

Chikhaoui, M., Dupuy, C. and Dostal, J., 1978, Geochemistry of late Proterozoic volcanic rocks from Tassendjanet Area. Contrib. Mineral. Petrol. 66 ,pp. 157-164.

Church, S.E. and Tilton, G.R., 1973, Lead and strontium isotope studies in the Cascade Mountains: bearing on andesite genesis. Geol. Soc. Amer. Bull. 84 ,pp. 1135-1154.

Clague, D.A. and Jarrard, R.D., 1973, Tertiary Pacific plate motion deduced from the Hawaiian Emperor Chain. Geol. Soc. Amer. Bull. 84 ,pp. 1135-1154.

Coates, J.A., 1974, Geology of the Manning Park area, British Columbia. Geol. Surv. Can. Bull. 238 , 177p.

Dickinson, W.R., 1973, Widths of modern arc-trench gaps in relation to past duration of igneous activity in association with magmatic arcs. J. Geophys. Res. 78,pp. 3376-3389.

Drake, M.J. and Weill, D.F., 1975, Partition of Sr,Ba,Ca,Y,Eu^{2+},Eu^{3+}, and other REE between plagioclase feldspar and magmatic liquid: an experimental study. Geochim. Cosmochim. Acta 39 ,pp. 689-712.

Duchesne, J.-C., 1978, Quantitative modelling of Sr, Ca, Rb, and K in the Bjerkrem-Sogndal layered lopolith (S.W. Norway). Contrib. Mineral. Petrol. 66 ,pp. 175-184.

Duchesne, J.-C. and Demaiffe, D., 1978, Trace elements and anorthosite genesis. Earth Planet. Sci. Lett. 38 ,pp. 249-272.

Dudas, M.J., Schmitt, R.A. and Harward, M.E., 1971, Trace element partitioning between volcanic plagioclase and dacitic pyroclastic matrix. Earth Planet. Sci. Lett. 11,pp. 440-446.

Eggler, D.H., 1972, Water-saturated and undersaturated melting relations in a Paricutin andesite and an estimate of water content in the natural magma. Contrib. Mineral. Petrol. 34,pp. 261-271.

Eggler, D.H., 1974, Application of a portion of the system CaAl Si O -NaAlSi O -SiO -MgO-Fe-O -H O-CO to genesis of the calc-alkaline suite. Amer. J. Sci. 274 ,pp. 297-315.

Eggler, D.H. and Burnham, C.W., 1973, Crystallization and fractionation in the system andesite-H O-CO -O at pressures to 10 kb. Geol. Soc. Amer. Bull. 84 ,pp. 2517-2532.

Eichelberger, J.C., 1978, Andesitic volcanism and crustal evolution. Nature 275 ,pp.21-27.

Elston, W.E., Rlhodes, R.C., Coney, P.J. and Deal, E.G., 1976, Progress report on the Mogollon Plateau volcanic field, Southwestern New Mexico, No. 3 - Surface expression of pluton. in Cenozoic Volcanism in Southwestern New Mexico, Elston, W.E. and Northrop, S.A.,eds., New Mexico Geol. Soc., Special Publication No. 5, pp.3-28.

Ewart, A., Bryan, W. and Gill, J., 1973, Mineralogy and geochemistry of the Younger volcanic islands of Tonga, S.W. Pacific. J. Petrol. 14 ,pp. 429-465.

Ewart, A., Green, D.C., Carmichael, I.S.E. and Brown, F.H., 1971, Voluminous low temperature rlhyolitic magmas in New Zealand. Contrib. Mineral. Petrol. 33 ,pp. 128-144.

Ewart, A. and Stipp, J.J., 1968, Petrogenesis cf the vclcanic rocks of the Central North Island, New Zealand, as indicated by a study of $^{87}Sr/^{86}Sr$ ratios, and Sr, Rb, K, U, Th abundances. Geochim. Cosmochim. Acta 32 ,pp. 699-736.

Ewart, A. and Taylor, S.R., 1969, Trace element gecchemistry of the rhyolitic volcanic rocks of Central North Island, New Zealand. Phenocryst data. Contrib. Mineral. Petrol. 22 ,pp. 127-146.

Ewart, A., Taylor, S.R. and Capp, A.C., 1968, Trace and minor element geochemistry cf the rhyolitic volcanic rocks of Central North Island, New Zealand. Total rcck and residual liquid data. Contrib. Mineral. Petrol. 18 ,pp. 76-104.

Ferrara, G. and Treuil, M., 1974 Petrological implications of trace element and Sr isotope distributions in basalt-pantellerite series. Bull. Volcanologique 38 ,pp. 548-574.

Fisher, R.V., 1966, Rocks composed of volcanic fragments and their classification. Earth Sci. Review 1 ,pp. 287-298.

Flanagan, F.J., 1973, 1972 values for international gecchemical reference samples. Geochim. Cosmochim. Acta 37,pp. 1189-1200.

Gary, M., McAfee, R.,Jr. and Wolf, C.L.,eds., 1972, Glcssary of Geolcgy, American Geological Institute, Washington, D.C., 805p.

Gill, J.B., 1978, Role of trace lement partition coefficients in models of andesite genesis. Geochim. Cosmcchim. Acta 42,pp. 709-724.

Green, N.L., 1977, Multistage andesite genesis in the Garibaldi Lake area, southwestern British Columbia. Ph.D. Thesis, University of British Columbia, 246p.

Green, T.H., 1972, Crystallization of calc-alkaline andesite under controlled high-pressure hydrous conditions. Contrib. Mineral. Petrol. 34 ,pp. 150-166.

Green, T.H. and Ringwood, A.E., 1967, Crystallizatien cf basalt and andesite under high pressure hydrous conditions. Earth Planet. Sci. Lett. 3 ,pp. 481-489.

Green, T.H. and Ringwood, A.E., 1968, Genesis of the calc-alkaline igneous suite. Contrib. Mineral. Petrol. 18 ,pp. 105-162.

Griffin, W.L. and Murthy, V.R., 1969, Distribution of K, Rb, Sr, and Ba in some minerals relevant to basalt genesis. Geochim. Cosmochim. Acta 33 ,pp. 1389-1414.

Grutzeck, M.W., Kridelbaugh, S.J. and Weill, kD.F., 1974, The distribution of Sr and the REE betweeen diopside and silicate liquid. Geophys. Res. Lett. 1 ,pp. 273-275.

Gunn, B.M., 1974, Systematic petrochemical differences in andesite suites. Bull. Volcanologique 38 ,pp. 481-492.

Haggerty, S.J., 1976, Opaque minerals in terrestrial igneous rocks. in Oxide Minerals, Mineralogical Soc. Amer. Short Course Notes 3 ,pp. 101-300.

Hakli, T.A. and Wright, T.L., 1967, The fracticnation of nickel between olivine and augite as a geothermometer. Geochim. Cosmochim. Acta 31 ,pp. 877-884.

Hamilton, D.L., Burnham, C.W. and Osborn, E.F., 1964, The solubility of water and effects of oxygen fugacity and water content on crystallization in mafic magmas. J. Petrol. 5 ,pp. 21-39.

Hart, S.R. and Brooks, C., 1974, Clinopyroxene-matrix partitioning of K, Rb, Cs, Sr, and Ba. Geochim. Cosmochim. Acta 38 ,pp. 1799-1806.

Hatherton, T. and Dickinson, W.R., 1969, The relationship between andesitic volcanism and seismicity in Indonesia, the Lesser Antilles, and other island arcs. J. Geophys. Res. 74 ,pp. 5301-5310.

Higuchi, H. and Nagasawa, H., 1969, Partition of trace elements betwen rock-forming minerals and the host volcanic rocks. Earth Planet. Sci. Lett. 7 ,pp. 281-287.

Hutchinson, C.S., 1974, Laboratory Handbook of Petrographic Techniques. John Wiley and Sons, New York, 527p.

Irvine, T.N. And Baragar, W.R.A., 1971, A guide to the chemical classification of the common volcanic rocks. Can. J. Earth Sci. 8,pp. 523-548.

Irving, A.J., 1978, A review of experimental studies of crystal/liquid trace element partitioning. Geochim. Cosmochim. Acta 42 ,pp. 743-770.

Korringa, M.K. and Noble, D.C., 1971, Distribution of Sr and Ba between natural feldspar and igneous melt. Earth Planet. Sci. Lett. 11 ,pp. 147-151.

Kudo, A.m. and Weill, D.F., 1970, An igneous plagioclase thermometer. Contrib. Mineral. Petrol. 25 ,pp. 52-65.

Kushiro, I., 1974, Melting of hydrous upper mantle and possible generation of andesitic magma: an approach from synthetic systems. Earth Planet. Sci. Lett. 22 ,pp. 294-299.

Kushiro, I., 1978, Density and viscosity of hydrous calc-alkaline magma at high pressures. Carnegie Inst. Wash. Yearbook 77 ,pp. 675-677.

Lambert, M.B., 1974, The Bennett Lake cauldron subsidence complex, British Columbia and Yukon Territory. Geol. Surv. Can. Bull. 227 , 213p.

Lambert, R.S.J., Holland, J.G. and Owen, P.F., 1974, Chemical petrology of a suite of calc-alkaline lavas from Mount Ararat, Turkey. J. Geol. 82 ,pp. 419-438.

Larson, R.L., 1972, Bathymetry, magnetic anomalies, and plate tectonic history of the mouth of the Gulf of California. Geol. Soc. Amer. Bull. 83 ,pp. 3345-3360.

Leake, B.E., 1978, Nomenclature of amphiboles. Mineralog. Mag. 42 ,pp. 533-563.

Leeman, W.P., 1974, Experimental determination of partitioning of divalent cations between olivine and basaltic liquid. Ph.D. Thesis, Part II, University of Oregon, pp. 231-303.

Leeman, W.P., 1976, Petrogenesis of McKinney (Snake River) olivine tholeiite in light of rare-earth element and Cr/Ni distributions. Geol. Soc. Amer. Bull. 87 ,pp. 1582-1586.

Leeman, W.P. and Lindstrom, D.J., 1978, Partitioning of Ni^{2+} between basaltic and synthetic melts and olivines - an experimental study. Geochim. Cosmochim. Acta 42,pp. 801-816.

Leeman, W.P., Ma, M.-S., Murali, A.V. and Schmitt, R.A., 1978, Empirical estimation of magnetite/liquid distribution coefficients for some transition elements. A correction. Contrib. Mineral. Petrol. 66 ,p. 429.

Le Maitre, R.W., 1976, Some problems of the projection of chemical data into mineralogical classifications. Contrib. Mineral. Petrol. 56 ,pp. 181-189.

Lindstrom, D.J., 1976, Experimental study of the partitioning of the transition metals between clinopyroxene and coexisting silicate liquids. Ph.D. Thesis, University of Oregon, 188p.

Lindstrom, D.J. and Weill, D.F., 1978, Partitioning of transition metals between diopside and coexisting silicate liquids. I. Nickel, cobalt, and manganese. Geochim. Cosmochim. Acta 42 ,pp. 817-832.

Lipman, P.W., 1965, Chemical composition of glassy and crystalline volcanic rocks. U.S. Geol. Surv. Bull. 1201-d,pp. D1-D24.

Mathez, E.H., 1973, Refinement of the Kudo-Weill plagioclase thermometer and its application to basaltic rocks. Contrib. Mineral. Petrol. 41 ,pp. 61-72.

Mazullo, L.J., Dixon, S.A. and Lindsley, D.H., 1975, T-fO relationships in Mn-bearing Fe-Ti oxides. Geol. Soc. Amer. Abst. with Prog. 7 ,p. 1192.

McIntyre, G.A., Brooks, C., Compston, W. and Turek, A., 1966, The statistical assessment of Rb-Sr isochrons. J. Geophys. Res. 71 ,pp. 5459-5468.

McKay, G.A. and Weill, D.F., 1976, Petrogenesis of KREEP. Proc. Seventh Lunar Sci. Conf.,pp. 2427-2447.

McKay, G.A. and Weill, D.F., 1977, KREEP revisited. Proc. Eighth Lunar Sci. Conf.,pp. 2339-2355.

Minster, J.F. and Allegre, C.J., 1978, Systematic use of trace elements in igneous processes. Part III: inverse problem of batch partial melting in volcanic suites. Contrib. Mineral. Petrol. 68 ,pp. 37-52.

Minster, J.F., Jordan, T.H., Molnar, P. And Haines, E., 1974, Numerical modelling of instantaneous plate tectonics. Geophys. J. R. Astr. Soc. 36,pp. 541-576.

Monger, J.W.H., 1969, Hope map-area, British Columbia. Geol. Surv. Can. Paper 69-47, 75p.

Mysen, B.O., 1978a, Experimental determination of nickel partition coeficients between liquid, pargasite, and garnet peridotite minerals and concentration limits of behvior according to Henry's Law at high pressure and temperature. Amer. J. Sci. 278 ,pp. 217-243.

Mysen, B.O., 1978b, The role of descending plates in the formation of andesitic melts beneath island arcs. Carnegie Inst. Wash. Yearbook 77 ,pp. 797-801.

Mysen, B.O., 1978c, Experimental determination of rare earth element partitioning between hydrous silicate melt, amphibole, and garnet peridotite minerals at upper mantle pressures and temperatures. Geochim. Cosmochim. Acta 42,pp. 1253-1263.

Mysen, B.O. and Boettcher, A.L., 1975a, Melting of a hydrous mantle: I. Phase relations of natural peridotite at high-pressures and temperatures with controlled activities of water, carbon dioxide, and hydrogen. J. Petrol. 16 ,pp. 520-548.

Mysen, B.O. and Boettcher, A.L., 1978b, Melting of a hydrous mantle: II. Geochemistry of crystals and liquids formed by anatexis of mantle peridotite at high-pressures and temperatures as a function of controlled activities of water, carbon dioxide, and hydrogen. J. Petrol. 16 ,pp. 549-593.

Nagasawa, H., 1970, Rare earth concentrations in zircons and apatites and their host dacites and granites. Earth Planet. Sci. Lett. 9 ,pp. 359-364.

Nagasawa, H. and Schnetzler, C.C., 1971, Partitioning of rare earth, alkali and alkaline earth elements between phenocrysts and acidic igneous magma. Geochim. Cosmochim. Acta 35 ,pp. 953-968.

Nicholls, I.A., 1971, Petrology of Santorini volcano, Cyclades, Greece. J. Petrol. 12 ,pp. 67-119.

Nicholls, I.A. and Ringwood, A.E., 1973, Effect of water on olivine stability in tholeiites and the production of silica-saturated magmas in the island-arc environment. J. Geol. 81 ,pp. 285-300.

Nicholls, I.A. and Whitford, D.J., 1976, Primary magmas associated with Quaternary volcanism in the western Sundra Arc, Indonesia. in Volcanism in Australasia, Johnson, R.W.,ed., Elsevier, New York,pp. 77-90.

Nixon, G.T., 1979, X-ray fluorescence analysis for major element oxides. Department of Geological Sciences, University of British Columbia.

Norrish, K. and Hutton, J.T., 1969, An accurate X-ray spectrographic method for the analysis of a wide range of geological samples. Geochim. Cosmochim. Acta 33,pp. 431-453.

Onuma, N., Higuchi, H., Wakita, H. and Nagasawa, H., 1968, Trace element partition between two pyroxenes and the host volcanic rocks. Earth Planet. Sci. Lett. 5 ,pp. 47-51.

Osborn, E.F., 1969, Experimental aspects of the calc-alkaline differentiation. in Proceedings of the Andesite Conference, McBirney, A.R.,ed., Oreg. Dept. Geol. Miner. Ind. Bull. 65 ,pp. 33-42.

Papike, J.J., Cameron, K.L. and Baldwin, K., 1974, Amphiboles and pyroxenes: characterization of other than quadrilateral components and estimation of ferric iron from microprobe data. Geol. Soc. Amer. Abst. With Prog. 6,pp. 1053-1054.

Pearce, T.H., Gorman, B.E. and Birkett, T.C., 1977, The relationship between major element chemistry and tectonic environment of basic and intermediate volcanic rocks. Earth Planet. Sci. Lett. 36,pp. 121-132.

Philpotts, J.A. and Schnetzler, C.C., 1970, Phenocryst-matrix partition coefficients for K, Rb, Sr and Ba, with applications to anorthosite and basalt genesis. Geochim. Cosmochim. Acta 34,pp. 307-322.

Pitman III, W.C., Larson, R.L. and Herron, E.M., 1974, Geol. Soc. Amer. Map, MC-6.

Richards, T., 1971, Plutonic rocks between Hope, B.C. and the 49 parallel. Ph.D. Thesis, University of British Columbia, 178p.

Riddihough, R.P., 1977, A model for recent plate interactions off Canada's West Coast. Can. J. Earth Sci. 14,pp. 384-396.

Riddihough, R.P. and Hyndman, R.D., 1976, Canada's active western margin - the case for subduction. Geoscience Can. 3,pp. 269-278.

Robertson, J.K. and Wyllie, P.J., 1971, Rock-water systems, with special reference to the water-deficient region. Amer. J. Sci. 271,pp. 252-277.

Roeder, P.L. and Emslie, R.F., 1970, Olivine-liquid equilibrium. Contrib. Mineral. Petrol. 29,pp. 275-289.

Rucklidge, J.C. and Gasparrini, E.L., 1969, EMPADR VII, a computer program for processing electron microprobe analytical data. Department of Geology, University of Toronto.

Schnetzler, C.C. and Philpotts, J.A., 1968, Partition coefficients of rare earth elements and barium between igneous matrix material and rock-forming mineral phenocrysts -I. in Origin and Distribution of the Elements, Ahrens, L.H., ed., Pergamon,pp. 929-938.

Schnetzler, C.C. and Philpotts, J.A., 1970, Partition coefficients of rare-earth elements between igneous matrix material and rock-forming mineral phenocrysts -II. Geochim. Cosmochim. Acta 34, pp. 331-340.

Schreiber, H.D. and Haskin, L.A., 1976, Chromium in basalts: experimental determination of redox states and partitioning among synthetic silicate phases. Proc. Seventh Lunar Sci. Conf., pp. 1221-1259.

Shaw, D.M., 1970, Trace element fractionation during anatexis. Geochim. Cosmochim. Acta 34, pp. 237-243.

Shimizu, N., 1974, An experimental study of the partitioning of K, Rb, Cs, Sr, and Ba between clinopyroxene and liquid at high pressures. Geochim. Cosmochim. Acta 38, pp. 1789-1798.

Smith, R.L., 1960a, Ash flows. Geol. Soc. Amer. Bull. 71, pp. 795-842.

Smith, R.L., 1960b, Zones and zonal variations in welded ash flows. U.S. Geol. Surv. Prof. Paper 374-F, pp. 49-59.

Smith, R.E. and Smith, S.E., 1976, Use of Ti, Zr, Y, Sr, K, P, Nb in classification of basaltic magmas. Earth Planet. Sci. Lett. 32, pp. 114-120.

Souther, J.G., 1977, Volcanism and tectonic environmnets in the Canadian cordillera - a second look. in Volcanic Regimes in Canada, Baragar, W.R.A., Coleman, L.C. and Hall, J.M., eds., Geol. Ass. Can. Special Paper No. 16, pp. 3-24.

Staatz, M.H., Tabor, R.W., Weis, P.L., Robertson, J.F., Van Noy, R.M., Pattee, E.C. and Holt, C.C., 1971, Mineral resources of the Pasayten Wilderness Area, Washington. U.S. Geol. Surv. Bull. 1325, 255p.

Steiger, R.H. and Jager, E., 1977, Subcommission on geochronology: Convention on the use of decay constants in geo- and cosmochronology. Earth Planet. Sci. Lett. 36, pp. 359-362.

Sun, C.-O., Williams, R.J. and Sun, S-S., 1974, Distribution coefficients of Eu and Sr for plagioclase-liquid and clinopyroxene-liquid equilibria in oceanic ridge basalt: an experimental study. Geochim. Cosmochim. Acta 38, pp. 1415-1433.

Sun, S-S. and Hanson, G.N., 1976, Rate earth element evidence for the differentiation of the McMurdo volcanics, Ross Island, Antarctica. Contrib. Mineral. Petrol. 54, pp. 139-155.

Tanaka, T. and Nishizawa, O., 1975, Partitioning of REE, Ba, and Sr between crystal and liquid phases for a natural silicate system at 20 kb pressure. Geochem. J. 9,pp. 161-166.

Thorpe, R.S., Potts, P.J. and Francis, P.W., 1976, Rare earth data and petrogenesis of andesite from the North Chilean Andes. Contrib. Mineral. Petrol. 54,pp. 65-78.

Tuttle, O.F. and Bowen, N.L., 1958, Origin of granite in the light of experimental studies in the system NaAlSi O - KAlSi O -SiO -H O. Geol. Soc. Can. Mem. 74, 153p.

Vance, J.A., 1965, Zoning in igneous plagioclase; patchy zoning. J. Geol. 73,pp. 636-651.

Verhoogen, J., 1962, Distribution of titanium between silicates and oxides in igneous rock series. Amer. J. Sci. 260,pp. 211-220.

Watters, B.N., 1975, X-ray fluorescence spectrometry analytical techniques. Department of Geological Sciences, University of British Columbia.

Weill, D.F. and McKay, G.A., 1975, The partitioning of Mg, Fe, Sr, Ce, Sm, Eu, and Yb in lunar igneous systems and a possible origin of KREEP by equilibrium partial melting. Proc. Sixth Lunar Sci. Conf.,pp. 1143-1158.

Whitford, D.J., Nicholls, I.A. And Taylor, S.R., 1979, Spatial variations in the geochemistry of Quaternary lavas across the Sundra arc in Java and Bali. Contrib. Mineral. Petrol. (in press).

Wilkinson, J.F.G., 1971, The petrology of some vitrophyric calc-alkaline volcanics from the Carboniferous of New South Wales. J. Petrol. 12,pp. 587-619.

Winchester, J.A. and Floyd, P.A., 1977, Geochemical discrimination of different magma series and their differentiation products using immobile elements. Chem. Geol. 20,pp. 325-343.

Wise, W.S., 1969, Geology and petrology of the Mt. Hood area: a study of High Cascade volcanism. Geol. Soc. Amer. Bull. 80,pp. 969-1006.

Wood, B.J. and Banno, S., 1973, Garnet-orthopyroxene and orhopyroxene-clinopyroxene relationships in simple and complex systems. Contrib. Mineral. Petrol. 42,pp. 109-124.

Wright, T.H. and Doherty, P.C., 1970, A linear programming and least squares computer method for solving petrologic mixing problems. Geol. Soc. Amer. Bull. 81,pp. 1995-2008.

Wyllie, P.J., 1973, Experimental petrology and global tectonics: a review. Tectonphysics 17,pp. 189-209.

Zielinski, R.A., 1975, Trace element evaluation of a suite of rocks from Reunion Island, Indian Ocean. Geochim. Cosmochim. Acta 39,pp. 713-734.

APPENDIX I: WHOLE-ROCK ANALYTICAL DATA

Whole-rock analyses performed by X-ray flucrescence spectrometry include 10 major elements, and the trace elements Cr, V, Ni, Sr, Rb, Ba, Nb, Y, Zr, Ce, and Nd. Concentraticns of major elements, with the exception of sodium, were determined from glass discs diluted with Chemplex Grade III flux in the manner discussed by Norrish and Hutton (1969). Sodium and trace element concentrations were determined from undiluted pressed powder pellets.

The technique for analysis and data reduction of major elements is presented by Nixon (1979). Techniques for trace element analysis, and reduction program procedures are presented in Appendix IVa and IVb.

Total water and carbon dioxide contents were determined on an apparatus designed after Hutchinson (1974), and the analytical procedures are discussed in Appendix IVc. Ferrous iron concentrations were determined by wet chemical methods outlined in Appendix IVd.

Major element analyses are presented on the following pages for twenty-six samples (locations shown cn Plate II) of the Coquihalla Volcanic Complex. These analyses have been recalculated to 100%, but the reported sums are for the original XRF analyses. Trace element concentrations are reported in parts per million. Normative compositions were calculated on a volatile-free basis, after the ferrous iron content of all rocks had been adjusted by the procedure of Le Maitre (1976), in order to normalize the suite of rocks to oxidation states more representative of their original compositicns. The normative

calcite contents reported are taken from separate norm calculations done on a volatile-included basis.

APPENDIX I: WHOLE-ROCK ANALYSES

	-PYROXENE ANDESITE-		-HORNBLENDE ANDESITE-		
	251	61	380	252	30
SIO2	52.10	57.32	56.44	54.48	55.19
TIO2	0.98	0.80	0.98	1.04	0.86
AL2O3	17.12	15.89	16.89	17.25	17.24
FE2O3	4.72	3.62	4.62	4.90	5.08
FEO	3.46	3.72	2.81	3.28	2.31
MNO	0.17	0.15	0.15	0.15	0.15
MGO	4.25	4.21	3.27	3.08	3.51
CAO	9.26	6.38	6.48	7.76	7.71
NA2O	2.79	3.02	3.69	3.00	3.05
K2O	1.00	2.22	1.74	1.32	1.41
P2O5	0.27	0.22	0.30	0.27	0.27
CO2	2.79	0.15	0.35	1.06	0.35
H2O	1.10	2.32	2.25	2.37	2.86
SUM	99.16	100.31	98.80	99.17	100.40
	TRACE ELEMENT CHEMISTRY				
NI	23	9	8	10	14
CR	50	64	11	13	21
V	241	197	195	218	186
SR	578	480	579	572	592
RB	21	53	37	15	31
BA	589	873	906	672	691
ZR	107	156	150	126	125
Y	26	28	29	28	28
NB	5	7	7	6	6
CE	29	48	52	22	41
ND	16	29	29	19	21
	NORMATIVE COMPOSITION				
Q	8.66	11.10	9.56	10.53	10.25
OR	6.21	13.53	10.61	8.18	8.68
AB	26.32	27.98	34.19	28.26	28.52
AN	32.82	23.99	25.17	31.17	30.40
DI	10.88	5.76	4.63	5.90	6.08
EN	7.31	9.76	7.60	6.93	7.90
FS	0.61	2.83	2.66	3.31	3.04
MT	5.18	3.42	3.46	3.61	3.29
IL	1.43	1.15	1.41	1.52	1.25
AP	0.59	0.47	0.71	0.59	0.59
C	0.0	0.0	0.0	0.0	0.0
CC	7.17	0.39	0.91	2.78	0.92
D.I.	41.18	52.61	54.36	46.97	47.45

APPENDIX I: (CONT.)

----------HORNBLENDE ANDESITE---------

	66	38	171	4	635
SIO2	57.73	56.86	56.01	59.48	59.95
TIO2	0.86	0.91	0.95	0.83	0.78
AL2O3	17.11	16.93	16.85	17.22	16.93
FE2O3	4.39	4.42	7.34	4.23	6.03
FEO	2.58	2.87	0.0	1.74	0.0
MNO	0.14	0.12	0.13	0.13	0.15
MGO	3.12	2.63	2.96	2.36	2.42
CAO	6.15	6.20	6.51	5.85	5.11
NA2O	2.87	2.41	3.30	3.08	3.89
K2O	1.74	2.30	1.80	2.29	2.36
P2O5	0.24	0.29	0.29	0.25	0.29
CO2	0.64	1.55	0.71	0.60	0.06
H2O	2.42	2.50	3.15	1.95	2.03
SUM	100.85	99.26	100.04	100.41	99.55
		TRACE ELEMENT CHEMISTRY			
NI	10	11	7	9	6
CR	12	14	11	11	8
V	172	170	173	137	115
SR	575	555	506	568	572
RB	46	51	38	50	59
BA	831	1040	833	863	1089
ZR	145	161	165	166	164
Y	28	29	31	30	29
NB	8	8	7	7	8
CE	41	41	61	50	56
ND	24	21	27	24	28
		NORMATIVE COMPOSITION			
Q	15.03	15.67	11.30	15.74	13.04
OR	10.73	14.40	11.16	14.02	14.29
AB	26.89	22.93	31.09	28.66	35.81
AN	29.92	30.30	27.13	27.36	22.32
DI	0.23	0.13	3.82	0.82	1.39
EN	8.90	7.65	7.20	6.45	6.33
FS	3.32	3.47	2.84	2.32	2.08
MT	3.21	3.41	3.43	2.87	3.00
IL	1.25	1.34	1.39	1.20	1.11
AP	0.52	0.69	0.64	0.54	0.62
C	0.0	0.0	0.0	0.0	0.0
CC	1.68	4.07	1.87	1.56	0.16
D.I.	52.64	53.00	53.55	58.43	63.14

APPENDIX I: (CONT.)

-------COQUIHALLA MOUNTAIN STOCK-------

	632	311	318	366	310
SIO2	54.58	56.49	56.82	59.60	61.66
TIO2	1.03	0.96	0.95	0.81	0.78
AL2O3	16.98	17.44	17.43	16.73	16.93
FE2O3	4.00	4.31	2.26	3.41	3.36
FEO	5.07	3.71	6.64	3.46	2.31
MNO	0.15	0.17	0.15	0.16	0.16
MGO	4.58	3.54	3.05	3.19	2.00
CAO	8.02	6.66	6.33	6.02	4.78
NA2O	3.17	4.04	3.72	3.24	4.51
K2O	1.61	1.67	1.97	2.02	1.96
P2O5	0.28	0.29	0.24	0.23	0.25
CO2	0.06	0.08	0.12	0.03	0.16
H2O	0.47	0.64	0.32	1.09	1.15
SUM	100.20	98.73	99.67	99.44	100.31
		TRACE ELEMENT CHEMISTRY			
NI	13	11	13	10	8
CR	22	18	37	23	9
V	225	167	181	154	121
SR	512	566	489	454	511
RB	44	37	55	56	48
BA	668	823	685	785	1001
ZR	132	142	152	158	168
Y	30	30	30	31	28
NB	7	6	8	9	8
CE	34	36	35	53	58
ND	22	19	23	22	26
		NORMATIVE COMPOSITION			
Q	5.45	6.28	7.81	13.64	13.38
OR	9.63	9.96	11.78	12.17	11.74
AB	28.80	36.60	33.82	29.68	41.07
AN	27.68	24.75	25.36	25.65	20.45
DI	8.59	5.35	3.88	2.63	1.56
EN	9.88	8.07	7.34	8.10	5.09
FS	4.68	3.94	4.72	3.87	2.69
MT	3.24	3.09	3.43	2.61	2.38
IL	1.45	1.35	1.34	1.15	1.10
AP	0.59	0.61	0.51	0.49	0.53
C	0.0	0.0	0.0	0.0	0.0
CC	0.15	0.20	0.31	0.08	0.41
D.I.	43.88	52.84	53.41	55.49	66.20

APPENDIX I: (CONT.)

	--ALTERED ANDESITE--			HORNBLENDE ----DACITE---		ALTERED DACITE
	296	253	59	283	192	240
SIO2	57.40	54.09	55.01	63.29	65.52	65.89
TIO2	0.80	0.86	1.03	0.58	0.56	0.60
AL2C3	16.90	16.64	16.89	16.65	16.13	16.99
FE2O3	3.63	3.16	4.48	2.13	2.61	1.58
FEO	2.93	4.00	3.46	2.78	1.60	1.56
MNO	0.14	0.18	0.20	0.12	0.12	0.09
MGO	3.34	3.17	3.48	2.05	1.44	0.85
CAO	5.65	5.44	4.68	4.21	2.68	2.60
NA2O	3.12	3.05	4.40	4.13	4.48	4.62
K2O	1.78	2.35	2.07	2.19	2.48	3.39
P2O5	0.22	0.26	0.32	0.29	0.21	0.16
CO2	1.35	3.41	1.00	0.09	0.47	0.10
H2O	2.71	3.39	2.96	1.49	1.67	1.58
SUM	99.96	99.29	99.73	100.70	99.47	99.85
	TRACE ELEMENT CHEMISTRY					
NI	11	10	9	4	5	5
CR	20	10	11	4	7	3
V	157	187	193	99	68	33
SR	531	345	467	488	490	369
RB	48	51	43	58	62	81
BA	650	737	998	1085	1076	1280
ZR	167	127	160	171	184	239
Y	31	27	31	29	27	37
NB	7	6	8	9	9	10
CE	61	41	52	48	52	102
ND	27	20	24	25	29	43
	NORMATIVE COMPOSITION					
Q	13.99	10.09	5.50	17.40	20.91	18.25
OR	11.04	15.00	12.71	13.18	15.00	20.32
AB	29.41	29.59	41.08	37.77	41.19	42.09
AN	27.93	26.77	21.03	19.35	12.21	12.03
DI	0.0	0.45	0.75	0.0	0.0	0.0
EN	9.68	9.29	9.70	5.77	4.07	2.38
FS	3.10	3.41	3.12	2.24	1.18	0.45
MT	3.10	3.50	3.91	2.27	2.27	1.76
IL	1.17	1.29	1.49	0.82	0.80	0.85
AP	0.48	0.59	0.70	0.62	0.45	0.34
C	0.11	0.0	0.0	0.58	1.91	1.52
CC	3.52	8.90	2.60	0.23	1.21	0.26
D.I.	54.44	54.69	59.29	68.35	77.11	80.66

APPENDIX I: (CONT.)

RHYOLITE

	319	112	26	712	173
SIO2	71.10	72.82	73.92	75.53	72.87
TIO2	0.37	0.27	0.31	0.14	0.27
AL2O3	15.58	15.32	13.90	12.97	13.46
FE2O3	1.12	0.64	0.80	0.91	0.68
FEO	1.29	0.81	0.92	0.0	1.51
MNO	0.11	0.06	0.08	0.05	0.07
MGO	0.66	0.57	0.59	0.14	0.31
CAO	1.22	0.50	0.27	0.67	0.24
NA2O	4.49	4.96	4.75	3.72	5.64
K2O	3.06	2.21	2.37	3.80	3.71
P2O5	0.06	0.04	0.07	0.04	0.03
CO2	0.10	0.15	0.17	0.21	0.13
H2O	0.84	1.69	1.85	1.72	1.12
SUM	99.76	99.96	99.80	100.56	99.56
		TRACE ELEMENT CHEMISTRY			
NI	8	5	5	2	7
CR	13	7	5	2	23
V	37	20	21	11	11
SR	184	243	175	95	120
RB	88	61	55	92	84
BA	1033	1210	1247	1006	1593
ZR	160	156	168	79	203
Y	30	17	23	28	26
NB	12	9	9	12	11
CE	55	54	62	29	89
ND	27	25	23	16	29
		NORMATIVE COMPOSITION			
Q	27.72	31.65	33.97	36.04	23.29
OR	18.29	13.28	14.34	23.15	22.09
AB	40.79	45.31	43.68	34.44	51.03
AN	5.73	2.26	0.90	3.16	0.46
DI	0.0	0.0	0.0	0.0	0.44
EN	1.84	1.60	1.67	0.40	0.69
FS	0.49	0.22	0.27	0.15	0.20
MT	1.38	0.83	1.01	0.55	1.35
IL	0.52	0.38	0.44	0.20	0.38
AP	0.13	0.09	0.15	0.09	0.06
C	3.10	4.39	3.57	1.82	0.0
CC	0.26	0.39	0.44	0.55	0.33
D.I.	86.81	90.24	91.99	93.63	96.42

APPENDIX II: MICROPROBE MINERAL ANALYSES

All mineral analyses were performed by an ARI-SEMQ electron microprobe. The accelerating voltage was 15 KV, the specimen current 50 nannoamperes, and a beam width of 10-20 microns was generally used. Most analyses were reduced using the correction procedures of Bence and Albee (1968) and Albee and Ray (1970); analyses which include vanadium were reduced by classical correction procedures using the EMPADR VII computer program of Rucklidge and Gasparrini (1969). A combination of natural and synthetic minerals were used as standards.

Formula bases, ferric iron contents, and end-member compositions were calculated using the MINTABLE program discussed in Appendix Vd. This program utilizes the reduction procedures of Cawthorne and Collerson (1974) for pyroxenes, Anderson (1968) and Carmichael (1967) for iron- titanium oxides, and Papike et al. (1974) for amphiboles.

Mineral analyses are presented on the following pages, and elements which were not determined in particular analyses are indicated by dashes (--).

APPENDIX IIA: PYROXENE ANALYSES

	---DIORITE---		PYROXENE --ANDESITE---		HORNBLENDE ---ANDESITE--	
	632	318	251	251	252	252
SIO2	52.02	52.64	50.38	52.41	50.22	50.13
TIO2	0.16	0.29	1.09	0.56	0.73	0.71
AL2O3	0.53	0.99	4.51	1.75	4.63	2.88
CR2O3	--	--	--	--	--	0.03
V2O3	--	--	--	--	--	0.07
NIO	--	--	--	--	--	0.0
FEO	9.60	10.61	9.12	7.95	6.88	8.14
MNO	0.34	0.47	0.24	0.49	0.28	0.29
MGO	14.25	14.08	14.93	16.04	14.66	14.96
CAO	22.93	20.91	20.16	20.21	22.66	21.59
BAO	0.07	0.0	0.06	0.0	0.12	0.0
NA2O	0.28	0.39	0.32	0.36	0.32	0.38
K2O	0.02	0.0	0.0	0.02	0.04	0.0
SUM	100.20	100.38	100.81	99.79	100.54	99.18
	FORMULA BASED ON 6 OXYGENS					
SI	1.9550	1.9677	1.8614	1.9442	1.8574	1.8870
AL IV	0.0235	0.0323	0.1386	0.0558	0.1426	0.1130
TI	0.0045	0.0082	0.0303	0.0156	0.0203	0.0201
AL VI	0.0	0.0114	0.0578	0.0207	0.0592	0.0148
CR	--	--	--	--	--	0.0009
V	--	--	--	--	--	0.0021
NI	--	--	--	--	--	0.0
FE2+	0.3017	0.3317	0.2818	0.2466	0.2128	0.2563
FE3+	0.0080	0.0010	0.0	0.0	0.0	0.0
MN	0.0109	0.0150	0.0076	0.0155	0.0088	0.0093
MG	0.7982	0.7845	0.8222	0.8869	0.8082	0.8394
CA	0.9233	0.8375	0.7981	0.8033	0.8980	0.8708
BA	0.0010	0.0	0.0009	0.0	0.0017	0.0
NA	0.0204	0.0283	0.0229	0.0259	0.0229	0.0277
K	0.0010	0.0	0.0	0.0009	0.0019	0.0
CA	45.39	42.54	41.79	41.14	46.58	44.07
MG	39.24	39.85	43.06	45.43	41.92	42.48
FE	15.37	17.61	15.15	13.43	11.50	13.44
XY	2.06	2.02	2.02	2.02	2.03	2.04
Z	1.98	2.00	2.00	2.00	2.00	2.00
	MOLE PERCENT END MEMBERS					
JD	1.39	2.69	2.33	2.64	2.57	2.66
AC	0.77	0.09	0.0	0.0	0.0	0.0
FECATS	0.0	0.0	0.0	0.0	0.0	0.14
TICATS	0.44	0.80	2.96	1.54	1.96	1.93
CATS	0.0	0.0	5.48	0.91	6.51	2.87
WO	44.27	40.81	34.83	38.33	39.17	39.34
EN	38.46	38.60	40.23	43.67	39.07	40.30
FS	14.68	17.01	14.16	12.91	10.71	12.75

APPENDIX IIA: (CONTINUED)

	-HORNBLENDE ANDESITE--			DACITE	---DIORITE---	
	252	635	004	283	318	632
SIO2	52.16	52.54	50.93	52.13	51.72	51.47
TIO2	0.16	0.47	0.65	0.29	0.44	0.33
AL2O3	0.81	1.45	2.52	1.07	1.04	0.86
CR2O3	0.01	--	--	0.01	--	--
V2O3	0.0	--	--	0.08	--	--
NIO	0.0	--	--	0.01	--	--
FEO	8.83	7.66	8.37	8.43	24.49	21.77
MNO	0.68	0.56	0.36	0.65	0.73	0.62
MGO	14.59	15.44	15.35	14.93	20.26	22.68
CAO	21.97	21.44	21.77	21.95	1.95	2.07
BAO	0.0	0.10	0.04	0.0	0.0	0.0
NA2O	0.30	0.36	0.30	0.36	0.01	0.02
K2O	0.02	0.05	0.05	0.0	0.0	0.02
SUM	99.53	100.07	100.34	99.91	100.64	99.84
	FORMULA BASED ON 6 OXYGENS					
SI	1.9614	1.9503	1.8963	1.9496	1.9475	1.9332
AL IV	0.0359	0.0497	0.1037	0.0472	0.0462	0.0381
TI	0.0045	0.0131	0.0182	0.0082	0.0125	0.0093
AL VI	0.0	0.0137	0.0069	0.0	0.0	0.0
CR	0.0003	--	--	0.0003	--	--
V	0.0	--	--	0.0024	--	--
NI	0.0	--	--	0.0003	--	--
FE2+	0.2777	0.2378	0.2606	0.2637	0.7712	0.6838
FE3+	0.0	0.0	0.0	0.0	0.0	0.0
MN	0.0218	0.0177	0.0114	0.0207	0.0234	0.0199
MG	0.8178	0.8543	0.8519	0.8323	1.1371	1.2697
CA	0.8852	0.8527	0.8685	0.8796	0.0787	0.0833
BA	0.0	0.0015	0.0006	0.0	0.0	0.0
NA	0.0219	0.0259	0.0217	0.0261	0.0007	0.0015
K	0.0010	0.0024	0.0024	0.0	0.0	0.0010
CA	44.20	43.45	43.59	44.06	3.91	4.05
MG	40.84	43.53	42.76	41.69	56.56	61.74
FE	14.96	13.02	13.65	14.25	39.53	34.21
XY	2.03	2.02	2.04	2.03	2.02	2.07
Z	2.00	2.00	2.00	2.00	1.99	1.97
	MOLE PERCENT END MEMBERS					
JD	2.22	2.92	2.36	2.53	0.07	0.23
AC	0.0	0.0	0.0	0.0	0.0	0.0
FECATS	0.01	0.0	0.0	0.13	0.0	0.0
TICATS	0.44	1.29	1.75	0.79	1.22	0.90
CATS	0.20	0.37	2.38	0.23	1.01	0.82
WO	42.75	41.00	39.60	42.11	2.75	3.15
EN	39.80	41.90	40.86	40.40	55.89	61.06
FS	14.58	12.53	13.05	13.80	39.06	33.84

APPENDIX IIB: HORNBLENDE ANALYSES

	---HORNBLENDE ANDESITE---				-HORNBLENDE DACITE-		
	252	252	635	004	283	283	164
SIO2	41.26	43.06	43.64	45.20	45.20	43.95	43.62
TIC2	3.32	3.07	3.22	2.64	2.64	2.81	3.07
AL2O3	10.63	11.04	9.70	8.55	9.40	9.27	11.11
CR2O3	--	0.01	--	--	0.02	0.01	--
V2O3	--	0.11	--	--	0.14	0.10	--
NIO	--	0.01	--	--	0.01	0.0	--
FEO	12.37	11.71	11.92	11.78	12.46	12.10	11.76
MNO	0.36	0.23	0.40	0.44	0.36	0.36	0.31
MGO	15.09	14.59	14.63	15.23	14.54	14.40	14.80
CAO	11.26	11.17	11.04	11.54	11.52	11.13	11.45
BAO	0.16	--	0.18	0.05	--	--	0.0
NA2O	2.54	2.47	2.40	2.22	2.19	2.24	2.50
K2O	0.44	0.42	0.54	0.50	0.49	0.45	0.47
SUM	97.43	97.89	97.67	98.15	98.97	96.82	99.09
	FORMULA BASED ON 23 OXYGENS						
SI	6.1494	6.3172	6.4358	6.6103	6.5645	6.5249	6.3237
AL IV	1.8506	1.6828	1.5642	1.3897	1.4355	1.4751	1.6763
TI	0.3721	0.3387	0.3571	0.2903	0.2883	0.3137	0.3347
AL VI	0.0167	0.2262	0.1218	0.0841	0.1735	0.1470	0.2221
CR	--	0.0012	--	--	0.0023	0.0012	--
V	--	0.0129	--	--	0.0163	0.0119	--
NI	--	0.0012	--	--	0.0012	0.0	--
FE2+	1.2885	1.4367	1.4702	1.4408	1.5134	1.5024	1.4258
FE3+	0.2534	0.0	0.0	0.0	0.0	0.0	0.0
MG	3.3523	3.1905	3.2159	3.3199	3.1475	3.1866	3.1981
MN	0.0458	0.0288	0.0503	0.0549	0.0446	0.0456	0.0383
CA	1.7981	1.7558	1.7444	1.8083	1.7926	1.7704	1.7785
NA	0.0	0.0080	0.0402	0.0017	0.0203	0.0212	0.0024
BA	0.0093	--	0.0104	0.0029	--	--	0.0
NA	0.7340	0.6946	0.6461	0.6278	0.5964	0.6236	0.7003
K	0.0837	0.0786	0.1016	0.0933	0.0908	0.0852	0.0869
CA	27.73	27.38	26.92	27.30	27.59	27.22	27.61
MG	51.70	49.76	49.62	50.12	48.44	48.99	49.65
FE	20.58	22.86	23.46	22.58	23.98	23.80	22.73
Z	8.00	8.00	8.00	8.00	8.00	8.00	8.00
Y	5.06	5.00	5.00	5.00	5.00	5.00	5.00
X	2.06	2.00	2.00	2.00	2.00	2.00	2.00
W	0.83	0.77	0.76	0.72	0.69	0.71	0.79

APPENDIX IIC: FELDSPAR ANALYSES

	DIORITE			PYROXENE ANDESITE		HORNBLENDE ANDESITE	DACITE		RHYOLITE			DIORITE
	632	318	318	251	061	252	164	192	173	712	223	632
SIO2	53.08	50.45	60.50	49.17	55.09	54.18	49.19	58.23	61.50	62.50	71.68	66.39
TIO2	0.11	0.02	0.04	0.07	0.09	0.07	0.05	0.10	0.07	0.05	0.25	0.04
AL2O3	28.74	30.41	23.88	32.29	27.90	27.72	32.32	26.79	23.60	22.96	14.99	18.80
FEO	0.43	0.51	0.21	0.40	0.45	0.44	0.31	0.12	0.31	0.26	0.19	0.47
MNO	0.00	0.01	0.02	0.04	0.00	0.08	0.00	0.00	0.07	0.06	0.09	0.02
MGO	0.04	0.01	0.02	0.06	0.00	0.07	0.04	0.03	0.04	0.04	0.04	0.00
CAO	11.77	14.36	6.69	15.95	10.38	10.80	15.68	7.56	5.64	5.24	0.36	0.79
BAO	0.10	--	--	--	--	0.08	--	0.01	0.15	0.25	0.32	0.38
NA2O	4.88	3.46	7.88	2.55	5.45	5.45	2.71	7.23	8.01	8.31	1.24	2.62
K2O	0.37	0.12	0.43	0.16	0.50	0.24	0.12	0.21	0.57	0.71	11.44	10.07
SUM	99.52	99.35	99.67	100.69	99.86	99.13	100.42	100.28	99.96	100.38	100.60	99.66
	FORMULA BASED ON 8 OXYGENS											
ST	2.4241	2.3201	2.7102	2.2394	2.4936	2.4761	2.2433	2.5972	2.7419	2.7745	3.1939	3.0077
AL	1.5470	1.6483	1.2608	1.7333	1.4884	1.4931	1.7372	1.4083	1.2401	1.2013	0.7872	1.0081
TI	0.0038	0.0007	0.0013	0.0024	0.0031	0.0024	0.0017	0.0034	0.0023	0.0017	0.0084	0.0014
FE	0.0164	0.0196	0.0079	0.0152	0.0170	0.0168	0.0118	0.0045	0.0116	0.0097	0.0071	0.0178
MN	0.0000	0.0004	0.0008	0.0016	0.0000	0.0031	0.0000	0.0000	0.0027	0.0023	0.0034	0.0008
MG	0.0027	0.0007	0.0013	0.0041	0.0000	0.0048	0.0027	0.0020	0.0027	0.0026	0.0027	0.0000
CA	0.5759	0.7076	0.3211	0.7783	0.5034	0.5288	0.7662	0.3613	0.2694	0.2492	0.0172	0.0383
BA	0.0018	--	--	--	--	0.0014	--	0.0002	0.0026	0.0043	0.0056	0.0067
NA	0.4321	0.3085	0.6844	0.2252	0.4783	0.4829	0.2396	0.6252	0.6924	0.7152	0.1071	0.2301
K	0.0216	0.0070	0.0246	0.0093	0.0289	0.0140	0.0070	0.0119	0.0324	0.0402	0.6503	0.5820
XY	1.0543	1.0445	1.0414	1.0361	1.0307	1.0543	1.0291	1.0085	1.0161	1.0253	0.8017	0.8771
Z	3.9711	3.9684	3.9711	3.9727	3.9820	3.9692	3.9806	4.0055	3.9820	3.9757	3.9811	4.0158
AN	55.94	69.16	31.17	76.85	49.81	51.56	75.65	36.18	27.10	24.81	2.22	4.51
AB	41.97	30.15	66.44	22.23	47.33	47.08	23.66	62.62	69.64	71.19	13.83	27.06
OR	2.09	0.69	2.39	0.92	2.86	1.36	0.69	1.20	3.26	4.00	83.95	68.43

APPENDIX IID: BIOTITE ANALYSES

	DIORITE	RHYOLITE					GRANITE
	310	173	173	712	223	180	183
SIO2	39.76	38.62	38.06	36.78	36.68	36.78	35.35
TIO2	4.56	4.07	4.03	4.04	4.36	4.19	3.39
AL2O3	11.90	14.55	13.96	13.81	13.97	13.84	15.58
CR2O3	--	--	0.0	--	--	--	--
V2O3	--	--	0.12	--	--	--	--
NIO	--	--	0.01	--	--	--	--
FEO	9.57	13.75	13.57	17.66	16.58	15.33	20.70
MNO	0.26	0.55	0.31	0.58	0.60	0.57	0.49
MGO	18.96	16.15	16.11	13.62	14.08	14.09	9.23
CAO	0.08	0.10	0.03	0.11	0.10	0.10	0.08
BAO	0.62	1.25	--	0.53	0.85	0.71	0.68
NA2O	0.23	0.75	0.80	0.72	0.70	0.55	0.24
K2O	9.64	7.01	7.86	8.70	8.64	8.70	9.32
SUM	95.58	96.80	94.86	96.55	96.56	94.86	95.06
			FORMULA BASED ON 22 OXYGENS				
SI	5.8081	5.6297	5.6400	5.5350	5.5041	5.5763	5.5016
AL IV	2.0488	2.3703	2.3600	2.4495	2.4707	2.4237	2.4984
TI	0.5009	0.4462	0.4491	0.4572	0.4920	0.4777	0.3968
AL VI	0.0	0.1295	0.0782	0.0	0.0	0.0495	0.3594
CR	--	--	0.0	--	--	--	--
V	--	--	0.0143	--	--	--	--
NI	--	--	0.0012	--	--	--	--
FE2+	1.1692	1.6763	1.6817	2.2226	2.0807	1.9438	2.6942
MN	0.0324	0.0684	0.0392	0.0745	0.0768	0.0737	0.0651
MG	4.1283	3.5091	3.5584	3.0551	3.1493	3.1842	2.1411
CA	0.0125	0.0156	0.0048	0.0177	0.0161	0.0162	0.0133
BA	0.0355	0.0714	--	0.0312	0.0500	0.0422	0.0415
NA	0.0651	0.2120	0.2299	0.2101	0.2037	0.1617	0.0724
K	1.7964	1.3036	1.4858	1.6702	1.6539	1.6826	1.8503
Z	7.86	8.00	8.00	7.98	7.97	8.00	8.00
Y	5.83	5.70	5.74	5.81	5.80	5.68	5.30
X	1.91	1.60	1.72	1.93	1.92	1.90	1.98

APPENDIX IIE: MAGNETITE ANALYSES

	DIORITE			PYROXENE ANDESITE		HORNBLENDE ANDESITE		DACITE		RHYOLITE		
	632	318	310	251	061	252	252	283	192	173	173	712
SIO2	1.20	0.14	0.29	0.45	0.29	0.41	0.25	0.65	0.07	0.31	0.15	0.62
TIO2	3.75	3.12	2.53	17.62	11.85	14.57	13.44	8.16	8.19	6.29	5.82	5.22
AL2O3	1.13	1.52	0.72	0.53	2.04	3.54	3.32	1.20	3.08	1.78	1.62	1.75
CR2O3	0.07	--	--	--	--	--	0.03	0.03	--	--	0.0	--
V2O3	0.0	--	--	--	--	--	1.36	1.10	--	--	0.62	--
NIO	0.0	--	--	--	--	--	0.0	0.02	--	--	0.03	--
FEO	85.52	87.58	89.56	77.06	78.71	75.24	75.89	82.47	83.50	81.90	81.98	80.11
MNO	0.24	0.25	0.46	1.07	0.59	0.88	0.68	0.15	0.80	2.27	1.49	2.89
MGO	0.03	0.09	0.14	0.14	0.05	0.13	0.09	0.05	0.16	0.67	0.88	0.11
CAO	0.03	0.05	0.09	0.07	0.34	0.17	0.06	0.14	0.01	0.14	0.0	0.21
BAO	0.0	0.0	0.17	0.11	0.0	0.24	0.0	0.0	0.02	0.18	0.0	0.23
NA2O	0.0	0.0	0.09	0.02	0.03	0.06	0.0	0.03	0.04	0.08	0.02	0.05
K2O	0.0	0.01	0.08	0.03	0.04	0.06	0.02	0.03	0.02	0.08	0.01	0.08
SUM	91.97	92.76	94.13	97.10	93.94	95.30	95.14	94.03	95.89	93.70	92.62	91.27
RECALCULATED ON ULVOSPINEL BASIS -- PROCEDURE OF ANDERSON (1968)												
FEO	33.88	34.04	32.95	46.32	41.61	44.90	44.80	38.83	39.80	34.00	34.14	32.26
FE2O3	57.39	59.50	62.91	34.16	41.23	33.72	34.56	48.50	48.57	53.24	53.16	53.18
SUM	97.72	98.72	100.44	100.52	98.07	98.68	98.60	98.89	100.76	99.04	97.95	96.60
%USP	11.55	9.49	7.44	50.17	36.49	46.34	43.74	25.16	25.21	17.34	17.61	14.83
RECALCULATED ON ULVOSPINEL BASIS -- PROCEDURE OF CARMICHAEL (1967)												
FEO	35.79	34.26	33.47	47.07	42.07	45.63	45.19	39.88	39.91	34.55	34.40	33.32
FE2O3	55.26	59.26	62.34	33.33	40.72	32.91	34.11	47.34	48.44	52.63	52.88	52.01
SUM	97.51	98.70	100.38	100.44	98.02	98.60	98.56	98.77	100.75	98.98	97.92	96.48
%USP	15.62	9.57	8.33	51.32	35.17	42.69	39.01	25.92	23.15	19.13	17.38	17.77

APPENDIX IIF: ILMENITE ANALYSES

	---DIORITE---		HORNBLENDE ANDESITE	DACITE	RHYOLITE
	632	632	252	283	180
SIO2	0.0	0.40	2.57	0.21	0.28
TIO2	45.14	43.76	50.88	51.08	33.34
AL2O3	0.03	0.0	0.10	0.0	0.19
CR2O3	--	--	--	0.01	--
V2O3	--	--	--	0.47	--
NIO	--	--	--	0.03	--
FEO	53.58	51.46	39.01	35.98	57.33
MNO	1.72	1.15	6.62	10.56	1.14
MGO	0.07	0.13	0.16	0.24	1.03
CAO	0.05	0.05	0.28	0.02	0.11
BAO	0.32	--	0.40	0.0	0.26
NA2O	0.01	0.0	0.05	0.0	0.03
K2O	0.03	0.0	0.08	0.0	0.08
SUM	100.95	96.95	100.15	98.60	93.79
	RECALCULATED BY PROCEDURE OF ANDERSON (1968)				
FEO	38.50	37.88	38.17	34.71	26.72
FE2O3	16.76	15.09	0.94	1.41	34.02
SUM	102.63	98.46	100.24	98.74	97.20
%FE2O3	16.46	15.20	1.45	3.06	36.82
	RECALCULATED BY PROCEDURE OF CARMICHAEL (1967)				
FEO	38.69	38.36	39.01	35.42	27.44
FE2O3	16.55	14.56	0.0	0.62	33.22
SUM	102.61	98.41	100.15	98.66	97.12
%FE2O3	15.49	14.12	0.15	1.09	33.00

APPENDIX IIG: ANALYSES OF SECONDARY MINERALS

	PREHNITE	----EPIDOTE----		SPHENE	MUSCOVITE
	1	2	3	4	5
SIO2	42.57	37.53	33.53	30.09	44.77
TIO2	0.07	0.02	0.11	29.40	0.09
AL2O3	20.81	23.96	33.66	6.93	27.40
FEO	4.46	10.95	8.94	0.58	6.73
MNO	0.12	0.24	0.28	0.01	0.21
MGO	0.04	0.04	0.04	0.02	5.29
CAO	26.79	23.46	20.03	29.09	0.80
BAO	--	--	--	0.02	0.49
NA2O	0.05	0.0	0.0	0.02	0.39
K2O	0.03	0.0	0.02	0.01	8.06
SUM	94.94	96.21	96.61	96.17	94.23
		FORMULA BASES			
SI	6.6041	3.2095	2.7949	4.0563	6.7843
TI	0.0086	0.0015	0.0067	2.9803	0.0101
AL	3.8053	2.4152	3.3060	1.1011	4.8937
FE	0.5780	0.7832	0.6233	0.0650	0.8532
MN	0.0160	0.0177	0.0198	0.0013	0.0264
MG	0.0097	0.0046	0.0049	0.0048	1.1959
CA	4.4529	2.1499	1.7888	4.2004	0.1302
BA	--	--	--	0.0009	0.0288
NA	0.0141	0.0	0.0	0.0091	0.1147
K	0.0061	0.0	0.0022	0.0014	1.5573

---

1 vug filling in hornblende dacite (164); 24 oxygens
2,3 vug filling in hornblende dacite (164); 13 oxygens
4 titanomagnetite alteration product in hornblende dacite (240); 20 oxygens
5 plagioclase alteration product in pyroxene andesite (251); 24 oxygens

APPENDIX IV: COMPILATION OF MINERAL/LIQUID DISTRIBUTION COEFFICIENTS OF CLINOPYROXENE, HORNBLENDE, PLAGIOCLASE, BIOTITE, APATITE, AND ZIRCON FOR THE ELEMENTS CHROMIUM, VANADIUM, NICKEL, STRONTIUM, BARIUM, RUBIDIUM, NEODYMIUM, AND CERIUM

CHROMIUM

D	Reference	Remarks
Clinopyroxene		
2.6*	Lindstrom and Weill, 1978	Di-Ab-An; 1290°C
2.5-3.7*	Schreiber and Haskin, 1976	Fo-An-Di; 1350°C; 1 atm; k dec with dec fO_2
0.3-32	Ewart et al.,1973	basaltic andesite to dacite; k dec inc Fe/(Fe+Mg) of cpx
10	Leeman, 1976	estimated from range of experimental and natural data
Hornblende		
23-36	Gill, 1978	andesite to dacite
12	Leeman, 1976	calculated from hb/cpx and cpx/liquid ratios
Magnetite		
100-620*	Lindstrom, 1976	alkalic basalt; 1111-1168°C, 1 atm $fO_2=10^{-4}$ to 10^{-12} atm
27-58	Ewart et al., 1973	andesite to dacite
9-26	Leeman, 1978	calculated from Rayleigh model of basalts
1-58	Gill, 1978	andesite to dacite
Biotite		
12.6±4.8	Higuchi and Nagasawa, 1969	dacite
17	Andriambololona et al.,1975	dacite
7	Leeman, 1976	calculated from mica/cpx and cpx/liquid ratios

* indicates to experimentally determined values
'inc' = 'increases 'dec' = 'decreases'

VANADIUM

D	Reference	Remarks
Clinopyrcxene		
0.03-10*	Lindstrom, 1976	basalt; 1125-1315°C; 1 atm; k dec with inc fO_2
0.8-2	Ewart et al., 1973	andesite to dacite
Hornblende		
18-45	Gill, 1978	andesite to dacite
Magnetite		
0-67*	Lindstrom, 1976	basalt; 1112-1135°C; 1 atm; k dec with inc fO_2
24-63	Ewart et al., 1973	andesite to dacite
4.9-17	Leeman, 1978	calculated frcm Rayleigh model of basalts
Biotite		
50	Andriambololona et al.,1975	dacite

NICKEL

D	Reference	Remarks
Clinopyroxene		
2.2-4.4*	Hakli and Wright, 1967	Makaopuhi basalt; 1050-1160°C; 1 atm k dec with inc T°C
1.5-11.7*	Lindstrom and Weill, 1978	Ab-An-Di; 1150-1350°C; 1 atm k dec with inc T°C
2.55*	Mysen, 1978a	Ab(45) An(45) Fo(7) Q(3); 1025°C; 20 kbs.
2.0	Leeman, 1976	estimate from experimental and natural data
3.5-8	Gill, 1978	andesite
Hornblende		
2.9*	Mysen, 1978a	An(41) Ab(41) Fo(16) Q(2); 1000°C; 15 kb
3.7	Leeman, 1976	calculated from hb/cpx and cpx/liquid ratios
7-8	Gill, 1978	andesite to dacite
Magnetite		
12.2-19.4*	Leeman, 1974	picritic tholeite; 1300-1252°C; 1 atm
20-77*	Lindstrom, 1976	alkalic basalt; 1111-1168°C; $fO_2 = 10^{-4}$ to 10^{-13} atm
4-19	Gill, 1978	andesite to dacite
Biotite		
13	Andriambololona *et al.*, 1975	andesite
3.7	Leeman, 1976	calculated from mica/cpx and cpx /liquid ratios

STRONTIUM

D	Reference	Remarks
Clincpyroxene		
0.06-0.08*	Shimizu, 1974	Di(50)Ab(25)An(25); 1100-1200°C; 15-30kb; $fO_2=10^{-8}$ to 10^{-4} atm
0.18-0.3*	Sun et al., 1974	basalt; 1110-1140°C; 1 atm
0.07-0.11	Hart and Brooks, 1974	ankaramite, basaltic andesite
0.12-0.43	Philpotts and Schnetzler, 1970	basalt-zoned phenocrysts
0.01-0.06	"	andesite
0.52	"	rhyodacite
0.11	Onuma et al.,1968	
0.12	Sun and Hanson, 1976	megacryst in basalt
Hornblende		
0.31	Griffin and Murthy, 1969	basalt
0.2-0.5	Ewart and Taylor, 1969	andesite to rhyclite
0.55-0.64	Philpotts and Schnetzler, 1970	basalt
0.19	"	andesite
Plagioclase		
1.5-2.2*	Sun et al., 1974	basalt; 1110-1140°C; 1 atm
1.2-3.3*	Drake and Weill, 1975	tholeite,andesite; 1150-1400°C; 1 atm; k inc with dec T°C
1.4-2.8	Schnetzler and Philpotts, 1970	basalt
1.3-1.8	"	andesite
2.8	"	dacite
2.4-4.5	Dudas et al., 1971	dacite
1.5-7	Korringa and Noble,1971	k inc from An(90) to An(30)
1.4-1.8	Ewart et al.,1973	An(84-88) in basaltic andesite
1.9-2.6	"	An(80-85) in dacite
2.6	"	An(85) in rhyclite
4.6	Sun and Hanson,1976	basalt
2.0-3.9	Duchesne,1978	k inc from An(50) to An(31)
2.3	Duchesne and Demaiffe,1978	An(47) in jotunite
Biotite		
0.08	Philpotts and Schnetzler,1970	basalt
0.12	"	dacite
0.67	"	rhyodacite
Apatite		
0.41	Duchesne,1978	calculated from anorthosite
1.5	Sun and Hanson,1976	basalt

BARIUM

D	Reference	Remarks
Clinopyroxene		
<0.01*	Shimizu, 1974	Di(50) Ab(25) An(25); 1100-1200°C; 15-20 kb
<0.01	Hart and Brooks, 1974	ankaramite and basaltic andesite
<0.01	Onuma et al., 1968	alkali-clivine basalt
0.03-0.05	Schnetzler and Philpotts, 1968	basalt
0.01-0.39	Philpotts and Schnetzler, 1970	basalt - zoned phenocryst
0.13	"	rhyodacite
0.01-0.04	"	andesite
0.03	Sun and Hanson, 1976	basalt megacryst
Hornblende		
0.45	Griffin and Murthy, 1969	basalt
0.42-0.73	Philpotts and Schnetzler, 1970	basalt
0.10	"	andesite
0.4	Leeman, 1976	calculated from hb/cpx and cpx/liquid ratios
0.32	Sun and Hanson, 1976	kaersutite megacryst in basalt
Plagioclase		
0.2-0.7*	Drake and Weill, 1975	natural tholeite, andesite 1150-1400°C; 1 atm; k inc with dec T
0.15-0.59	Philpotts and Schnetzler, 1970	basalt
0.05-0.24	"	andesite
0.36	"	dacite
0.16-0.42	Korringa and Noble, 1971	k inc from An(90) to An(30)
0.34-1.43	Dudas et al., 1971	dacite
0.12-0.17	Ewart et al., 1973	basaltic andesite to andesite
0.11-0.17	"	dacite
0.16	"	rhyolite
1.47	Sun and Hanson, 1976	basalt
0.39	Duchesne and Demaiffe, 1978	An(47) in jotunite
Biotite		
9.7±1.3	Higuchi and Nagasawa, 1969	dacite
1.09	Philpotts and Schnetzler, 1970	phlogopite in basalt
6.36	"	biotite in dacite
15.3	"	biotite in rhyodacite

RUBIDIUM

D	Reference	Remarks
Clinopyroxene		
<0.01*	Shimizu,1974	Di(50)Ab(25)An(25); 1100-1200°C; 15-30 kb
<0.01	Hart and Brooks,1974	ankaramite and basaltic andesite
0.02-0.28	Philpotts and Schnetzler,1970	basalt
0.03	"	rhyodacite
0.01-0.04	"	basaltic andesite
Hornblende		
0.27	Griffin and Murthy,1969	basalt
0.01	Nagasawa and Schnetzler,1971	dacite
0.41-0.43	Schnetzler and Philpotts,1970	basalt
0.05	"	andesite
0.4	Leeman,1976	calculated from amph/cpx and cpx/liquid ratios
Plagioclase		
0.02*	McKay and Weill,1976	synthetic lunar basalt; 1200°C; 1 atm
0.08*	McKay and Weill,1977	synthetic low-K basalt; 1240°C;1 atm
0.12-0.25	Duchesne,1978	k inc from An(50) to An(31)
0.03-0.19	Philpotts and Schnetzler,1970	andesite
0.06-0.49	Dudas et al.,1971	dacite
0.05	Sun and Hanson,1976	basalt
0.12-0.25	Duchesne and Demaiffe,1978	k inc from An(50) to An(20)
Biotite		
2.24±.47	Higuchi and Nagasawa,1969	dacite
3.06	Philpotts and Schnetzler,1970	phonolite
3.26	"	dacite
0.94	"	rhyodacite
3.0	Leeman,1976	calculated from mica/cpx and cpx/liquid ratios

NEODYMIUM

D	Reference	Remarks
Clinopyroxene		
0.21-0.24*	Grutzeck et al.,1974	Ab-An-Di; 1265°C ; 1 atm
0.35*	Tanaka and Nishizawa,1975	basalt; 1200°C ; 20 kb
0.26-0.32	Schnetzler and Philpotts,1968	basalt
0.17-0.18	Schnetzler and Philpctts,1970	basalt
0.07-0.65	"	andesite
1.28	"	rhyodacite
0.94	Nagasawa and Schnetzler,1971	dacite
0.38	Sun and Hanson,1976	basalt
Hornblende		
0.5*	Frey (in Irving,1978)	tholeite; 1000°C ; 5 kb
0.16	Schnetzler and Philpotts,1968	basalt
0.19	Schnetzler and Philpotts,1970	andesite
1-4.25	Nagasawa and Schnetzler,1971	dacite
0.85-3.21	Sun and Hanson,1976	basalt
Plagioclase		
0.04-0.06*	Weill and McKay,1975	synthetic lunar basalt; 1200-1340°C ; k dec with dec T
0.08-0.13*	Drake and Weill,1975	tholeite, andesite, and Ab-An-Di 1150-1400°C ; 1 atm; k inc with dec T
0.04	Higuchi and Nagasawa,1969	basalt
0.11	Schnetzler and Philpotts,1968	basalt
0.02-0.07	Schnetzler and Philpotts,1970	basalt
0.02-0.2	"	andesite
0.17	"	dacite
0.14-0.29	Dudas et al.,1971	dacite
0.17	Sun and Hanson,1976	basalt
Biotite		
0.03	Schnetzler and Philpotts,1970	basalt
0.04	"	dacite
0.34	"	rhyodacite
Apatite		
27.4-81.1	Nagasawa,1970	dacite
21	Nagasawa and Schnetzler,1971	dacite
1.4-16	Sun and Hanson,1976	calculated for basalt
Zircon		
2-6.5	Nagasawa,1970	dacite

CERIUM

D	Reference	Remarks
Clinopyroxene		
0.1-0.12*	Grutzeck et al.,1974	same conditions as for Nd
0.2*	Tanaka and Nishizawa,1975	same conditions as for Nd
0.3*	Mysen,1978c	basalt; 950°C ;20 kb
0.17	Onuma et al.,1968	alkali-clivine basalt
0.12-0.18	Schnetzler and philpotts,1968	basalt
0.36	Nagasawa and Schnetzler,1971	dacite
0.08-0.1	Schnetzler and Philpotts,1970	basalt
0.04-0.51	"	andesite
0.65	"	rhyodacite
0.1	Leeman,1976	estimated from experimental and natural data
0.18	Sun and Hanson,1976	basalt
Hornblende		
0.3*	Frey(in Irving,1978)	tholeite; 1000°C ; 5 kb
0.04*	Mysen,1978c	An(41)Ab(41)Fo(16)Q(2); 1000°C ; 15 kb
0.12	Schnetzler and Philpotts,1968	basalt
0.34	Higuchi and Nagasawa,1969	basalt
0.09	Schnetzler and Philpotts,1970	andesite
0.49-1.98	Sun and Hanson,1976	basalt
0.43-1.77	Nagasawa and Schnetzler,1971	dacite
0.2	Leeman,1976	estimate from experimental and natural data
Plagioclase		
0.07-0.14*	Drake and Weill,1975	same conditions as for Nd
0.05-0.07*	Weill and McKay,1975	same conditions as for Nd
0.09	Higuchi and Nagasawa,1969	basalt
0.02-0.11	Schnetzler and Philpotts,1970	basalt
0.08-0.3	"	andesite
0.24	"	dacite
0.16-0.4	Dudas et al.,1971	dacite
0.22	Sun and Hanson,1976	basalt
0.1	Leeman,1976	estimate from experimental and natural data
Biotite		
0.32	Higuchi and Nagasawa,1969	dacite
0.03	Schnetzler and Philpotts,1970	basalt
0.04	"	dacite
0.23	"	rhyodacite
Apatite		
18-52.5	Nagasawa,1970	dacite
16.6	Nagasawa and Schnetzler,1971	dacite
1.1-12	Sun and Hanson,1976	calculated for basalt
Zircon		
2.3-7.4	Nagasawa,1970	dacite

APPENDIX IV: CONTRIBUTIONS TO LABORATORY ANALYTICAL TECHNIQUES

APPENDIX IVA: OPERATING CONDITIONS FOR TRACE ELEMENT ANALYSIS BY X-RAY FLUORESCENCE SPECTROMETRY

Tables 7-11 list the operating conditions for the analysis of five sets of trace elements: chromium-vanadium, barium, nickel, niobium-zirconium-yttrium-strontium-rubidium, and cerium-neodymium. These trace elements are run in the above groups due to the proximity of two theta positions, and the presence of some interferences between elements of a given group.

The following procedure should be followed in setting up the X-ray fluorescence spectrometer for analysis of any set of trace elements (for an explicit description of general analysis procedures, the reader is referred to the XRF Guidebook):

-- Turn water supply to machine on (red light on)

-- Turn main power on

-- Wait several minutes for machine to 'click' on

-- Slowly turn Kv dial up to desired setting

-- Slowly turn Ma dial up to desired setting

-- Check argon flow if the flow proportional counter is to be used; regulator on argon tank=10 lb/inch; flow gauge in XRF=6-7

-- Wait at least one hour for machine to warm up

-- Set all machine parameters to values listed in operating condition tables

-- Using standards or correction pellets with high concentrations of the elements of interest, do 2% scans to determine lower level and window settings; these settings can change markedly from day to day

-- Using the same high concentration samples, determine peak

positions by counting for 10 seconds at two theta intervals of .01°; repeat this procedure until consistent peak positions are located

-- From these peak positions, subtract or add the values listed in the tables of operating conditions in order tc determine the two theta positions of all background measurements

-- Run two theta scans on several standards and unknowns in order to check for correct positioning of peak and background measurements

-- Proceed with analyses, bracketing all runs on unknowns between runs on the group of standard rccks selected for calibration

The following sections discuss modifications in the operating conditions set up by Watters (1975).

Chromium-Vanadium

These two elements need to be analyzed together due to the interference of CrK_{α} (2.2896A°) by VK_{β} (2.2843A°) radiation. In addition VK_{α} (2.503A° is interfered with by TiK_{β} (2.5138A°) radiation. Vanadium (1000 ppm V)- and titanium (TiO_2 -B)-spiked correction pellets are run to evaluate these interference effects.

These elements are analyzed using the mclybdenum tube set at 60 Kv and 40 Ma. Although WL_{α} radiation (1.476A°) is closer to the absorption edge of Cr (2.07) than McK_{α} (.709A°), the lower power (50 Kv and 40 Ma) of the tungsten tube gives lcwer intensities than the molybdenum tube.

Both the flow proportional and scintillatien counters are

used for this series of elements as the scintillation counter alone yields very low intensities. Using both ccunters and the fine collimator, resolution between the vanadium an titanium peaks is poor; the two peak positions must by determined using each correction pellet in turn. Although correction factors are quite large, excellent regression lines for vanadium are achieved with this method.

Unfortunately, the molybdenum tube (and the tungsten tube) appear to have minor amounts of chromium alloyed with the metal of the tube casing, and large chromium peaks are produced on blank samples. This leads to regression lines with large negative intercepts (over -100), and low peak/background ratios. For this reason, an aluminum filter is use to block out most of this primary Cr radiation.

The chromium peak and backgrounds on both sides are measured using this filter and the coarse collimator; the vanadium peak, titanium peak, and background for these peaks are measured without this filter and with the fine collimator.

The vanadium correction pellet should be run on all peak and background positions; the titanium correction pellet need be run on only the vanadium and titanium peaks and the associated background.

The background positions around the chromium peak have been chosen so as to avoid large barium and cerium peaks; care should be taken to check background positions from two theta scans run on rocks with high concentrations of these elements.

The lower level and window settings for Cr, V, and Ti are all similar and should be set by running 2% scans on PCC or DTS

for Cr, and the appropriate correction pellet for V and T. These settings should be extended at least 10-15% on both sides in order to avoid drastic reductions in count rate that can occur due to small voltage shifts with time.

It is recommended that ultramafic rocks be used with caution in calibration lines (for nickel, too), as there are large discrepancies in the quoted concentrations from different sources (cf. Abbey, 1977 and Flanagan, 1973). In addition, calibration lines weighted by the high concentrations of ultramafic standards will lead to overestimation of the concentrations of normal (1-400 ppm) rocks.

Barium

Barium is analyzed using the chromium tube as its L_α absorption edge (2.36A°) lies just to the long wavelength side of CrK_α radiation (2.29A°). The TiO_2-B pellet is run in order to calibrate the interference of TiK_β with BaL_α. Use of the flow proportional counter and the fine collimator yield good intensities and acceptable resolution between the two peaks. Only one background position need be run as backgrounds are flat across the two peak positions.

Nickel

Nickel is analyzed using a molybdenum target (.711A°) and settings of 60 Kv and 40 Ma. Intensities are better than with the tungsten tube (50Kv and 40Ma), even though tungsten radiation (1.476A°) is closer to the K absorption edge of Ni (1.488A°). If nickel is analyzed at the same time as zinc and

copper, however, the chromium tube should be used as the MoK and WL peaks interfere with the Zn peak and background measurements around it.

The flow proportional and scintillation counters are used together as intensities with the scintillation counter alone are unacceptably low. The aluminum filter is used to reduce primary nickel radiation (due to a nickel alloy in the target) to an acceptable level.

Niobium-Zirconium-Yittrium-Strontium-Rubidium

These elements are analyzed using the tungsten tube because MoK interferes with the niobium peak. Interferences of RbK_{β} on YK_{α} and SrK_{β} on ZrK_{α} are calibrated by running the strontium and rubidium-spiked pellet (Rb+Sr in silicic and boric acid) on all peak and background positions.

Intensities on most rock samples are great enough that counting times on peak need be no greater than forty seconds. The background position between the niobium and zirconium peaks can be ignored as it is distorted in most sample due to the prescence of the ThL_{α} peak. The Zr and Y peak positions should be located using rocks which have high concentrations of these elements and low concentrations of Sr and Rb (due to the interferences discussed above).

Cerium-Neodymium

These elements are analyzed using the molybdenum tube at settings of 60Kv and 40Ma. Use of the flow proportional and scintillation counters yield optimum intensities, and resolution

between the overlapping tails of both peaks is adequate. A cerium-spiked pellet (Cerium in silicic+boric acid) is run to calibrate the interference on NdK_{α} . At present no supply of neodymium has been located; ideally, a neodymium-spiked pellet should be run to calibrate the interference on CeL_{α} .

TABLE 7: OPERATING CONDITIONS FOR CHROMIUM-VANADIUM

Peak, Bkd #	bkd-1	pk-1	bkd-2	bkd-3	pk-2	pk-3
Counting Positions	bkd	Cr	bkd	bkd	V	Ti
Two Theta Angles	Cr-2.20	69.35	Cr+1.50	V-1.86	76.86	77.21
Count Times	40	100	40	40	100	40
Target (Kv-Ma)	Molybdenum Tube (60-40)					
Crystal	LIF(200)					
Counter(Voltage)	FPC(8.6)+Sc(10.8)					
Gain	128					
Collimator	Coarse ———			Fine ———		
Filter	Aluminum Filter ———			No Filter ———		
Lower Level-Window	180-240					
Counts on AGV	8244	27606	5458	1809	22063	27588
Regression Equation		24.2x-14.13			108.7x+9.6	
Standard Deviation		1.79			5.6	
Composition Range		6-53			5-410	

TABLE 8: OPERATING CONDITIONS FOR BARIUM

Peak, Bkd #	pk-1	pk-2	bkd-1
Counting Positions	Ti	Ba	bkd
Two Theta Angles	86.07	87.01	Ba+4.0
Count Times	10	10	10
Target (Kv-Ma)	Chromium Tube (50-40)		
Crystal	LIF (200)		
Counter (Voltage)	FPC (8.7)		
Gain	128		
Collimator	Fine		
Filter	No Filter		
Lower Level-Window	360-320		
Counts on AGV	258115	17478	424
Regression Equation		1236.2x-25.8	
Standard Deviation		3.4-13.6	
Composition Range		440-1860	

TABLE 9: OPERATING CONDITIONS FOR NICKEL

Peak,Bkd #	bkd-1	pk-1	bkd-2
Counting Positions	bkd	Ni	bkd
Two Theta Angles	Ni-.63	48.63	Ni+1.37
Count Times	20	40	20
Target (Kv-Ma)	Molybdenum Tube (60-40)		
Crystal	LIF(200)		
Counter(Voltage)	FPC(8.6)+Sc(10.8)		
Gain	128		
Collimator	Coarse		
Filter	Aluminum Filter		
Lower Level-Window	300-300		
Counts on AGV	17220	39042	13083
Regression Equation		16.72x-.47	
Standard Deviation		1.02 (3.27)	
Composition Range		6-17 (6-200)	

TABLE 10: OPERATING CONDITIONS FOR NIOBIUM-ZIRCONIUM-YITTRIUM-STRONTIUM-RUBIDIUM

Peak, bkd #	bkd-1	pk-1	pk-2	bkd-3	pk-3	bkd-4	pk-4	bkd-5	pk-5	bkd-6
Counting Positions	bkd	Nb	Zr	bkd	Y	bkd	Sr	bkd	Rb	bkd
Two Theta Angles	Nb-.35	21.23	22.40	Y-.25	23.63	Sr-.4	25.01	Rb-.4	26.49	Rb+1.4
Count Times	20	40	40	20	40	20	40	20	40	20
Target (Kv-Ma)	Tungsten Tube (50-40)									
Crystal	LIF(200)									
Counter (Voltage)	Scintillation (8.45)									
Gain	128									
Collimator	Fine									
Filter	No Filter									
Lower Level-Window	300-450									
Counts on AGV	22281	46432	126211	15807	39064	13332	208309	10723	37119	8135
Regression Equation	11.8x+3.8		227.5x-15.7		18.5x+3.6		658.6x+7.4		69.1x-.3	
Standard Deviation	.84		2.7		3.4		9.0		2.4	
Composition Range	9.5-29		105-500		12-37		190-660		21-250	

TABLE 11: OPERATING CONDITIONS FOR CERIUM-NEODYNIUM

Peak,Bkd #	bkd-1	pk-1	pk-2	bkd-2
Counting Positions	bkd	Ce	Nd	bkd
Two Theta Angles	Ce-.85	71.56	72.05	Ce+1.30
Count Times	40	100	100	40
Target (Kv-Ma)	Molybdenum Tube (60-40)			
Crystal	LIF(200)			
Counter(Voltage)	FPC(8.4)+Sc(9.5)			
Gain	128			
Collimator	Fine			
Filter	No Filter			
Lower Level-Window	200-500			
Counts on AGV	5750	19540	16750	5108
Regression Equation		138.3x-46.9	37.6x-1.5	
Standard Deviation		6.2	3.4	
Composition Range		21-410	16-148	

TABLE 12: CONCENTRATIONS (PPM) AND MASS ABSORPTION COEFFICIENTS FOR STANDARD ROCKS

	Concentrations (parts per million)											Mass Absorption Coefficients				
	Cr	V	Ba	Ni	Nb	Zr	Y	Sr	Rb	Ce	Nd	@Cr	@V	@Ba	@Sr	@Nd
AGV	12	125	1090	17	15.0	220	26	660	67	74	35	134.4	164.2	230.1	11.6	146.2
W-1	120	240	160	78	9.5	105	25	190	21	21	16	144.3	176.2	246.1	14.3	156.8
G-2	9	34	1860	6	14.0	300	12	480	170	168	54	130.4	161.6	226.9	9.4	141.9
GSP	13	49	1300	9	29.0	500	32	230	250	410	148	133.8	165.1	231.6	10.4	145.6
BCR	16	410	680	13	14.0	185	37	330	47	53	28	138.4	164.5	230.1	14.2	150.5
GA	12	38	850	7	10?	150	21	310	175	70	25?	130.0	161.5	226.7	9.5	141.4
GH	6	5	22	3	85?	150	70	10	390	50?	21?	127.2	159.4	224.0	8.6	138.5
SY-2	10?	50	460	10		270	130	270	220	213	73	145.1	180.9	269.3	12.2	157.8
SY-3	8?	51	440	11	145?	340	740	300	210	2000?	500?	145.5	181.5	253.7	12.3	158.2
NIM-P		240		560		30	4?	34?	5?			115.8	144.4	203.1	13.2	126.1
NIM-S	13	10	2600?	6	3.5?	45?	3?	64	550			156.1	195.2	273.1	10.6	169.8
NIM-N	34	210	95?	120	2.0?	22?	7	260	5?			142.6	177.5	248.0	13.1	155.0
NIM-G	14	2	110?	8	52.0	290	125	10	330			128.4	160.8	225.9	8.9	139.8
NIM-D	2900	41	10?	2100		10?		3?				104.2	130.7	184.3	14.1	113.6
NIM-L	14?	78	460?	6?	920		23	4600	195			132.6	164.1	229.8	13.3	144.2
JG	53	24	460	8?		110?	31?	185	185			129.3	161.1	226.3	9.1	140.7
JB	400	210	490	135		155	26?	440	41			141.1	171.2	239.4	13.1	153.4
MRG	420	520		200	20.0?	100	20?	260	8			157.8	182.0	253.6	18.3	171.4
DTS	4400	13		2400								103.8	130.3	184.1	10.3	113.1
PCC	3000	31		2500								102.2	128.3	181.2	10.0	111.4
QLO		52.5	1401	7?		170?		350?				131.5	162.4	227.9	10.3	143.1
RGM		14.7	882			210?		110?	170?			127.7	159.2	223.6	8.8	139.0
BHVO	320?	306	132.5	140?	19?	160?	27?	400?	10?			149.7	176.3	246.2	15.1	162.6

Source for concentrations is Abbey(1977)--'?' indicates less certain value

Mass absorption coefficients calculated from major element chemisty(Abbey,1977);

Mass attenuation values taken from the Handbook of Spectroscopy(1974)

Appendix IVb: Trace Element Reduction Program

BASIC language computer programs have been written for the reduction of trace element data. As conditions for each set of trace elements differ with respect to shape of backgrounds, interferences, and counting times, five separate programs have been written for the reduction of the five sets of trace elements discussed above.

The general reduction procedures for all the trace elements are presented below; specific differences and data input formats for each set of elements are discussed under separate headings.

General reduction technique

A complete run for a given set of trace elements includes counting the intensities of peaks and backgrounds for each element of interest, and for any elements which give rise to interferences. Data reduction involves the following steps:

- Reduction of raw counts on all peaks and backgrounds to counts per second
- Subtraction of background counts per second from peak counts per second to give net peak counts per second
- Calculation of the intensity of any interferences and subtraction of the appropriate amounts from the net peak counts per second
- Multiplication of net peak counts per second times the mass absorption coefficient for the appropriate wavelength
- Calculation of the ratio of the above product for each rock with that of AGV-1
- Calibration of the standard rocks by regression of the above

ratios against nominal concentrations

- Comparison of nominal concentrations of standards with concentrations calculated from the regression line, and rejection of any standards which differ by more than two standard deviations of the regression
- Recalculation of the regression line if any standards have been rejected
- Calculation of unkown concentrations from the regression line derived from standard rocks
- Calculation of 95% confidence limits for each of the computed concentrations

Program Options

Several options for data reduction are made available to the user with the us of input statements which demand 'yes' or 'no' answers (the number '1' signifies 'yes'; the number '0' signifies 'no').

Option One: 'Compiled Regression Statistics'

This option enables the user to compile the results of a specific run with previous runs. It also allows unknown samples to be processed without running any standard rocks (AGV-1 must always be run as it is the reference standard); it is recommended that this be done for qualitative work only.

A 'yes' response brings back a demand to input the previous regression statistics for each element being analyzed. These statistics can be read off any previous computer outputs. The data should be typed on one line, with all entries separated by commas.

Option Two: 'Print Suppressor'

A 'yes' response generates a full printout of preliminary calculations prior to printing of the regression equation and statistics. This printout includes a tabulation of the net counts per second times mass absorption coefficient for each standard, a list of nominal concentrations versus concentrations calculated from the regression line for each standard, and statistics of the fit of the background curves for the niobium-rubidium program.

A 'no' response considerably shortens the computer printout and the time take in data reduction. The regression equation and associated statistics are printed and the calculated concentrations for unknown rocks are tabulated.

Option Three: 'Weighted Least Squares Fit'

A 'yes' response causes the calibration line to be calculated using a statistical weighting of the standard rock compositions. The weighting factor, defined at line # 140, is equal to the reciprocal of the squared concentration; this weighting factor can be altered by changing line # 140. It is suggested that a weighted fit be used only if a wide range of standard compositions are used in the regression line. The best fit is obtained by using an unweighted fit to standards which closely bracket the expected concentrations of unknown rocks.

During operation of the reduction program, the user is required to respond to one additional input question:

'Number of Standards?'

The user must input the number of standard rocks which are to be used in the calibration line. This number must agree with the

number of data lines which have been written for the standard rocks(data statements are discussed below). The number of correction pellets run for any set of trace elements is not included in the number of standards input at this time.

Data Input and Reduction Program Procedures

In order to operate the reduction program, it is critical that data be input in the correct format and in the proper order. All data is input in the form of data statements which have the form:

'line number-DATA-any data entries separated by commas'

where '-' refers to a blank space in the line. If a comma is the last entry of a data line, the computer will interpet this to mean that another data entry has been made with the default value of '0'. Any number of data entries can be made in a single line(space is the only limitation); the computer reads sequentially through these data lines in order to find as many data entries as it needs to satisfy any 'data read' statements that it encounters.

In order to avoid ambiguity, specific formats for each set of trace elements are presented below. The numbers associated with peaks and backgrounds refer to the same numbers listed in the tables of operating conditions. The number '0' must be entered in the data statements after all data for any correction pellet, standard, or unknown has been typed; this tells the computer that the data which follows the '0' is data for the next rock. Data for more than one run on a given rock follows sequentially without separation with a '0'; for all peak and

background positions, type the counts for the first run, and then type the counts for any additional runs, using commas to separate all data entries.

Recommended values for the concentrations of the various trace elements for the standard rocks, and mass absorption coefficients for the required wavelengths are listed in Table 12.

In the data format sections below, numbers at the beginning of lines refer to the line numbers at which the data statements should be typed; 'ppm' refers to the concentration in parts per million; 'mac' refers to the mass absorption coefficient at the appropriate wavelength.

Data Format for Chromium-Vanadium Series

5990: date of run(in quotation marks)

5999: two theta positions for bkd-1,pk-1,bkd-2

6000-6009: counts for TiO -correction pellet--bkd-3,pk-2,pk-3--repeat for all runs

6010-6019: counts for Vanadium correction pellet--bkd-1,pk-1,bkd-2,bkd-3,pk-2,pk-3 for all runs

6020: AGV(in quotes),Cr ppm,Cr mac,V ppm,V mac

6021-6029: counts on AGV--bkd-1,pk-1,bkd-2,bkd-3,pk-2,pk-3-repeat for all runs

6030-6999: data for other standard rocks in same form as that for AGV

7000- : data for unknowns--name of sample(in quotes),Cr-mac,V mac,counts for all two theta positions in same order as above

The correction factor for Ti interference on V is equal to

the background-corrected counts/second on V/Ti, taken from the TiO_2-correction pellet. As the V peak overlaps the Ti peak, a correction factor equal to the background-corrected c/s on Ti/V is calculated from the V correction pellet. Because of these two mutual interferences, peak counts on standards and unknowns are computed by iteration with both correction factors until a constant value is reached. The V correction pellet also gives a correction factor for V interference on Cr, which is equal to the background-corrected c/s on V/Cr. The background intensity at the Cr peak is determined by putting a straight line through the background positions on either side of the peak.

Data Input and Reduction Procedures for Barium

5999: date of run (in quotes)

6000-6009: counts on TiO_2-correction pellet--pk-1, pk-2, bkd-1--repeat for all runs

6010: AGV (in quotes), Ba ppm, Ba mac

6011-6019: counts on AGV--same order as above--repeat for all runs

6020-6099: data for other standards--same form as for AGV

7000- : data for unknowns--name (in quotes), Ba mac, counts in same order as above

As backrounds are flat across both peak positions, the counts at the background position are subtracted from both peaks. The TiO_2-correction pellet gives a correction factor equal to the background-corrected c/s on Ba/Ti.

Data Input and Reduction Procedures for Nickel

5990: two theta positions for bkd-1,pk-1,bkd-2

5999: date of run(in quotes)

6000: AGV(in quotes),Ni ppm,Sr mac

6001-6009: counts for AGV in same order as above--repeat for all runs

6010-6999: data for other standards in same form as for AGV

7000- : data for unkowns--name(in quotes),Sr mac,counts in same order as above

No corrections are necessary for reduction of Ni data. Background intensity at the Ni peak is determined by putting a straight line through the backgrounds on either side of the peak.

Data Input and Reduction Procedures for Nicbium to Rubidium Series

5999: date of run(in quotes)

5990: two theta positions for all peaks and backgrounds --bkd-1,pk-1,pk-2,bkd-3,pk-3,bkd-4,pk-4,bkd-5,pk-5,bkd-6

6000-6010: counts for correction pellet--for all positions in same order as above--repeat for all runs)1 6020: AGV(in quotes),Sr mac,Nb ppm,Zr ppm,Y ppm,Sr ppm,Rb ppm

6021-6029: counts on AGV for all peaks and backgrounds in same order as above

6030-6999: data for other standards in same form as that for AGV

7000- : data for unknowns--name(in quotes),Sr mac, ccunts for all peaks and backgrounds in same order as above

Note: Due to the length of this program all data for

unknowns may not be able to be reduced at one time. After loading master program, enter data until computer prints the error message 'PTB'. Erase the data lines for the unkown rock preceding this message. Reduce data, and then delete data lines for those unknown rocks; type data for next batch of unknowns and reduce as above.

Backgrounds are determined at all peak positions by fitting an exponential curve to all background positions. The 'Rb+Sr' correction pellet is used to determine the correction factors for Sr interference on Zr, and Rb interference on Y. These factors are equal to the background corrected counts/second on Zr/Sr, and Y/Rb, respectively.

Data Input and Reduction Procedures for Cerium-Neodymium

5990: date of run(in quotes)

5999: two theta positions--bkd-1,pk-1,pk-2,bkd-2

6000-6009: counts for Ce correction pellet--same order as above--repeat for allruns

6020: AGV(in quotes),Nd mac,Ce ppm,Nd ppm

6021-6029: counts for AGV--same order as above--repeat for all runs

6030-6999: data for other standards--same form as for AGV

7000- : data for unknowns--name(in quotes),Nd mac,counts in same order as above

Background intensities are determined at peak positions by assuming a straight line fit between background postions. The Ce pellet gives a correction factor equal to the background-corrected c/s on Nd/Ce.

Operation of Reduction Program

-- Calculate mass absorption coefficients for the appropriate wavelegths for all unknown rocks; use BASIC program discussed in Appencix Va. As mass absorption coefficients for elements 28-47 are linearly related, use the mass absorption coefficient for Sr for reduction of data for nickel, and for the niobium to rubidium series. As Nd and Ce mass absorption coefficients are extremely close in their values, the Nd mass absorption coefficient is used for both elements.

-- Turn teletype switch to 'line'

-- Type 'SCR'; this clears the memory of the computer so that the reduction program can be loaded

-- Load the reduction program from the paper tape feeder

-- Enter data either by typing it in or by feeding it in from paper tape. All data should be stored on paper tape for future reference

-- Type 'RUN'

-- Answer the 3 option questions by typing '0' or '1', and then 'return'

-- Answer the '# of standards' question by typing 'x' and then 'return', where 'x' equals the number of standards not including correction pellets

-- After successful reduction of data and storage of data on paper tape(s), type 'SCR' which erases the memory of the computer and leaves the terminal ready for the next user.

APPENDIX IVC: DETERMINATION OF TOTAL WATER AND CARBON DIOXIDE

Description of Apparatus: The apparatus and procedure involved has been modified from that of Hutchinson (1974). Figure 36 presents a labelled sketch of the apparatus. It consists of an open-bore furnace with a three foot long, 18 mm internal diameter silica tube running throughit and in which samples are placed. It is attached at both ends to drying tubes by mean of tygon tubing and rubber stoppers wrapped in teflon tape. Nitrogen delivered from a storage tank, is cleaned by passsing through the first two drying tubes, sweeps thrcugh the silica tube, and then passes through the final drying tubes in which the amount of water and carbon dioxide gained frcm the sample is measured. Water is absorbed in the first drying tube (H2O) which is filled with magnesium perchlorate. Carbcn dicxide is absorbed in the second tube (CO_2) which contains ascarite. The one-way flcw of nitrogen ends in a beaker containing mineral oil, in which the flow rate can be visually estimated.

Supply: Magnesium perchlorate and ascarite can be ordered frcm Fisher Scientific; one-pound bottles of each are now kept in the X-ray lab. The drying tubes need not be refilled for scores of samples. Ascarite changes from a brcwn to white cclor when it is exhausted, and magnesium perchlorate should be changed only if blank values appear to be erratic or if the H2O tube lcses weight on blank runs.

Combustion boats and crucibles are kept in the X-ray lab. The collection consists of 5 five-centimeter vitreosil boats, 5 ten-centimeter vitreosil boats, 2 ten-centimeter Coors porcelain

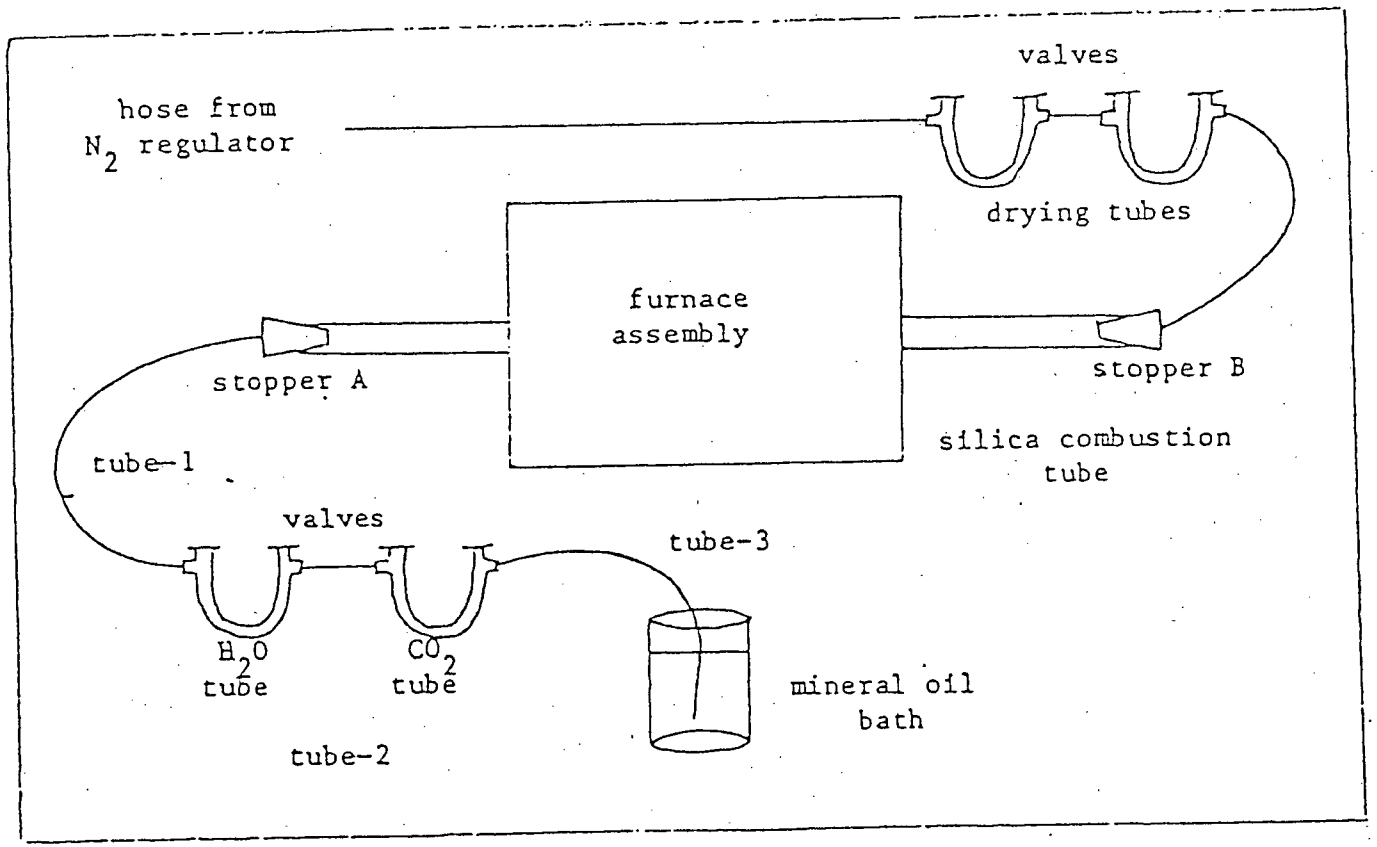

FIGURE 36: Schematic drawing of apparatus used for determination of total H_2O and CO_2.

boats, and 3 five-centimeter Coors porcelain boats. Porcelain boats should be used at temperatures above 1100 degrees Celsius.

Procedure: Switch variac on, turn up to 115 volts, and allow to warm up for 2 hours. Temperature should be in the range 1050-1100 degrees Celsius, but will climb slowly with time. After 4-5 hours turn the variac down to 110 volts. A calibration chart of temperature versus variac voltage is attached to the variac.

Open all valves in the four drying tubes, open the pressure valve on the nitrogen tank, and open the needle valve on the regulator. Slowly turn the main adjusting valve on the regulator until bubbles of nitrogen can be seen in the mineral oil bath. Flow should be continuous and just slow enough that bubbles can be counted individually.

Determination of Blank: As the flow of nitrogen gas alone causes the water and carbon dioxide collection tubes to gain weight, a blank value should be determined before each batch of samples is run. These correction factors should not be more than 0.3 mg and 2 mg per hour for CO_2 and H_2O, respectively.

Using a lint free cloth to handle drying tubes, close valves on H_2O and CO_2 tubes, remove tygon tubing, accurately weigh each tube, and reconnect. As pressure will build up once the valves are closed, disconnect tygon tube 1 from the H_2O tube as soon as the first valve is closed. Disconnect tube 2 from the H_2O tube, unscrew clamp and weigh tube. Reclamp in position and reconnect tube 2; disconnect tube 2 and tube 3 from the CO_2 tube, unscrew clamp, weigh, reclamp, and reconnect tubes 2 and 3. Open valves in both drying tubes and reconnect tube 1. Adjust flow rate as above.

Note time. Run blank for 1 hour. Following the weighing procedure above, obtain the weight gained by each drying tube, and divide by the time of the run to arrive at a correction value for both H2O and CO2.

Determination of H_2O^- in samples: Accurately weigh approximately one gram of each sample into Coors porcelain crucibles. Dry at 110 degrees centigrade for one hour. Cool and reweigh. Weight loss equals H_2O^-. Store samples in dessicator for determination of H_2O^+ and CO2.

Determination of H_2O^+ and CO2 in sample: Accurately weigh approximately one gram of sample into small vitreosil combustion boat. If sample is to be reused later for further chemical analyses, use larger vitreosil or Coors porcelain combustion boats lined with nickel foil in order to avoid contamination between samples.

Note time. If more than 15 minutes has passed since the last weighing of the drying tubes, it is best to reweigh to obtain initial values.

Reconnect tube 1 to the H2O tube and immediately pull stopper A from the silica tube. The flow of nitrogen through the tube prevents air from entering the system. Place combustion boat with sample into the end of the silica tube and, using the iron push rod, push the boat into the furnace until the red mark on the push rod is aligned with the end of the silica tube. Quickly, but smoothly, remove the push rod and replace the stopper at the end of the silica tube. Check the mineral oil

bath for the flow of nitrogen. Adjust the rate of flow by means of the regulator or needle valve so that bubbles are continuous but just slow enough to be individually counted. This gives a flow of approximately 3 liters per hour. Care should be taken that the rate of flow is the same as that during the blank determination.

Vapour will condense on the inside of the silica tube, slowly progress down the tube, into the pyrex tube inserted in rubber stopper A, and eventually onto the arm of the H2O tube. The run can be terminated when condensation droplets are no longer visible on the arm of the H2O tube.

Note time. Close valves on the H2O and CO2 tubes, and remove rubber stopper A. Push sample as far as possible with the flattened end of the push rod. Remove stopper B, and with the other end of the push rod, hook the combustion boat and draw it out of the silica tube until it overhangs the edge enough to be grasped with a pair of tweezers. Set the boat on the asbestos pad to cool. Replace stopper B, then stopper A, and disconnect tube 1 from the H2O tube.

Weigh the two drying tubes according to the procedure outlined above. Load next sample into the combustion apparatus to begin second determination. Weigh the combustion boat plus sample which, by then, should be cool enough to touch.

Calculations: Obtain the weight gained by each drying tube by subtracting the initial weights of the tubes from the weights after the run. Subtract the appropriate correction values (adjusted to the length of the run). Divide each of these values by the initial weight of the sample to obtain the weight

per cent of H_2O^+ and CO_2 in the sample. Subtract the final weight of the combustion boat plus sample from the initial value and divide by the initial weight of the sample, to obtain the total weight per cent of sample lost. This value should agree with the sum of the H_2O^+ and CO_2 values to within 5%. If not, a duplicate run should be made.

Shut Down: Turn down voltage on variac and switch off. Release pressure of nitrogen by backing off on regulator. Wait for bubbles to stop in mineral bath; then close needle valve on nitrogen regulator and main pressure valve on tank, and shut all valves on drying tubes. This insures that no air will enter the system and that nitrogen pressure will not build up within the system.

APPENDIX IVD: DETERMINATION OF FERROUS IRON

equipment:	
5-10	Teflon Test Tubes + Caps
1	Sand Bath And Hotplate
1	Plastic Coated Wire Rack
1	Microburet Plus Stand
1	Magnetic Stirrer
2-5	Magnetic Stirring Rods
2-3	100 Ml Volumetric Flasks
1	1 Litre Volumetric Flask
1	10 Ml Graduated Cylinder
5-10	600 Ml Pyrex Beakers
2	100 Ml Pyrex Beakers
1	Glass Stirring Rod
1	Timer(10 Minutes)
1	Metal Tongs

reagents:

- Boric Acid(10 G/sample)
- Barium Diphenylamine Sulfonate(.01 G/10
- Potassium Dichromate(.6825 G)
- Phosphoric Acid (50ml/10 Samples)
- Hydroflouric Acid In Dispensing Bcttle (2ml/sample)
- Sulfuric Acid In Dispensing Bottle (2 Ml/sample)
- Distilled Water (400 Ml/sample)

Supply:

All reagents and equipment are kept in Dr. K. Fletcher's lab (room 213), with the following exceptions:

A timer can be borrrowed from the department darkroom, and metal tongs from the X-ray lab.

Distilled water, and hydroflouric and sulphuric acid in dispensing bottles are available from the strcntium chemistry lab. Boric acid (crystals) are available from geology supplies.

Method:

Prepare the following solutions (solutions 1 and 2 can be made one week early but sclution 3 should be made just before the rest of the procedure is done):

1) Indicator solution: dissolve 0.01 g barium diphenylamine sulfonate in 50 ml water. Add 50 ml phosphoric acid and dilute to 100 ml. It is not critical that all the barium diphenylamine is dissolved completely; it only effects the intensity of the colour of the final solution.

2) Titration solution: dissove .6825 g potassium dichromate (dried at110°C for 2 hours) in water and dilute to 1 liter. Must be accurate.

3) Boric acid solution: dissolve 10 g boric acid in 400 ml water (in 600 ml beaker) and bring to vigorous boil. Allow solution to cool. Repeat for each sample to be analyzed. This solution forms a complex with the ferrous ion to prevent oxidation to ferric ion.

Weigh accurately samples of approximately 400 mg each into a series of teflon test tubes. Rinse sample down sides of test tube with as little water as possible. Add 2 ml sulfuric acid to test tube and then 2 ml hydroflouric acid cap immediately and bring to rapid boil in sand bath for 10 minutes.

Note: Sample oxidizes readily once HF is added so be quick with procedure once it is added. If very little water was used to wash down sample in test tube, the acids can be mixed with a small amount of water in a teflon test and then added to sample. Since the mixture of these reagents involves a strongly exothermic reaction, addition of this hot acid mixture will allow sample to reach a boil more quickly. Use timer to make sure boiling time is not more than 10 minutes. Risk of oxidation of ferrous iron increases greatly with prolonged boiling.

While sample is boiling fill graduated cylinder with 10 ml

indicator solution.

Pour about 100 ml of boric acid from 600 ml beaker into 100 ml beaker. Using metal tongs, remove test tube from sand bath and immediate plunge it (cap side down) into 600 ml beaker containing 300 ml boric acid. Use glass stirring rod tc push cap off test tube. Keep test tube immersed (sample out of contact with air) while rinsing glass rod and test tube cap with boric acid from small beaker into large one. Lift test tube from beaker and quickly fill several times with boric acid from small beaker emptying contents each time into large beaker.

Add 10 ml indicator solution to 600 ml beaker containing boric acid plus sample and begin to stir on magnetic stirrer. Titrate with potassium dichromate solution until <u>permanent</u> purple tinge is obtained. Colour will often appear and then dissappear as mixing of solution proceeds.

<u>Note:</u> in the entire procedure, only three measurements are critical to the accurate determination of ferrous iron: the proportions of the titration solution, the weight of sample, and the volume of titration solution used.

<u>Calculations:</u>

the oxidation-reduction equation is:

$Cr2O7^{-2} + 14\ H^{+} + 6\ Fe^{+2} === 6\ Fe^{+3} + 2\ Cr^{+3} + 7\ H2O$

moles Cr2O7 = (.6825/294.2)*(volume tit.soln.in litres)

moles FeO = (wgt of sample(mg))(% FeO)/71.85

$$\% \text{ FeO} = \frac{6 * .6825 * 71.85 * \text{vol. Tit.sl(ml)} * 100}{294.2 * \text{wgt sample(mg)}}$$

%FeO = 100 * vol tit.sl(ml)/ wgt sample(mg)

APPENDIX V: COMPUTER PROGRAMS

Various programs have been written that facilitate reduction of whole-rock compositional data and representation of this data in a variety of ways useful to petrologists. These programs are designed to complement the X-ray fluorescence spectrometry analytical techniques recently established in the UBC Department of Geology, and should be used in the following manner:

1) raw XRF whole-rock data is reduced to a hydrous basis and mass absorption coefficients are calculated by the 'mass absorption coefficient' program described in Appendix Va.

2) whole-rock data from step 1 is run through a cation norm program and an output file is generated which contains the whole-rock chemistry and normative compositions of all rocks.

Steps 1 and 2 can be combined by utilizing the 'XRF calibration' program written by G.T. Nixon. This program puts analyses on an hydrous basis and generates a data file which is read by the norm program. Mass absorption coefficients are calculated in this version of the norm program.

3) whole-rock data is tabulated for presentation using the program described in Appendix Vb.

4) whole-rock data is graphically plotted using the program described in Appendix Vc, in conjunction with a program written by E.H. Perkins.

In addition, steps 3 and 4 have been adapted so that microprobe analyses of minerals can be tabulated and plotted using the programs described in Appendix Vd and VIe, respectively.

APPENDIX VA: MASS ABSORPTION COEFFICIENT COMPUTATION:

This program computes mass absorption coefficients for various wavelengths from major element analyses. Coefficients are computed for barium and neodymium (L alpha), and chromium, vanadium, strontium, and rubidium (K alpha) wavelengths, using mass attenuation values from The Handbook of Spectroscopy, 1974.

Several options are available for recalculating major element analyses prior to the computation of the mass absorption coeficients; these options are intended to complement two primary situations encountered in obtaining major element analyses by the fused disc, X-ray fluorescence technique used at UBC.

The first option is used for treating major element analyses of rocks used as standards in calibration curves. This option converts analyses from Abbey (1977), which are on a dry basis (H_2O^- removed), to analyses in a completely volatile-free and oxidized state; these analyses correspond to the state of these rocks in fused disc form and should be used as primary values in calibration curves. The analyses are then reconverted to a volatile-included basis, recalcualted to 100%, and mass absorption coefficients are computed.

The second option is used to treat analyses of unknown rocks which have been determined on fused discs by X-ray fluorescence. This option converts these analyses to a volatile-included basis, recalculates them to 100%, and computes mass absorption coefficients.

If neither of the above options are chosen, the program will calculate mass absorption coefficients without adjustment

of the major element chemistry.

Major element chemistry is supplied by the user in the form of data statements. These statements must occur between lines 1000 and 1999, or after line 2500. The data statements must be in the following form:

sample name(in quotes),SiO2,TiO2,Al2O3,Fe2O3,FeO,MnO,
MgO,CaO,Na2O,K2O,P2O5,H2O+,S,CO2,H2O-

All oxide data is in weight per cent. It is not important how much data appears on a single line, as long as the name of the sample and oxide data are in the proper order. Data for each sample should follow sequentially in the same order as listed above. If any of the above elements or oxides have not been determined, a zero must be entered in their place.

The only difference between data statements for standards and unknowns is that data for standards includes a nominal sum (including trace elements) which follows the last oxide entry. A second input-option in the program allows the user to specify which data format has been used.

In order to run the program, all analyses should be typed in data statements and kept on paper tape so that they can be reused at a later time if necessary.

Load the master program from the paper tape and enter the analyses from paper tape if they have not already been typed in.

Type 'RUNNH'. The program then asks the user which option is to be used. Type either '2', '1', or '0'. If '0' is typed, the program asks whether the data format is for unknown rocks or standard rocks. Type '1' or '2'.

APPENDIX VB: WHOLE-ROCK TABULATION PROGRAM

This program reads the output file of the ncrm program(refer to G.T. Nixon, 1979) which consists of major and trace element chemistry and normative ccmpositicns, and tabulates them in a file which can be run on the FMT system. The tables in Appendix I are examples of the final cutput of this program.

The program should be run from a terminal with the follcwing command:

```
$RUN OB.WRTABLE   3='DATAFILE'    7='OUTPUT'
```

where 'DATAFILE' contains the output from the ncrm program, and 'OUTPUT' will be the file read by the FMT system.

One option is presented to the user, and demands an input of how many columns/page are to appear in the final table. The program first asks 'same # of columns/page?'; the user must type '0' for 'yes', or '1' for 'no'. If the answer is 'yes' the program asks the user to input the number of cclumns to appear on each page. If the answer is 'no', the program asks how many pages of output are to be produced and the # of cclumns to appear on each page starting with page one(up to 20 pages). All information must be right justified in I2 format.

Before running the output file on the FMT system, this file should be edited by replacing lines 1-3 with the following lines:

```
NO LIST
NO PAGE
GO
```

Then issue the command:

```
$RUN *FMT SCARDS= 'OUTPUT' SPRINT= 'FINAL TABLE'
```

Release the final table to the special 'TN' printer with the follcwing commands:

```
$CONTROL *PRINT* HOLD PRINT=TN FORM=TYPE
$COPY 'FINAL TABLE' *PRINT*
$RELEASE *PRINT*
```

where 'TYPE' refers to the type of paper (8 x 11, or blank)

APPENDIX VC: WHOLE-ROCK PLOT PROGRAM

This program is designed so that various compcsitiocnal parameters and ccmbinations of these parameters can be plotted using plot programs written by E.H. Perkins. The program reads the output file of the norm program, so that major and trace elements, in addition to normative compositions, can be plotted. Each of these compositional parameters is given a reference number within the program, so that choices of plct parameters is performed by user input of the appropriate numbers. Examples of plots generated by use of this program are shown in all figures of this thesis that contain compositional data.

The program is run from conversational terminal by the command:

```
$RUN OB.WRPLOT 3='DATAFILE' 7='-FILE'
```

where 'DATAFILE' contains the output of the ncrm program, and '-FILE' is a temporary file which is read by the plot program.

The program is written so that the X- and Y-axes can contain ratios with numerators and denominators consisting of the sum of up to six compositional parameters. The choice of parameters is performed by four separate input statements for X-axis numerator, X-axis denominator, Y-axis numerator, and Y-axis denominator. The format of the input is 6I2, where each two-place integer is the reference number of a desired compositicnal parameter. If less than six parameters are desired, the remainder of an input line is left blank. A denominator (or numerator) can be set equal to '1', by input of the reference number '50' at the appropriate input question.

Triangular plots are created within the program by rearranging the data such that the X-axis numerator is translated to the lower right apex of an equilateral triangle, and the Y-axis numerator is translated to the top apex of the triangle. Both denominators must contain the sum of all parameters desired at the three apices of the triangle.

All parameters within numerators and denominators can be multiplied by chosen factors by responding 'yes' ('1') to the appropriate question. In this case the user is asked to input these multiplicative factors for each numerator and denominator. The input is in 6F6.3 format, and is easiest if all parameters are separated by commas. If less than six multiplicative factors are desired, the remaining part of the input line can be left blank.

Other input questions require 'yes' or 'no' responses, which are signified by typing (I1 format) '1' or '0', respectively. These options are for:

-- a large square plot as opposed to a smaller rectangular plot with long axis horizontal

-- all major elements plotted on a molecular basis (divided by molecular weights)

-- all major elements recalculated on a volatile-free basis

-- the natural log of all plot parameters

-- all iron converted to the ferrous state (for AFM diagrams)

-- all major elements converted to parts per million by multiplying by '10,000'.

If a rectangular plot is chosen, the program then prints

the minimum and maximum values for the X- and Y-axes. The user must then type the minimum and maximum values desired for both axes in 4F10.3 format. These values will normally be chosen so as to encompass the printed minimum and maximum values.

In the last input, the user enters labels for both axes which may contain up to twenty characters.

Triangular plots require neither of the final two inputs.

After termination of the program, the user can plot the data by using the command:

$RUN THB2:PLOIG.O 3='-FILE' (for rectangular plots), or

$RUN EHP:TRIIG.O 3='-FILE' (for triangular plots).

In either case, the user is then asked by this program 'what device are you on?', and responds by hitting the 'return' key. The plot will be drawn, and can be copied to a larger size by putting the cross-hairs on the 'copy' command, and typing '1'. To make a hard copy of the plot, press the 'copy' button on the right side of the Tektronix terminal. To return to command mode, press the 'return' key. To terminate the plot program, put the cross-hairs on the 'stop' command, and type '1'. Many other plot edit commands are available but use of them should not be attempted without further personal instructions.

NOTE: This plot program can only be run on the Tektronix terminal now located in Dr. T.H. Brown's computer room. His permission to use that terminal is a necessary condition for using this plot program.

APPENDIX VD: MINERAL TABULATION PROGRAM

This program calculates formula bases and various end member compositions for pyroxenes, amphiboles, feldspars, biotites, magnetites, and ilmenite analyses, and tabulates them in an output file which can be run on the FMT system. Examples of tables produced by this system are presented in Appendix II.

The program reads analyses including up tc 13 elements (format: A4,10F7.2,/,4x,3F7.2) for all minerals except feldspars, which contain up to 10 elements(format: A4,10F7.2). The order of the data input is:

sample name, SiO_2, TiO_2, Al_2O_3, FeO, MnC, MgO, CaO, BaO, Na_2O, K_2O, Cr_2O_3, V_2O_3, NiO.

The program should be run from a conversational terminal with the following command:

$RUN OB.MINTABLE 3='DATAFILE' 7='OUTPUT' 8='PLOTDATA'

where 'DATAFILE' contains the mineral analyses

'OUTPUT' is the file which will be run cn the FMT system and 'PLOTDATA' is a file which will contain the analyses and calculated formula bases of the tabulated minerals, and can be used to plot mineral compositions using the program described in Appendix Ve.

After issuing the above command, the program will ask the user to input the formula basis (# of oxygens) appropriate for the mineral compositions that it will read. In crder tc key the program into calculating appropriate end-member compositicns, the following formula bases should be used:

6=pyroxenes 8=feldspars 22=bictites

23=amphiboles 24=magnetites 32=ilmenites

The desired formula basis is input at the same time as the desired number of columns per page and the number of elements in the mineral analyses (3I2 format).

In addition to calculating formala bases, the program will calculate

-- Fe^{3+}, Al^{VI}, Al^{IV}, and end-member compositicns fcr pyroxenes using the procedures of Cawthorne and Collerson (1974)

-- feldspar end-member compositions

-- Fe^{3+} in amphibole analyses by solution of the charge balance equation of Papike et al. (1974):

$$Na(A)+K(A)+2Ba(A)+Al^{VI}+Fe^{3}+2Ti = Al^{IV}+Na(M4)$$

where letters in parantheses refer to amphiblcle sites

Na is distributed between the A and M4 sites by setting Na(M4) equal to the difference between the ideal sum of the X and Y sites (7) and the sum of the cations (Mg, Fe, Ni, Al^{VI}, V, Cr, Ca, Mn) filling these sites.

-- Fe^{3+} and ulvospinel contents of magnetites by the procedure of Anderson (1968) or Carmichael (1967)

-- Fe^{3+} and hematite contents of ilmenites by the procedure of Andersen (1968) or Carmichael (1967)

If Fe-Ti oxides are being tabulated, the program will ask the user which reduction procedure to use. Respcnd by inputting '0' for the procedure of Anderson (1968), or '1' for that of Carmichael (1967). It is often useful to run the program twice because the two reduction techniques can yield quite different results. These differences can lead to significant variations in calculated temperatures and oxygen fugacities if applied to the experimental data of Buddington and Lindsley (1964).

Before running the output file on the FMT system, edit the same changes in this file as discussed in Appendix Vb.

APPENDIX VE: MINERAL PLOT PROGRAM

This program enables users to plot mineral compositions using the programs written by E.H. Perkins. Examples of plots generated by this program are Figures 23 and 25 of this thesis.

The program is run from conversational terminal with the command:

$RUN OB.MINTABLE 3='DATAFILE' 7='-FILE'

where 'DATAFILE' is the file generated by the 'mineral tabulation' program described in Appendix Vd

and '-FILE' is the file which will be read by the plot program

The program is set up in a similar fashion to that of the 'whole-rock plot' program (Appendix Vb), and the compositional parameters to be plotted are designated in four input statements for the X- and Y-axis numerators and denominators (6I2 format).

Triangular, quadrilateral, or rectangular plots can be generated by responding '1','2', or '0', respectively to the appropriate input question.

After termination of the program, the data may be plotted using the command:

$RUN THB2:PLOIG.O 3='-FILE' (for rectangular plots), or

$RUN EHP:TRIIG.O 3='-FILE' (for triangular or quadrilateral plots).

Operation of these plot programs is described at the end of Appendix Vc.